The dynamics of liquefied sand under wave loading with applications to nearshore engineering

March, 2003

Junji MIYAMOTO

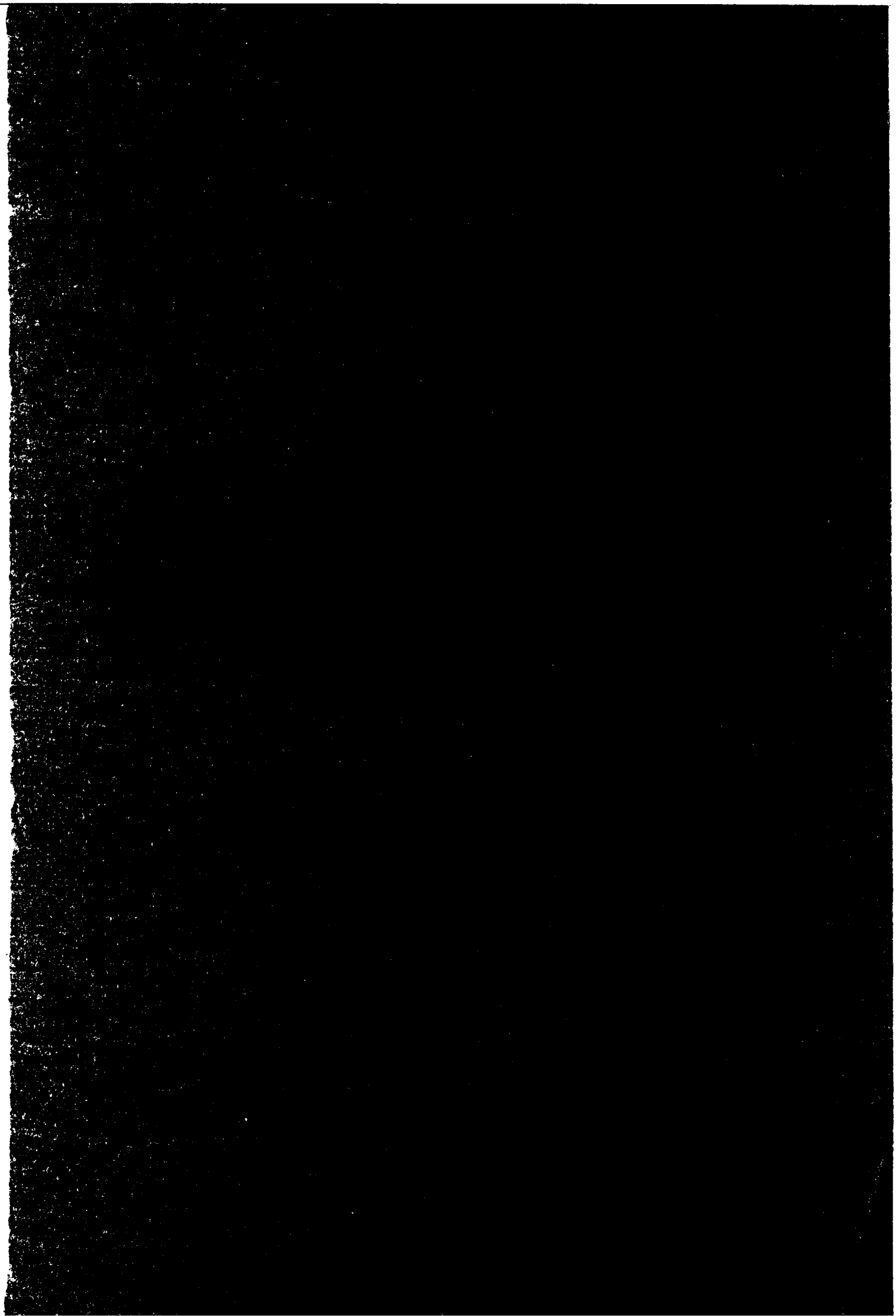

The dynamics of liquefied sand under wave loading with applications to nearshore engineering

March, 2003

Junji MIYAMOTO

Abstract

The purpose of this thesis is to discuss the behaviour of liquefied soil under fluid wave loading and to present a framework for predicting it. The emphasis is placed on investigating propagation of liquefied zone, solidification in liquefied sand, re-liquefaction characteristics, energy dissipation in liquefied sand and instability of the granular system on liquefiable sand bed. Centrifuge wave testing with viscous scaling was used to examine the soil behaviour under fluid wave trains.

The process of wave-induced liquefaction is of a progressive nature. Interestingly, after the progressive liquefaction, a layer of liquefied sand solidifies progressively from the base up while severe fluid-wave loading is imposed over a prolonged period of time. The propagation of the liquefied zone in sand beds and the progressive solidification in liquefied sand under wave loading are theoretically analyzed. It is shown that the solidification permits solid particles to rearrange into a state of remarkably dense compaction due to contractancy. This soil behaviour is accentuated through comparison with consolidation in a quiescent environment following liquefaction. The validity of the predicted results are assessed through comparison with the measured performance of centrifugal wave tank testing on loose sand beds.

The effects of preshearing in beds of sand on their performance at the subsequent wave loading stage were examined based on centrifugal wave tank tests. The experimental results emphasized the importance of distinguishing between low-level preshearing and high-level preshearing. The low-level preshearing, which by definition did not bring about liquefaction under particular wave trains, may increase significantly the liquefaction resistance to subsequent wave loading. The relation between the duration of high-level preshearing and the extent of re-liquefaction at the wave reloading stage were investigated. It was found that in the solidified zone the re-liquefaction resistance increased significantly due to the marked densification that had been brought about by the solidification. The extent of the liquefaction in the wave reloading stages became smaller as the solidification zone had developed larger. An analytical model proposed could reproduce the observed effects of high-level preshearing.

The energy dissipation in a system involving liquefied soil was discussed. The liquefied soil was distinguished into fully destructured liquefied soil and into structured liquefied soil. It was shown that the structured liquefied soil plays a vital role for dissipating a significant amount of wave energy in the entire system under consideration.

Finally, wave-induced liquefaction and flow deformation in soil beds below granular slopes were examined based on centrifuge wave tank tests. The experimental program focuses on the measurements of deformation in sand beds undergoing liquefaction, in addition to pore pressure measurements. The test results showed that the toe of a granular slope started settling upon the occurrence of liquefaction at shallow soil depth in the free field, and that the rate of settlement of the granular slope increased markedly in association with the spread of liquefied zone.

Acknowledgements

The research summarized in this thesis has been carried out at the Department of Civil Engineering, Faculty of Engineering, Kyoto University. I here wish to acknowledge the supervision, guidance, encouragement and assistance received from many people.

I wish to express my sincerest gratitude to my academic supervisor, Professor Hideo Sekiguchi, at the Disaster Prevention Research Institute (DPRI), Kyoto University, for his invaluable guidance, stimulating discussions and continuous encouragement throughout all the stages involved in the studies described in this thesis. Professor Hideo Sekiguchi guided my research from standpoints of not only soil mechanics and coastal engineering but also geology, marine environment and sedimentology. Furthermore, Professor Hideo Sekiguchi spent much time for helping me with writing papers in English, and gave me some opportunities to take part in international conferences.

Grateful acknowledgements are extended to Professor Tetsuro Sakai at the Department of Civil Engineering of Kyoto University and to Professor Fusao Oka at the Department of Civil Engineering of Kyoto University for their thorough review and making valuable comments on the draft of this thesis.

I would like to express my gratitude to Dr. Shinji Sassa, JSPS Research Fellow at DPRI, for his valuable comments and advises. Dr. Shinji Sassa taught me profundity of studies of fluid-soil performance and the attitude to researches. We would often discuss the latest scientific topics at the time of supper.

The author learned much about basics of the centrifuge and the technique of experiments from Mr. Masato Koyama who is the past member of the Waterfront Geotechnics Laboratory.

Finally, I would like to thank my parents for their much support and encouragement.

Table of contents

List of figures

List of tables

List of symbols

a_0 amplitude of vertical displacement of soil surface

D thickness of soil bed before wave loading

D_r relative density

d thickness of soil bed

e void ratio

G shear modulus of soil

g acceleration due to gravity

H fluid depth before wave loading, wave height

h fluid depth

k Darcy coefficient of permeability

L wavelength

M constrained modulus of soil skeleton

N scale factor

n porosity

S settlement of soil surface

T wave period

u_e excess pore pressure

$u_e^{(1)}$ fluctuating component of u_e

$u_e^{(2)}$ residual component of u_e

u_S amplitude of fluid pressure fluctuation at the depth of solidification front

u_0 amplitude of fluid pressure fluctuation at the soil surface

$u_{\xi 0}$ amplitude of fluid pressure fluctuation at the original level of soil surface before wave loading

$\dot{v}$ volumetric strain rate

$\dot{v}^c$ volumetric strain rate due to changes in σ_V'

$\dot{v}^p$ volumetric strain rate due to cyclic shearing

z coordinate taken from the soil surface

z_L location of bottom of liquefied soil in z-coordinate

z_S location of solidification front in z-coordinate

γ' initial submerged unit weight of soil

γ_f unit weight of fluid

κ wave number

ξ wave loading cycle

ρ_1 mass density of fluid

ρ_2 mass density of liquefied soil

σ_v' vertical effective stress

σ_{V0}' initial vertical effective stress

τ wave induced maximum shear stress at a given point of soil depth

χ wave induced cyclic stress ratio (τ/σ_v')

χ_0 wave induced cyclic stress ratio ($\kappa_0 u_0/\gamma'$) at the level of soil surface

ω angular frequency of waves

Z Lagrangian coordinate where reference configuration is at ξ=0

ζ Euler coordinate taken from the initial soil surface

Z_S location of solidification front in Z-coordinate

ζ_S location of solidification front in ζ-coordinate

Chapter 1

Introduction

The response of seabed deposits or sediment particles to storm waves has received increasing attention in nearshore engineering, with particular reference to the stability of coastal-defense systems and to the management of sediment transport. Recently, the emphasis of design for coastal-defense systems has been placed on not only safety of waterfront areas against storm waves but also nourishing a fertile environment (Isobe, 1994).

The soil response to storm waves takes a variety of forms including liquefaction, flow deformation, sediment transport and submarine landslide and so on. These responses may occur in sequence or in a combined fashion, causing serious damage to coastal-defense systems or to lifeline facilities such as pipeline or platforms (Fig. 1.1). For example, investigation of the settlement of concrete blocks covering breakwaters in Miyazaki Port in Japan suggested that liquefaction due to waves played a key role on the sinking of blocks (Gomyo et al. 1996). In order to address the problems of damage of coastal structures, it is important to achieve a full understanding as to how liquefaction develops, how the liquefied soil behaves under severe wave loading and how liquefaction is linked with the damages of coastal structures.

The purpose of this thesis is to discuss the behaviour of liquefied soil under fluid wave loading and to present a framework for predicting it. The emphasis is placed on investigating propagation of liquefied zone, solidification in liquefied sand, re-liquefaction characteristics, energy dissipation in liquefied sand and instability of the granular system on liquefiable sand bed. Centrifuge wave testing with viscous scaling was used to examine the soil behaviour under fluid wave trains.

The organization of this thesis is as follows (Fig. 1.2). Previous studies on wave-induced liquefaction are reviewed in chapter 2. The propagation of the liquefied zone and solidification in liquefied sand are discussed in chapter 3, based on an analytical model. In chapter 4, the progressive liquefaction and solidification in liquefied soil are discussed on the basis of the results from a range of centrifuge tests. Effects of wave loading history on re-liquefaction resistance and extent of re-liquefaction are discussed in chapter 5. Energy dissipation in a system of liquefied soil is discussed in chapter 6. The relation between instabilities of granular slopes on sand beds and wave-induced liquefaction is examined in chapter 7, on the basis of

centrifuge wave tank tests. The principal findings and conclusions obtained in the present thesis are summarized in chapter 8.

References

Isobe, M. (ed.) 1994. *Coastal and marine environments*. Asakura Press. 203. (*in Japanese*)

Gomyo, M. Sakai, K., Takayama, T., Suzuki, K. & Takahashi, S. (1996). Field investigations on wave-dissipating concrete blocks vertical wall breakwater. *Proceedings of the 25th International Conference Coastal Engineering, ASCE,* Chapter 129, 1652-1664.

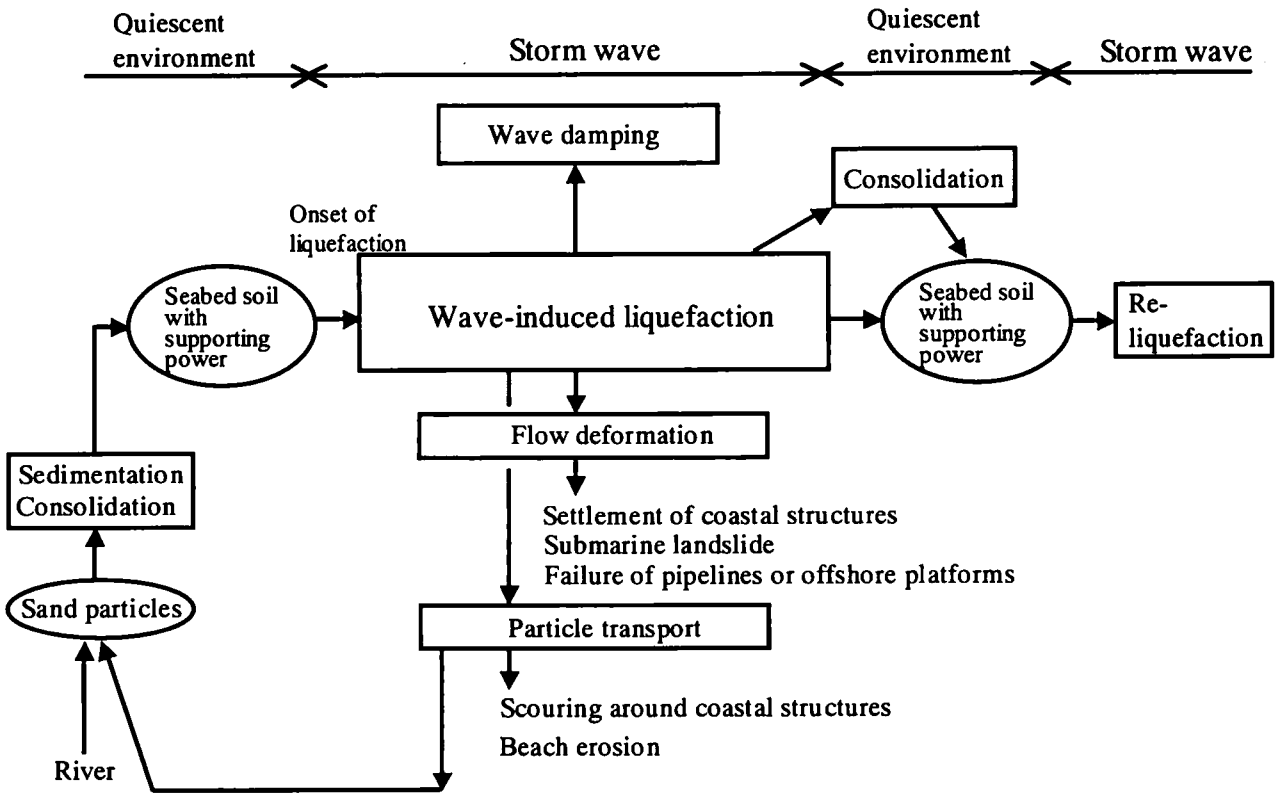

Fig. 1.1 Physical process of geo-hazard in water front area involving wave-induced liquefaction

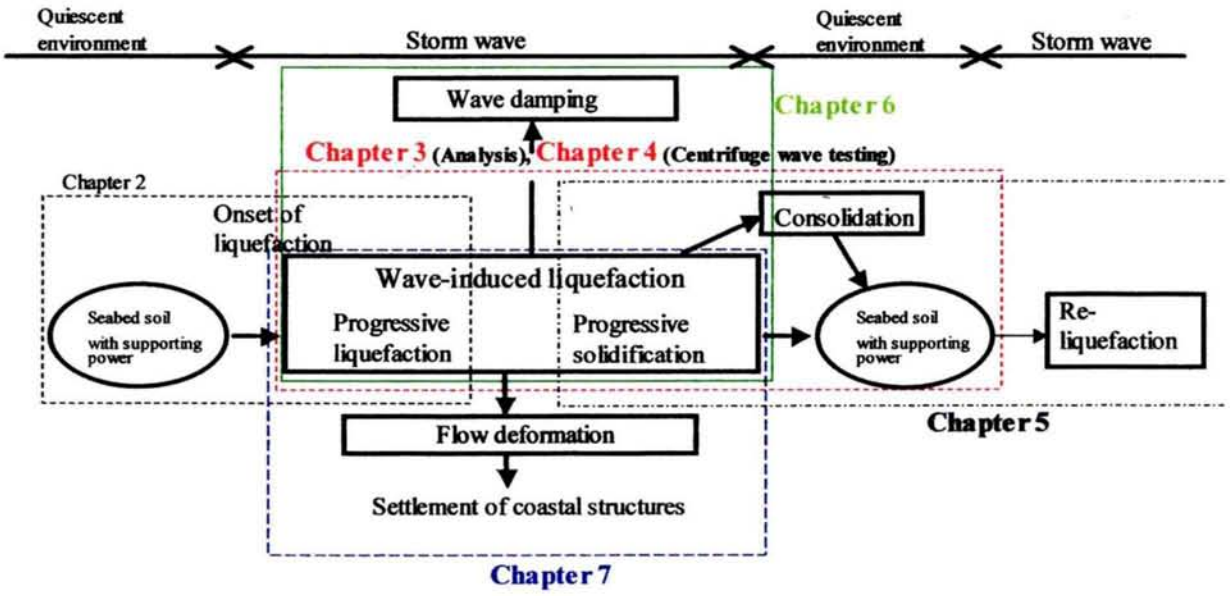

Fig. 1.2 Approaches to investigating dynamics of liquefied sand under sever wave loading

Chapter 2

Review of previous studies

2.1 PREVIOUS STUDIES OF WAVE-INDUCED LIQUEFACTION

Wave-induced liquefaction is generated mainly by two different mechanics (Sumer & Fredsoe, 2002), namely

1. by the upward vertical pressure gradient in the soil during the passage of a wave trough (momentary liquefaction); and
2. by the generation of residual pore pressure due to cyclic plasticity of the soil.

The momentary liquefaction is associated with the phase lag and amplitude decay of oscillatory pore pressures at different depth, relative to the fluid pressure at the soil surface. (Nago & Maeno, 1987; Zen & Yamazaki, 1990; Sakai et al., 1992, Jeng, 1997 among others). In the mechanism of the phase lag, the compressibility of the pore fluid plays an important role. The compressibility of the pore fluid becomes significant when air is presented in the fluid. If the soil is completely saturated, no phase lag in the pore pressure response is anticipated.

Many theoretical or analytical investigations of wave-induced build-up of residual pore pressures have been made, with contractive soil behaviour under wave loading being considered. Cyclic plasticity of the soil was incorporated in conventional one-dimensional analysis procedures (Seed & Rahman, 1978; Finn et al., 1983; Barends & Calle, 1985; Groot et al. 1991). Two-dimensional elasto-plastic analyses were carried out by Siddharthan (1987), Oka et al. (1991, 1994) and Sassa & Sekiguchi (2001). The cyclic plasticity due to wave loading was investigated with particular reference to stress paths induced in soil elements. Madson's (1978) solutions that are based on linear poro-elasticity theory indicate that the stress path induced by progressive wave loading is characterized by the continuous rotation of principal stress axes. The possible importance of the effect of stress axes rotation was initially proposed by Ishihara & Towhata (1983) and Ishihara & Yamazaki (1984). Sassa & Sekiguchi (2001) emphasized the consequence of wave-induced stress axes rotation in soil through their elastoplastic analyses, as will be described in the following section.

There have been relatively few experimental studies that reported the build-up of

residual pore pressures induced by waves. Clukey et al. (1985), Foda & Tzang (1994) and Sumer et al. (1999) observed build-up of residual pore pressures in silt beds. Van Kessel & Kranenburg (1998) examined liquefaction of a sloping cohesive sediment bed. Significant build-up of residual pore pressures in sand beds leading up to liquefaction were observed in Sekiguchi et al. (1995) and Sassa & Sekiguchi (1999). It is noted here that Sekiguchi et al. (1995) and Sassa & Sekiguchi (1999) used centrifuge modelling.

Centrifugal wave experiments were first attempted by Sekiguchi & Phillips (1991) using a drum centrifuge. Related developments, such as the incorporation of viscous scaling and the use of a workable wave absorption system, have broadened the potential of centrifugal wave tank testing for exploring wave-induced instability of sediments (Sekiguchi et al. 1998). What should be noted here is the capability to match the time-scaling of fluid wave propagation (the Froude law) to the time-scaling of consolidation. For details of the theoretical background to centrifuge wave testing, refer to Sassa & Sekiguchi (1999).

2.2 CHARACTERISTICS OF WAVE-INDUCED LIQUEFACTION DUE TO BUILD-UP OF RESIDUAL PORE PRESSURES IN SAND BEDS

Characteristics of wave-induced liquefaction of loosely packed, fresh deposits of sand under regular fluid wave loading were discussed using centrifugal wave-tank testing with viscous scaling (Sassa & Sekiguchi, 1999). They performed progressive-wave tests and standing-wave tests. The principal findings obtained are as follows:

(a) Under a severe wave loading, the loosely packed fresh deposits of sand underwent liquefaction due to the build-up of residual pore pressures.
(b) There exits a critical cyclic stress ratio, χ_{cr}, beyond which liquefaction occurs. The value of χ_{cr} under progressive-wave loading was smaller than that under standing-wave loading.
(c) The process of liquefaction featured a downward advance of the liquefaction front.

The characteristics of build-up of residual pore pressures due to wave loading leading up to liquefaction is schematically shown in Fig. 2.1. Specifically, this figure illustrates a time history of excess pore pressures at a generic point in a sand bed subjected to severe wave loading. The state of liquefaction occurs when the residual pore pressure reaches the level of the initial vertical effective stress, σ_{v0}', of the point, making the effective confining pressure zero.

The experimental results mentioned in (b) suggested that an important factor for the marked difference in liquefaction resistance is the rotation of the principal stress axes that occurs under progressive wave loading. Sassa & Sekiguchi (2001) proposed an elastoplastic constitutive model for describing the behaviour of sand under cyclic loading involving rotations of principal stress axes. A plane-strain finite element program for predicting the soil behaviour under progressive wave or standing-wave loading was developed with the proposed constitutive model being incorporated into a coupled stress-flow analysis procedure (Sassa & Sekiguchi, 2001). The finite-element analysis performed could predict accurately the onset of liquefaction at shallow soil depth of sand beds under severe wave conditions.

The progressive nature of liquefaction mentioned in (c) above has profound implications in wave-soil interaction. However, it is not easy to track the progressive nature of liquefaction with ordinary finite-element techniques in solid mechanics. The principal difficulty appears to arise from the lack of pertinent constitutive modeling for the completely liquefied state of soil with zero effective stress. Thus rational framework to predict the behaviour of liquefied soil under wave loading needs to be developed.

2.3 REPORTS ON GEO-HAZARDS IN WATERFRONTS ASSOCIATED WITH STORM WAVES

This section reviews several case histories which have been reported on geo-hazards in waterfronts associated with storm waves.

Breakwaters in a port of Awashima Island (Niigata pref. Japan) underwent significant settlements when storm waves (significant wave height $H_{1/3}$=3.4m, wave period $T_{1/3}$ =7s) struck them in March 1974 (Saito et al. 1976; Nakamura & Okusa, 1988). Tanaka (1993) pointed out that the observed extent and form of the damage could not be reproduced using conventional circular slip analysis and suggested the occurrence of liquefaction in foundation soil due to severe wave loading.

Three offshore platforms in the Mississippi River delta were displaced and damaged by Hurricane Camille, which struck the U. S. Gulf of Mexico coastline in August 1969. Surveys and analyses indicated that the foundation movements were induced by 20-m-high, hurricane-generated waves (Bea et al., 1983).

Prior et al. (1989) installed pore pressure transducers in seabed soil in the Hwang Ho Delta in China for measuring pore pressure changes in the sediments during storms. Three storms struck there during the period of measurements, and caused submarine landslides. The pore pressure transducers sank in the course of the storm loading

suggesting the occurrence of liquefaction in the sediments.

Gomyo et al. (1996) performed field investigations into the damage to breakwaters in Miyazaki Port, Japan from 1988 to 1990, during which several typhoons hit that area. It was found that long-term, gradual settlement of concrete blocks covering breakwaters occurred associated with the sinking of the blocks into the foundation soil. As probable causes of the damage, liquefaction due to wave loading as well as scouring around the toe of the slopes consisting of the blocks were referred to.

Sections of detached breakwaters on the Niigata Coast of Japan settled by more than 10m due to wave attack over a period of several stormy seasons. Based on extensive field surveys, Nishida et al. (1985) found that a large number of blocks had sunk into the foundation soil. As possible mechanism of this damage, wave-induced liquefaction and sediment transport through the blocks were pointed out.

References

Barends, F. B. J. & Calle, E. O. F. (1985). A method to evaluate the geotechnical stability of off-shore structure founded on a loosely packed seabed sand in a wave –loading environment, *Proc. 4th BOSS, Delft*, 643-652.

Bea, R. G, Wright, S. G., Sicar, P. & Niedoroda, A. W. (1983). Wave-induced slides in South Pass Block 70, Mississippi delta, *J. Geotech. Engng Div., ASCE* 109, 619-644.

Clukey, E. C., Kulhawy, F. H., Liu, P. L.-F. & Tate, G. B. (1985). The impact of wave loads and pore-water pressure generation on initiation of sediment transport, *Geo-Marine Lett.* **5**, 177-183.

Finn, W. D. L., Siddharthan, R. & Martin, G. R. (1983). Response of seafloor to ocean waves. *J. Geotech. Engng Div., ASCE* **109**, No. 4, 556-572.

Foda, M. A. & Tzang, S. –Y. (1994). Resonant fluidization of silty soil by water waves. *J. Geophys. Res.* **99**, 463-475.

Gomyo, M. Sakai, K., Takayama, T., Suzuki, K. & Takahashi, S. (1996). Field investigations on wave-dissipating concrete blocks vertical wall breakwater.

Proceedings of the 25th International Conference Coastal Engineering, ASCE, Chapter 129, 1652-1664.

Groot, M. B. de, Lingenberg, J. & Meijers, P. (1991). Liquefaction of sand used for soil improvement in breakwater foundations. *Proc. Int. Symp. Geo-coast'91, Yokohama,* 555-560.

Ishihara, K. & Towhata, I. (1983). Sand response to cyclic rotation of principal stress directions as induced by wave loads. *Soils & Foundations*, **23**, No. 4, 11-26.

Ishihara, K. & Yamazaki, A. (1984). Analysis of wave-induced liquefaction in seabed deposits of sand. *Soils & Foundations*, **24**, No. 3, 85-100.

Jeng, D.-S. (1997). *Wave-induced seabed response in front of a breakwater*. PhD thesis, The University of Western Australia.

Madson, O. S. (1978). Wave-induced pore pressures and effective stresses in a porous bed. *Geotechnique,* **28**, No. 4, 377-393.

Nago, H. & Maeno, S. (1987). Pore pressure and effective stress in a highly saturated sand bed under water pressure variation on its surface, *J. Natural Disaster Sci.* **9**, No. 1, 23-35.

Nakamura, T. & Okusa, S. (1988). Submarine landslides around the Japanese Islands, *Coastal Oceanography, Coastal Oceanography Committee, The Oceanographical Society of Japan*, **26**, No. 1, 55-63. (*in Japanese*)

Nishida, H., Yamaguchi, Y., Kondo, T. & Shimizu, K., 1985. A study on sinking of blocks of detached breakwaters using elastic wave exploration. *Proceedings of Coastal Engineering, JSCE* 32, 365-369. (*in Japanese*)

Oka, F., Yashima, A., Shibata, T. & Kato, M. (1991). A finite element analysis of liquefaction of seabed due to wave action. *Proc. Int. Symp. Geo-Coast '91, Yokohama*, 3-6.

Oka, F., Yashima, A., Shibata, T., Kato, M. & Uzuoka, R. (1994). FEM-FDM coupled

liquefaction analysis of a porous soil using an elastoplastic model. *Appl. Sci. Res.* **52**, 209-245.

Prior, D. B., Suhayda, J. N., Lu, N. –Z., Bornhold, B. D., Keller, G. H., Wiseman, W. J., Wright, L. D. & Yang, Z. –S. (1989). Storm wave reactivation of a submarine landslide, *Nature*, **341**, No. 7, 47-50.

Saito, S., Hashimoto, H. & Tanioka, S. (1976). A study on the damages of Ports at Awashima Island, *Proceedings of Coastal Engineering, JSCE,* **23**, 262-267 (*in Japanese*).

Sakai, T., Hatanaka, K. & Mase, H. (1992). Wave-induced effective stress in seabed and its momentary liquefaction. *J. Waterway, Port, Coast, Ocean Engng Div, ASCE*, **118**, No. 2, 202-206.

Sassa, S. & Sekiguchi, H. (1999). Wave-induced liquefaction of beds of sand in a centrifuge. *Geotechnique,* **49**, No.5, 621-638.

Sassa, S. & Sekiguchi, H. (2001). Analysis of wave-induced liquefaction of sand beds. *Geotechnique,* **51**, No.2, 115-126.

Seed, H. B. & Rahman, M. S. (1978). Wave-induced pore pressure in relation to ocean floor stability of cohesionless soils. *Marine Geotechnology*, **3**, No. 2, 123-150.

Sekiguchi, H. & Phillips, R. (1991). Generation of water waves in a drum centrifuge. *Proc. Int. Conf. Centrifuge 91*, Boulder, 343-350.

Sekiguchi, H., Kita, K. & Okamoto, O. (1995). Response of poro-elastoplastic beds to standing waves. *Soils & Foundations*, **35**, No. 3, 31-42.

Sekiguchi, H., Kita, K., Sassa, S. & Shimamura, T. (1998). Generation of progressive fluid waves in a geo-centrifuge. *Geotechnical Testing Journal*, **21**, No. 2, 95-101.

Siddharthan, R. (1987). Wave-induced displacements in seafloor sands, *Int. J. Numer. Anal. Methods Geomech.* **11**, 155-170.

Sumer, B. M., Fredsoe, J., Christensen, S. & Lind, M. T. (1999). Sinking/floatation of pipelines and other objects in liquefied soil under waves. *Coastal Engineering*, **38**, 53-90.

Sumer, B. M. & Fredsoe, J. (2002). *The mechanics of scour in the marine environment*, World Scientific, 446.

Tanaka, N. (1993). Littoral drift and scouring of sea bottom due to waves, *Tsuchi-to-Kiso, The Japanese Society of Soil Mechanics and Foundation Engineering*, **41**, No.3, Ser. No. 422, 31-36. (*in Japanese*)

Van Kessel, T. & Kranenburg, C. (1998). Wave-induced liquefaction and flow of subaqueous mud layers. *Coast Engng* **34**, 109-127.

Zen, K. & Yamazaki, H. (1990). Oscillatory pore pressure and liquefaction in seabed induced by ocean waves. *Soils & Foundations*, **30**, No. 4. 147-161

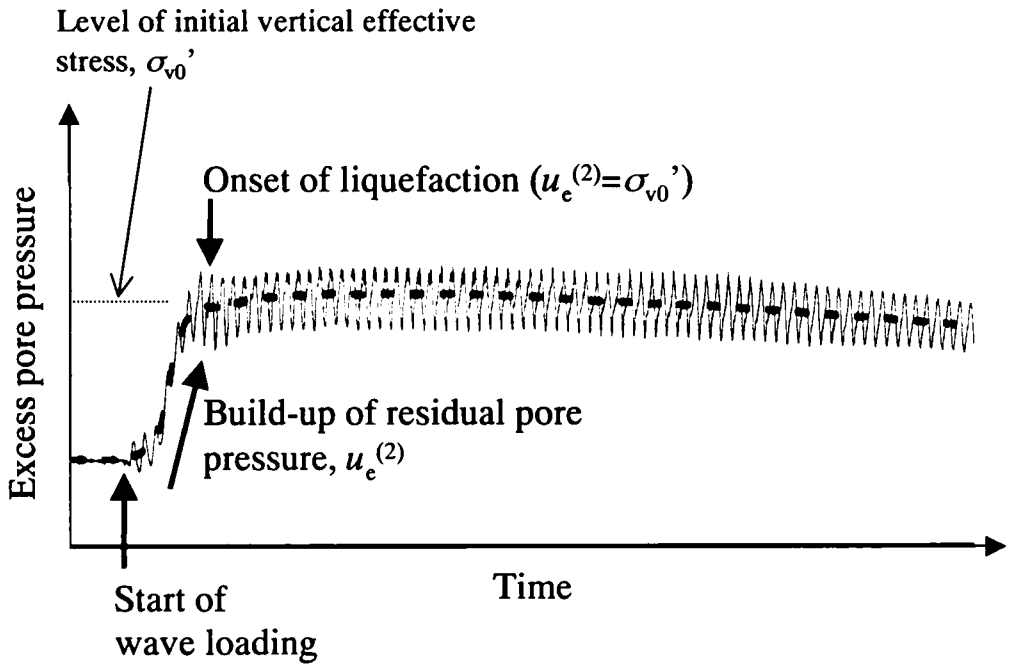

Fig. 2.1 Sketch showing the development of excess pore pressure at a generic point in a sand bed due to severe wave loading

Chapter 3

Analysis of progressive liquefaction and solidification in sand beds

3.1 INTRODUCTION

The behaviour of cohesionless soil undergoing a state of liquefaction is of profound interest to engineers in association with assessing the consequence of liquefaction. The primary consequence is concerned with the loss of the supporting power of seabed soil causing stability problems for offshore pipelines (Sumer et al., 1999; Sumer & Fredsøe, 2002) and composite breakwaters (Gomyo et al., 1995). This increased interest in liquefaction phenomena calls for a full understanding of not only the process of occurrence of liquefaction but also the behaviour of liquefied soil under fluid-wave loading.

The process of wave-induced liquefaction in loosely packed fresh deposits of sand was investigated using centrifugal wave testing with viscous scaling (Sassa & Sekiguchi, 1999). It was found that the loosely packed deposits of sand subjected to severe wave loading underwent liquefaction due to the build-up of the residual pore pressures. The process of wave-induced liquefaction is of a progressive nature: liquefaction is induced at uppermost layer of a sand deposit and then the liquefaction front advances downward.

The soil behaviour up to the onset of liquefaction at shallow soil depth could be predicted by the finite-element analysis combined with a constitutive model of cyclic plasticity (Sassa & Sekiguchi, 2001). The propagation of the liquefied zones after the occurrence of liquefaction at shallow soil depth was theoretically analyzed as a moving boundary problem (Sassa et al. 2001). In this model, the completely liquefied state of sand is modeled as an inviscid fluid. This assumption enabled the model to predict the marked fluidity of the liquefied soil under wave loading. However, if we suppose that the liquefied sand continues to be subjected to severe wave loading (Fig. 3.1), the following question may arise: 'Does the soil bed continues to undergo the state of liquefaction in the course of prolonged wave loading?'

Recent centrifuge wave tank tests have shown that when the bed of liquefied sand continues to be subjected to the severe wave loading, the residual pore pressure in the liquefied soil dissipates (Fig. 3.1), which is called the *solidification*, and then the

solidification front advances upward to the soil surface (Miyamoto et al. 2002). Interestingly, the soil region that experienced the solidification underwent more marked densification than the densification which would be brought about in the process of consolidation under a quiescent environment following liquefaction.

The nature of the liquefied sand under cyclic loading has received considerable attention in relation to the densification of the sand from the researchers concerning seismic liquefaction. Nagase & Ishihara (1988) and Ishihara (1993) performed simple shear tests in multi-directional condition, and showed that the volumetric strain during the reconsolidation following liquefaction depended on the magnitude of maximum shear strain induced during cyclic loading after the occurrence of liquefaction. In order to model the effect of cyclic loading applied to the liquefied sand on the volumetric strain during the subsequent reconsolidation, Yoshida et al. (1994) assumed that the liquefied sand has a small stiffness whose degree depends on the magnitude and the number of cyclic loading applied to the liquefied sand.

This chapter proposes an analytical model for predicting the behaviour of liquefied soil under fluid-wave loading, with the emphasis on the progressive liquefaction and solidification in liquefied sand.

The organization of this chapter is as follows: The theoretical framework will be described first, and then the procedure for the solution of the entire system will be described. The predicted features of the behaviour of liquefied soil will then be discussed. Here, the description of the predicted features consists of two parts. The first part focuses on the downward propagation of the liquefaction front. The second part focuses on the progressive solidification in liquefied sand during wave loading as well as the densification of soil bed due to the solidification. This will be followed by a discussion of an expression for the relation between the velocity of the solidification front and the changes in density of liquefied soil due to the solidification.

3.2 THEORETICAL FRAMEWORK OF PROGRESSIVE LIQUEFACTION AND SOLIDIFICATION IN LIQUEFIED SAND

3.2.1 Problem definition

Consider a situation where sinusoidal fluid wave trains propagate over a level bed of cohesionless soil. The passage of fluid wave trains induces the oscillation in the fluid

pressure acting on the soil bed. The wave pressure oscillation causes excess pore pressure u_e at a generic point in the soil bed to develop. Note that the excess pore pressure u_e may be divided into two components: the oscillatory component designated as $u_e^{(1)}$ and the residual component designated as $u_e^{(2)}$. The temporal average, $\bar{u}_e^{(1)}$, over any wave cycle is zero by definition. The residual component stems from the contractive behaviour of the sand due to cyclic loading. When the residual pore pressure $u_e^{(2)}$ reaches the level of the initial vertical effective stress σ_{v0}' at the soil horizon, the state of liquefaction occurs. The residual pore pressure at a generic point in the liquefied soil may be expressed as

$$u_e^{(2)} = \sigma_{v0}'. \tag{3.1}$$

After the onset of liquefaction, the liquefaction front advances downwards, and then stops at a certain soil depth or the rigid base. If the wave loading continues, solidification starts at the bottom of the liquefied soil layer.

Suppose that at time t the bottom of the liquefied soil has been at $z=z_L$ (Fig. 3.2). A thin layer where the liquefied soil starts solidifying is introduced at the bottom of the liquefied sand ($z_L<z<z_S$). The thin soil layer where solidification starts is called a *transition layer*. Note that the transition layer is a part of the liquefied soil layer, and the liquefied soil in the transition layer is assumed to have a marginally discernible stiffness yet the effective stress is zero by definition. The liquefied soil in the transition layer is called *structured liquefied soil*.

The liquefied soil overlying the transition layer is assumed to have zero stiffness and called *fully destructured liquefied soil*. The boundary between the fully destructured liquefied soil and the structured liquefied soil ($z=z_S$) is called a *solidification front*. The solidification front advances upward with the transition layer being accompanied in the course of wave loading. Accordingly, the sub-liquefied soil layer increases in thickness with time.

The entire system under consideration now consists of exterior fluid ($0<z<h$), fully destructured liquefied soil ($z_S<z<0$), structured liquefied soil ($z_L<z<z_S$) and sub-liquefied soil ($-d<z<z_L$) (Fig. 3.3).

3.2.2 Formulation for the entire system

The fully destructured liquefied soil is modelled as an inviscid fluid. The exterior

fluid layer and the fully destructured liquefied soil layer compose a two-layer fluid region ($z_S<0<h$). A classical theory of wave propagation in a two-layer fluid (Lamb, 1932) is applied to the two-layer fluid region (Sassa et al. 2001). From the two-layer fluid theory, several formulations are made: the dispersion relationship for the two-layer fluid, $\tilde{u}_0$ the fluid pressure oscillation at the soil surface ($z=0$), $\tilde{u}_s$ the fluid pressure oscillation at the depth of the solidification front ($z=z_S$), a_0 the amplitude of vertical movements of the soil surface, and $u_e^{(1)}$ the oscillatory pore pressure at a generic point in the fully destructured liquefied soil ($z_S<z<0$). Since in the present study the settlement of the soil surface S is considered, the four physical quantities $\tilde{u}_0$, $\tilde{u}_s$, $u_c^{(1)}$ and a_0 can be formulated as functions of $\tilde{u}_{\zeta 0}$ the fluid pressure oscillation at the original level of the soil surface ($z=S$). The amplitudes of $\tilde{u}_0$, $\tilde{u}_s$ and $u_e^{(1)}$, and a_0 are expressed in equations (3.29), (3.31), (3.30) and (3.26) respectively in Appendix 1 of this chapter. In the present study, the amplitude $u_{\zeta 0}$ is assumed to be a constant value.

The structured liquefied soil is modelled as an elastoplastic material, which has zero effective stress and a marginally discernible stiffness. The sub-liquefied soil is modelled as an elastoplastic material. The volumetric strain rate $\dot{v}$ in the elastoplastic soil under cyclic loading may consist of a component $\dot{v}^C$ depending on the vertical effective stress rate $\dot{\sigma}_v'$ and a component $\dot{v}^P$ due to the cyclic shearing. Namely,

$$\dot{v} = \dot{v}^c + \dot{v}^p \tag{3.2}$$

The component $\dot{v}^P$ may reflect the contractive nature of the loosely packed sand subjected to cyclic shearing. The component $\dot{v}^c$ may be related to the vertical effective stress rate $\dot{\sigma}_v'$ with constrained modulus of the soil skeleton, M, as follows:

$$\dot{v}^c = \frac{1}{M}\dot{\sigma}_v' \tag{3.3}$$

We will now formulate a storage equation for describing the build-up or dissipation of the residual pore pressures, $u_e^{(2)}$, in the elastoplastic soil. The storage equation used in Sassa et al. (2001) had been derived on the basis of an infinitesimal deformation theory (Sassa & Sekiguchi, 1999). However, the solidification in liquefied sand may be accompanied by significant densification. In the present study, a storage equation considering finite deformation is derived.

Consider the soil body consolidating one-dimensionally in the course of wave loading (Fig. 3.4). The coordinate ζ represents locations of soil elements from the initial level of the soil surface. Note that ζ is related to z with settlement of the soil surface, S, as follows: $\zeta=z-S$. Hence, the bottom of the soil bed in ζ coordinate is $-D=-d-S$ and the mean level of the exterior fluid $H=h-S$. At time $t=0$ wave loafing starts. Each element in the soil bed is labelled throughout its subsequent motion by its initial location. For the labelling of the elements, Z-coordinate is introduced. Now, an element in the soil body lying $\zeta=Z$ at $t=0$ is considered. The boundary of the soil element always encapsulates the same soil particles throughout its subsequent motion. Suppose that, at time t the solidification front is located at $\zeta=\zeta_S$, the soil surface is located at $\zeta=-S$ and the soil element at $\zeta(Z, t)$. At this time, the soil element has effective stress σ_v' and excess pore pressure u_e. In the following description, the time average of a wave cycle is considered. Therefore, water level is constant $\zeta=H$ and the fluctuating component of excess pore pressure $u_e^{(1)}$ becomes zero.

The soil solids and the pore fluid are assumed to be incompressible. Conservation of mass for solid phase and conservation for fluid into and out of the soil lead to the equations

$$\dot{v} = -\frac{\dot{e}}{1+e} = \frac{\partial q_\zeta}{\partial \zeta} \tag{3.4}$$

where a superimposed dot represents material time derivative, $\dot{v}$ is the volumetric strain rate, e is the void ratio and q_ζ is the relative discharge velocity of the fluid (Carter et al. 1979).

The fluid flow through the soil may be governed by Darcy's law.

$$q_\zeta = -k\frac{\partial h}{\partial \zeta} = -\frac{k}{\gamma_f}\frac{\partial u_e^{(2)}}{\partial \zeta} \tag{3.5}$$

where k is the Darcy coefficient of permeability, γ_f is the unit weight of the fluid and h is the total head. Note that $h = H+D+u_e^{(2)}/\gamma_f$.

From equations (3.2) and (3.3), constitutive relationship of the soil is assumed as follows:

$$\dot{v} = \frac{1}{M}\dot{\sigma}_v' + \dot{v}^p \tag{3.6}$$

Combination of equations (3.4)-(3.6) yields,

$$\dot{\sigma}_v' = -\frac{M}{\gamma_f}\frac{\partial}{\partial \zeta}\left(k\frac{\partial u_e^{(2)}}{\partial \zeta}\right) - M\dot{v}^p \tag{3.7}$$

The vertical effective stress rate $\dot{\sigma}_v'$ and the material time derivative of the residual pore pressure, $\dot{u}_e^{(2)}$, should be related as follows:

$$\dot{\sigma}_v' + \dot{u}_e^{(2)} = 0 \tag{3.8}$$

For detail of the derivation of equation (3.8), refer to Appendix 2 of this chapter. From equation (3.8), equation (3.7) is expressed as

$$\dot{u}_e^{(2)} = \frac{M}{\gamma_f}\frac{\partial}{\partial \zeta}\left(k\frac{\partial u_e^{(2)}}{\partial \zeta}\right) + M\dot{v}^p \tag{3.9}$$

Equation (3.9) is expressed in Z coordinate as follows, noting that $\dot{u}_e^{(2)}(\zeta) = \partial/\partial t\{u_e^{(2)}(\mathrm{Z})\}$:

$$\frac{\partial u_e^{(2)}}{\partial t} = \frac{M}{\gamma_f}\frac{\partial}{\partial \mathrm{Z}}\left(k\frac{\partial u_e^{(2)}}{\partial \mathrm{Z}}\frac{\partial \mathrm{Z}}{\partial \zeta}\right)\frac{\partial \mathrm{Z}}{\partial \zeta} + M\frac{\partial v^p}{\partial t} \quad for\ -D<Z<Z_S \tag{3.10}$$

where Z_S the location of the solidification front in Z-coordinate. The soil element in Z-coordinate always embraces the same mass of sand grains. Therefore,

$$\frac{\partial \mathrm{Z}}{\partial \zeta} = \frac{1-n}{1-n_0} \tag{3.11}$$

where n is the current porosity and n_0 is the initial porosity.

With wave loading cycle ξ ($=\omega t/2\pi$) and non-dimensional parameter $\kappa_0 Z$, where κ_0 is the initial wave number, the equation (3.10) may be rewritten as

$$\frac{\partial u_e^{(2)}}{\partial \xi} = 2\pi\frac{M}{\gamma_f \omega}\kappa_0^2\frac{\partial}{\partial(\kappa_0 \mathrm{Z})}\left[k\frac{\partial u_e^{(2)}}{\partial(\kappa_0 \mathrm{Z})}\cdot\frac{1-n}{1-n_0}\right]\cdot\frac{1-n}{1-n_0} + M\frac{\partial v^p}{\partial \xi} \quad for\ -D<Z<Z_S \tag{3.12}$$

The above-equation is the basic equation that governs the process of the build-up or dissipation of the residual pore pressure in the elastoplastic soil layer. The second term on the right-hand side of equation (3.12), $M\partial v^p/\partial\xi$, corresponds to the 'source term' due to the cyclic plasticity of the soil. Detail of the constitutive relationship of this term is described later. In the derivation of equation (3.12), the variations in constrained modulus M and permeability k have been taken into account. The permeability k may be a function of the void ratio e. The following relation (Taylor, 1948) is used in the present study:

$$k = C\frac{\gamma_f}{\mu}\cdot\frac{e^3}{1+e} \tag{3.13}$$

where C is a parameter, which depends on the grain size and the arrangement of sand grains and μ is the dynamic viscosity of the pore fluid. The constrained modulus, M, may increase with increasing vertical effective stress σ_v'. The relation between M and σ_v' is described later in detail.

The base of the soil bed is assumed to be rigid impermeable. Therefore, no fluid flow occurs on the base of the soil bed. Namely,

$$\frac{\partial u_e^{(2)}}{\partial Z} = 0 \qquad on\ Z = -D \tag{3.14}$$

From equation (3.1), the boundary condition on the solidification front Z_S is that

$$u_e^{(2)} = \sigma_{v0}' \qquad on\ Z = Z_S \tag{3.15}$$

Note that the initial vertical effective stress at the soil horizon Z is obtained from $\sigma_{v0}'=-\gamma' Z$, where γ' is the submerged unit weight of the soil.

3.2.3 Remarks on constitutive relationship

A constitutive relationship of the source term of the storage equation is assumed as follows (Sassa et al. 2001):

$$\frac{\partial v^p}{\partial \xi} = \beta\left[v_\infty^p(\chi) - v^p\right] \tag{3.16}$$

where β is a material parameter, v_∞^p stands for the amount of volumetric strain due to cyclic shearing that is attained ultimately with ξ approaching infinity and χ is the cyclic stress ratio, which is defined as

$$\chi = \frac{\tau}{\sigma_{vi}} \tag{3.17}$$

Here, τ is the maximum cyclic shear stress at a given horizon of soil z in the elastoplastic soil and σ_{vi}' is the vertical effective stress. The relation between v_∞^p and χ is defined so that the ultimate volumetric strain v_∞^p may not exceed a critical value v_{max}. That is to say,

$$v_\infty^p(\chi) = v_{max} \cdot \left[1 - \exp\{-(A\chi)^B\}\right] \quad (B>1) \tag{3.18}$$

where A and B are material parameters. The critical value v_{max} is defined, in terms of the initial void ratio e_0 and the minimum void ratio e_{min}, as follows:

$$v_{max} = \frac{e_0 - e_{min}}{1 + e_0} \tag{3.19}$$

The critical value v_{max} represents the maximum volumetric strain with reference to the initial state of a soil element before wave loading.

Next discussion is on the constrained modulus of the soil skeleton, M. The proposed relation between the constrained modulus of soil skeleton M and the vertical effective stress σ_v' is shown in Fig. 3.5. Here, point A represents the initial state of a soil element which has initial vertical effective stress σ_{v0}'. After the start of wave loading, the residual pore pressure builds up and the vertical effective stress, σ_v', decreases. This allows M to decrease in a manner indicated as line ABD. On the linear line AD, when σ_v' reduces to zero, the constrained modulus M also reduces to zero. When the constrained modulus M approaches zero, the volumetric strain rate based on equation (3.3) becomes infinite. Therefore, it is assumed that if the vertical effective stress σ_v' is smaller than a reference stress σ_{vR}', the constrained modulus M is a constant. If the residual pore pressure in the soil element starts dissipating before or just when the

effective stress reaches point C, the constrained modulus increases on the curve CBA with the increase in vertical effective stress.

Point C represents the constrained modulus M of the structured liquefied soil and means that the soil element under consideration is in the transition layer. If the transition layer advances downwards accompanying the liquefaction front, the soil element under consideration is located above the transition layer. This means that the soil element becomes fully destructured liquefied soil and loses the stiffness completely (Point D). Suppose that the soil element is located in the transition layer again. The soil element becomes structured liquefied soil again and recovers a marginally discernible stiffness (Point E). When the residual pore pressure in the soil element dissipates, the effective stress increases. This allows M to be changed in a manner indicated as curve EFG.

It is assumed that the constrained modulus M in the process E-F-G is smaller than that in the process C-B-A. This assumption stemmed from the experimental results from Lee & Albasisa (1974) and Yoshimi et al. (1975), where it was observed that the liquefied sand underwent compression more significantly during the subsequent consolidation, than the sand where liquefaction had not occurred underwent compression.

3.3 SOLUTION PROCEDURE

If the location of the solidification front after ξ cycles of wave loading is identified, the distribution of residual pore pressure in the elastoplastic soil layer is obtained by solving equation (3.12) under the boundary conditions. We adopted an implicit finite-difference scheme for numerically solving equation (3.12). In the implicit finite-difference scheme, using the constrained modulus M, permeability coefficient k and porosity n at ξ cycles, the residual pore pressures at $\xi+\Delta\xi$ cycles are obtained. The finite-difference representation of equation (3.12) used is given in Appendix 3 of this chapter. Here, $\Delta\xi$ is the increment of wave loading cycles.

With reference to Fig. 3.6, the elastoplastic soil layer in Z-coordinate ($-D<Z<Z_S$) is divided into $n+N$ increments of equal size ΔZ such that $(N+n)\Delta Z=-D-Z_S$. Here, $-n\Delta Z$ is the thickness of the transition layer and $-N\Delta Z$ is that of the sub-liquefied soil layer. Since the transition layer is assumed to be a thin layer, $-n\Delta Z \ll D$. The location of a soil element in the elastoplastic soil is represented by $Z_i=Z_S+i\Delta Z$ for $i=0, n+N$. Therefore, the location of the bottom of the liquefied soil Z_L is represented by Z_n ($=Z_S+n\Delta Z$). Similarly, the location of the bottom of the soil bed, $-D$, is represented by Z_{n+N}.

The flow chart for identification of Z_S and Z_L at $\xi+\Delta\xi$ cycles is shown in Fig. 3.7. Let residual pore pressure $u_e^{(2)}$ at soil depth Z_i at ξ cycles be denoted by $U_i(\xi)$. Note that the residual pore pressures in the transition layer $U_0(\xi)\sim U_n(\xi)$ are equal to the initial vertical effective stress σ_{v0}'. From equation (3.15), the residual pore pressure at the solidification front at $\xi+\Delta\xi$ cycles, $U_0(\xi+\Delta\xi)$, is also equal to σ_{v0}'. Therefore, the unknowns are a total of $N+n$ residual pore pressures, $U_1(\xi+\Delta\xi)\sim U_{n+N}(\xi+\Delta\xi)$. The source term $M\partial v^p/\partial\xi\,\Delta\xi$ of each soil element in the sub-liquefied soil is evaluated from equations (3.16)-(3.19). In equation (3.17), the maximum cyclic shear stress, τ, is obtained from equation (3.33) in Appendix 1 and the vertical effective stress σ_{vi}' is defined as $\sigma_{vi}'=-\gamma'(Z-Z_S)$. The finite-difference representation for equation (3.12) are solved using a Gaussian elimination method. If the calculated values of $U_{n+1}(\xi+\Delta\xi)\sim U_{n+m}(\xi+\Delta\xi)$ $(1\le m\le N)$ are larger than σ_{v0}', then the liquefied zone is judged to have extended to $Z_L(\xi)+m\Delta Z$. The transition layer accompanies the advance of Z_L. Namely, $Z_S(\xi+\Delta\xi)=Z_L(\xi+\Delta\xi)-n\Delta Z$. If the calculated value of $U_{n+1}(\xi+\Delta\xi)$ does not reach σ_{v0}', the residual pore pressures in the transition layer dissipate according to equation (3.12). The solidification front Zs advances upward with the transition layer being accompanied. Namely, $Z_S(\xi+\Delta\xi)=Z_S(\xi)-n\Delta Z$. Accordingly the liquefied zone reduces in thickness such that $Z_L(\xi+\Delta\xi)=Z_L(\xi)-n\Delta Z$.

With identified the value of Z_S or Z_L, updating are made for the void ratio e (porosity n), the constrained modulus M and the permeability coefficient k and so on for each soil element.

3.4 FEATURES OF PREDICTED PERFORMANCE: PROGRESSIVE LIQUEFACTION

This section describes predicted results using the proposed model, focusing on the progressive liquefaction. The wave conditions were set as follows: gravity acceleration 30g (i. e. N=30); fluid depth, H=80mm; wave frequency, f=8Hz; $u_{\zeta 0}$=3.0kPa. The soil parameters used are listed in Table 3.1. Note that the submerged unit weight of the soil, γ', is 30 times that in 1-g condition. Viscous scaling used, keeping the permeability coefficient, k, the same as under 1-g condition (see equation (3.13)). The wave and soil conditions correspond to those of a centrifuge wave test on a loose deposit of Silica sand #7- Batch A (test WJ12) as described later in chapter 4.

In the calculations we used time increments Δt equal to T/40 and depth increments ΔZ equal to -D/200. The number of elements consisting of the transition layer, n, was set as

1.

3.4.1 Propagation of liquefaction front

The predicted time histories of the wave-induced pore pressure fluctuations at different spatial points are shown in Fig. 3.8, together with the input wave forms, $\tilde{u}_{\zeta 0}$. It can be clearly seen that, in the course of continued wave loading, the liquefaction front advanced downwards. In accordance with the advance of the liquefaction front, the oscillatory pore pressure at each soil depth exhibits a significant amplification, particularly at deeper soil depth (ζ=-76*mm*). A close observation of the wave form at ζ=-76*mm* shows that the residual pore pressure started dissipating from t=4000 ms or so. This is an indication of the occurrence of solidification at this soil depth.

The predicted process of the downward advance of the liquefaction front can be more clearly seen in Fig. 3.9. The locations of the liquefaction front during wave loading are denoted by LLF in this figure. The shallow soil depths (ζ>-13*mm*) have undergone liquefaction at 1.6 cycles of wave loading. In the course of wave loading, the liquefaction front advances further downwards, bringing essentially all depth of soil into the state of complete liquefaction at 7.4 cycles of wave loading.

The predicted progress of the liquefaction front is shown in Fig. 3.10. In this figure the associated temporal changes in wave number, κ, are also shown. The liquefaction front starts moving downwards at t=740 ms and advances rapidly with time, terminating at ζ=-78*mm* when t=1650ms. During the wave loading the wave number, κ, decreases slightly from 0.0121mm^{-1} to 0.0102mm^{-1}.

3.4.2 Enhanced vertical vibration of liquefied soil

An idea of how the sand bed deforms in the course of the progressive liquefaction may be obtained from Fig. 3.11. Here the predicted vertical displacement of the soil surface is plotted. No vertical movement occurs before liquefaction takes place. However, upon the onset of liquefaction at shallow soil depth, the soil surface starts vibrating. The amplitude of the vibratory soil motion increases markedly with time, in association with the downward propagation of the liquefaction front. At the end of progressive liquefaction, the amplitude of the vibratory motion reaches a maximum value 6.3 *mm*. Note that this soil movement corresponds to a shear strain amplitude equal to $2a_0/L$=2.4%, where L is the wave length.

3.5 FEATURES OF PREDICTED PERFORMANCE: PROGRESSIVE SOLIDIFICATION

This section describes predicted results from a range of analyses using the proposed model, focusing on the progressive solidification in liquefied sand. The emphasis is placed on looking at the densification due to the solidification and the difference between the solidification and the consolidation following liquefaction under a quiescent environment.

A total of twelve cases were performed (Table 3.2). The number of wave loading cycles ranged from 9 to 1000. The gravity acceleration in the analyses was set at 30g. The wave conditions set and the soil parameters used are listed in Table 3.3. The wave and soil conditions correspond to those of a centrifuge wave test on a loose deposit of Silica sand #7- Batch B (test WJ40) as described later in chapter 4. The soil beds are assumed to be uniform before wave loading.

The time increments Δt is $T/40$ and depth increments $\Delta Z = -D/200$ which are the same as those in the calculation in section 3.4.

3.5.1 Features of advance of solidification front

The predicted time histories of the wave-induced pore pressure fluctuations at different spatial points in case A-800 are shown in Fig. 3.12, together with the input wave forms, $\tilde{u}_{\zeta 0}$. It can be clearly seen that, in the course of continued wave loading, the solidification front advanced upwards. In accordance with the advance of the solidification front, the gradual reduction in the amplitudes of the oscillatory pore pressures $u_e^{(1)}$ occurred in the region behind the solidification front. A close observation of the wave form at ζ=-17*mm* for instance shows that the residual pore pressure during the liquefaction gradually decreased with time. This is just an indication of the finite deformation effect. That is to say, the mass of the soil above the level of ζ=-17*mm* decreased due to the densification of the soil below the solidification front.

The advance of the solidification front can be seen in detail in Fig. 3.13. In this figure, the profiles of the residual pore pressure, $u_e^{(2)}$ with elevation ζ for seven different times in case A-800 are shown. The successive locations of the solidification front during the wave loading are denoted by ζ_s. Each line of the residual pore pressure against ζ above the solidification front corresponds to σ_{v0}' against ζ line at each time. Note that the temporal movement of the line σ_{v0}' - ζ above the solidification front is due to the

densification of the soil below the solidification front.

The predicted progress of liquefaction and solidification fronts in case A-800 is shown in Fig. 3.14 (a). The liquefaction front advanced rapidly with time, terminating at ζ=-82*mm* when ξ=9. After the full development of the liquefaction zone, the solidification front advanced upward in the course of continued wave loading. The solidification front reached the level of the soil surface at ξ=542. The settlement of the soil surface occurred in accordance with the progress of the solidification front. In this particular case, after the end of advance of the solidification front, the settlement of the soil surface is negligibly small.

The amplitude, a_0, of the soil surface vibration decreases in accordance with the progress of the solidification front in case A-800 can be noted in Fig. 3.14 (b). It is also noteworthy that the amplitude a_0 increased in association with the downwards advance of the liquefaction front. The vibratory soil motion is a good indication of the fluidities of liquefied soil.

The temporal change in the center of the vibration in Fig. 3.14 (b) represents the settlement of the soil surface. Since in the analytical model the liquefied sand above the solidification front, which is the fully destructured liquefied soil, is not densified, the settlement of the soil surface occurred due to the densification in the soil region below the solidification front. Therefore, the velocity of the settlement of the soil surface corresponds to the discharge velocity at the solidification front. Since the discharge velocity at the solidification front is equal to $k\gamma'/\gamma_f$, the velocity of the settlement of the soil surface in Fig. 3.14(b) may be represented by the following equation:

$$\dot{S} = k\frac{\gamma'}{\gamma_f} \tag{3.20}$$

The way in which void ratio profile changes with the progress of the solidification front typified in Fig. 3.15 on the basis of the result from case A-800. Note that in curve 2, the void ratio in the region behind the solidification front (ζ_s=-54*mm*) decreased significantly. The same pattern of the densification was observed from curve 3. It is also noteworthy that the soil bed underwent significant densification at all depth when the solidification extended to the soil surface (Curve 4).

3.5.2 Comparison between solidification and consolidation under quiescent environment

It is instructive to contrast the characteristics of the solidification and those of the consolidation following liquefaction under quiescent environment.

The rate of dissipation of the excess pore-pressure due to consolidation following liquefaction is larger than that due to solidification. This aspect can be seen clearly in Fig. 3.16 with three calculated traces being shown. Note that in case A-25 the wave loading was stopped at ξ=25, permitting the consolidation to occur in the liquefied soil. Essentially the same behaviour can be seen from case A-280 where the wave loading was stopped at ξ=280. Because of the effects of the pore pressure generation by the source term in equation (3.12), the rate of the dissipation of the pore pressure due to the solidification was smaller than that due to consolidation.

The amount of densification during consolidation following liquefaction depends on the way in which the soil has previously undergone solidification. This aspect can be seen in Fig. 3.17 with the changes in void ratio profile in case A-280 being shown. In fact, little further densification due to the consolidation occurred in the region where the solidification previously developed ($-82mm<\zeta<44mm$). By contrast, in the region where no solidification occurred, the appreciable densification ensued due to the consolidation.

Note that the amount of the densification due to the solidification can be brought about more significantly than that of densification due to the consolidation. One can confirm the above statement by comparing the profiles below and above the solidification front (ζ_S=-44*mm*). This aspect is shown more clearly in Fig. 3.18. The marked densification in the solidification process was essentially caused by the contractancy due to the cyclic loading.

3.5.3 Settlement of soil surface

Summary plots showing the relative importance of solidification and consolidation on the final settlement of sand deposits are presented in Fig. 3.19. In fact, for the final settlement, the settlement due to solidification becomes more dominant than that due to consolidation with increasing wave loading cycles. Note that the final settlement of the soil surface increases considerably as the settlement due to solidification becomes more dominant.

3.6 DISCUSSION: Revisit to Florin & Ivanov (1961) proposal

It has been observed that the advance of solidification front during wave loading is accompanied by the significant densification. The purpose of this section is to examine the relation between the densification due to the solidification and the velocity of the solidification front. It is shown that this relation is approximately represented by a simple equation which had been proposed by Florin & Ivanov (1961).

Florin & Ivanov (1961) proposed an equation for the upward velocity of the solidification front as follows:

$$(\textit{Velocity of the solidification front}) = \frac{\gamma'(1+e_1)k}{\gamma_f(e_1-e_2)} \tag{3.21}$$

where e_1 is the void ratio of the liquefied sand and e_2 is the void ratio at the end of consolidation. Scott (1986) used equation (3.21) with void ratio e_2 being redefined as the void ratio of the solidified sand. In order to clarify the meaning of equation (3.21), it is worthwhile re-examining the derivation procedure of the equation.

Consider a situation where a saturated sand bed is in a state of complete liquefaction under cyclic loading. The residual pore pressure starts dissipating at the base of the liquefied sand layer, and then the solidification front moves upward. The velocity of the solidification front is denoted here as dZ_s/dt. The underlying assumptions to derive at equation (3.21) may be summarized as follows:

(1) The void ratio of the liquefied sand, e_1, at the interface between the liquefied sand and the solidified sand, whose thickness is dZ_s, changes to the void ratio e_2 for the time, dt. Here, the change in void ratio is denoted as Δe ($=e_1$-e_2).
(2) The liquefied sand above the interface between the liquefied sand and the solidified sand is not densified.
(3) The changes in the void ratio of the saturated sand, Δe, should concurrently cause the pore water to be squeezed out of the void space of the sand.
(4) The pore-water flow follows Darcy's law.
(5) The hydraulic gradient of the flow corresponds to a critical gradient, γ'/γ_f.
(6) The permeability coefficient, k, and the submerged unit weight of the soil, γ', are constant.

Under these assumptions, the following equation can be obtained.

$$\frac{\Delta e}{1+e_1}\cdot\frac{d\,Z_S}{d\,t}=k\cdot\frac{\gamma'}{\gamma_f} \tag{3.22}$$

This equation is essentially the same as equation (3.21). Note that Δe in equation (3.22) represents the change in the void ratio which occurs at the interface between the liquefied sand and the solidified sand, not the change in the void ratio associated with the increase in the vertical effective stress, σ_v'. Namely, e_2 in equation (3.21) is the void ratio of the solidified sand, which is the one redefined by Scott (1986), not the void ratio at the end of consolidation.

In the obtaining equation (3.22), the settlement of the interface between the liquefied sand and the solidified sand, which is due to the densification in the region below the solidification front, is not considered. Therefore, the velocity of the solidification front in equation (3.21) or (3.22) represents the one in Lagrangian coordinate. Now, the velocity of the solidification front in Euler coordinate (ζ-coordinate), $d\,\zeta_S/d\,t$, is described. The rate of the settlement of the interface between the liquefied sand and the solidified sand is considered. Since the liquefied sand above the solidification front is assumed to be not densified, the rate of the settlement of the interface between the liquefied sand and the solidified sand corresponds to that of the soil surface settlement, $\dot{S}$. Remember that $\dot{S}$ is expressed in equation (3.20). The velocity $d\,\zeta_S/d\,t$ is expressed as follows:

$$\frac{d\,\zeta_S}{d\,t}=\frac{d\,Z_S}{d\,t}+(-\dot{S})=\frac{\gamma'}{\gamma_f}k\frac{(1+e_1)}{\Delta e}-\frac{\gamma'}{\gamma_f}k=\frac{\gamma'}{\gamma_f}k\frac{(1+e_2)}{\Delta e} \tag{3.23}$$

Equation (3.23) represents the relation between the velocity of the solidification front and the degree of densification due to the solidification, Δe. Now, this relation represented by equation (3.23) is compared with the relation obtained from the proposed model.

The predicted temporal changes in the void ratio profile in case A-800 is shown in Fig. 3.20(a). This figure shows the changes in the void ratio profile in the period of ξ= 50 to 550 in more detail than in Fig. 3.15. In Fig. 3.20(a), the location of the solidification front at each time is represented by that of the nearly horizontal part of each profile. The predicted velocity of the solidification front at each depth in case A-800 is shown in Fig. 3.20(b). The relation between the velocity of the solidification front and the degree of densification can be examined by comparing Fig. 3.20 (a) with

Fig. 3.20 (b). It is shown that in the region where the velocity of the solidification front is larger (ζ<-65*mm* or ζ>-25*mm*), the degree of densification is smaller, and that in the region where the velocity of the solidification front is smaller (-65*mm*<ζ<-25*mm*), the degree of densification is larger.

The densification of the sand due to the solidification obtained from equation (3.23) is superimposed in Fig. 3. 20 (a) (dotted line). In obtaining this line, the velocity of the solidification front in each soil depth shown in Fig. 3. 20 (b) are substituted into equation (3.23). In addition, the initial values of γ', k, and void ratio e in analysis of A-800 shown Table 3.3 are used for γ', k, and e_1 in equation (3.23) instead of those values of liquefied sand. This reason is that the initial values of γ', k, and void ratio e are nearly the same as those of liquefied sand in the analysis A-800. It is seen from Fig. 3. 20(a) that the degree of densification obtained from equation (3.23) corresponds reasonably to that obtained from the analytical model. This indicates that the relation between the velocity of the solidification front and the degree of densification is approximately represented by equation (3.23).

It is interesting to observe that the densification in association with the advance of the solidification front is represented by a simple expression based on a few assumptions of above-mentioned (1)-(6). However, it should be remembered that is noted that the densification due to the solidification could be back-calculated from equation (3.23), when the velocity of the solidification front at a soil depth is given. In order to predict both the velocity of the solidification front and the densification due to solidification, one should solve a moving-boundary problem as demonstrated in sections 3.1 through 3.5 of this chapter.

3.7 CONCLUSIONS

The progressive liquefaction and solidification processes in liquefied sand during continued wave loading have been discussed and a theoretical framework for describing them has been proposed. The formulation was made in view of levels of liquefaction. In fact, two levels of liquefied soil were introduced: *fully destructured liquefied soil* that has zero-stiffness; and *structured liquefied soil* that has a marginally discernible stiffness while the effective stress is zero. The structured liquefied sand thus defined has an ability to permit the excess pore pressure to dissipate according to a storage equation, thereby enabling solidification to develop in a liquefied soil layer.

The proposed theoretical framework has proven capable of describing not only the progressive solidification, but also the progressive liquefaction that should precede the

solidification process. Furthermore, in the framework, the solidification process has been distinguished from the consolidation process in liquefied sand under quiescent environment.

The principal conclusions obtained from the present study may be summarized as follows:

(a) After the full developments of the liquefied zone due to the progressive liquefaction, in the course of continued wave loading, the residual pore pressure at the bottom of the liquefied sand started dissipating, triggering the start of solidification. The solidification front advanced upward to the soil surface during the continued wave loading.

(b) The vibratory movements of the soil surface developed in association with the advance of the liquefaction front and decreased in association with the advance of the solidification front. The vibratory soil movements stopped when the solidification front reached the soil surface.

(c) The advance of the solidification front brought about marked densification in the region behind the front. This densification was caused by the contractancy due to cyclic loading.

(d) The degree of densification due to the solidification process was more significant than that brought about by the consolidation under quiescent environment after the cessation of the wave loading.

(e) The rate of the excess pore-pressure dissipation in the solidification process was smaller than that in the consolidation process, since the pore pressure was generated due to the contractancy of the sand in the solidification process.

(f) With increase in wave loading cycles, ξ_{FL}, following the full development of the liquefied zone, the settlement of the soil surface at the completion of the dissipation of the residual pore pressure was increased. This is because the solidification zone in the soil beds became larger with increasing ξ_{FL}.

(g) The relation between the velocity of the solidification front and the degree of densification due to the solidification is approximately represented by a simple expression presented by Florin & Ivanov (1961).

APPENDIX 1. FORMULATION FOR THE TWO-LAYER FLUID REGION

Suppose that a small-amplitude sinusoidal fluid wave having wavelength L and wave period T propagates in a two-layer fluid of a finite thickness equal to h-z_S as shown in

Fig. 3, under an Ng gravitational field. If the motion of the fluid is irrotational, velocity potentials should exist for both fluid layers: ϕ_1 for region I and ϕ_2 for region II. The concrete forms of ϕ_1 and ϕ_2 are shown in equations (36), (37) and (43)-(46) in Sassa et al. (2001). Note that the bottom of the two-layer fluid is z_L in Sassa et al. (2001). Therefore, the word z_L in equations (43) and (45) of Sassa et al. are replaced with z_S in the present study.

The dispersion relationship for the two-layer fluid is obtained from equation (47) of Sassa et al. (2001) as follows:

$$\left[1-\left(\frac{Ng\kappa}{\omega^2}\right)^2\right]\tanh(\kappa h)\tanh(\kappa z_S)=\frac{\rho_2}{\rho_1}\left(1-\frac{Ng\kappa}{\omega^2}\tanh(\kappa h)\right)\left(1+\frac{Ng\kappa}{\omega^2}\tanh(\kappa z_S)\right) \tag{3.24}$$

where ρ_1 and ρ_2 are the mass densities of the exterior fluid and of the liquefied soil, κ is the wave number ($=2\pi/L$) and ω is the angular frequency of waves ($=2\pi/T$).

The settlement of the soil surface S is considered. The fluid pressure oscillation $\tilde{u}_{\zeta 0}$ at the level $z=S$, which is the original level of the soil surface, is related to the velocity potential for the exterior fluid, ϕ_1, by using the linearised Bernoulli equation as follows:

$$\tilde{u}_{\zeta 0}=\rho_1\left.\frac{\partial\phi_1}{\partial t}\right|_{z=S} \tag{3.25}$$

Substituting the concrete form of ϕ_1 in equation (3.25) leads to

$$a_0=\frac{\kappa\sinh(\kappa z_S)}{(\rho_1-\rho_2)Ng\kappa\sinh(\kappa z_S)\cosh(\kappa S)-\rho_2\omega^2\cosh(\kappa z_S)\cosh(\kappa S)+\rho_1\omega^2\sinh(\kappa z_S)\sinh(\kappa S)}u_{\zeta 0} \tag{3.26}$$

Similarly, the fluid pressure oscillation at the current soil surface, $\tilde{u}_0$, is related to ϕ_1.

$$\tilde{u}_0=\rho_1\left.\frac{\partial\phi_1}{\partial t}\right|_{z=0} \tag{3.27}$$

Substituting the concrete form of ϕ_1 in equation (3.27) leads to

$$u_0 = -\frac{\rho_2\omega^2 + (\rho_2 - \rho_1)Ng\kappa\tanh(\kappa z_S)}{\kappa\tanh(\kappa z_S)}a_0 \tag{3.28}$$

Combination of equations (3.26) and (3.28) yields

$$u_0 = -\frac{\rho_2\omega^2 + (\rho_2 - \rho_1)Ng\kappa\tanh(\kappa z_S)}{(\rho_1 - \rho_2)Ng\kappa\tanh(\kappa z_S)\cosh(\kappa S) - \rho_2\omega^2\cosh(\kappa S) + \rho_1\omega^2\tanh(\kappa z_S)\sinh(\kappa S)}u_{\zeta 0} \tag{3.29}$$

The relation between u_0 and the amplitude of oscillatory pore pressure $u_e^{(1)}$ at a given horizon z in the fully destructured liquefied soil ($z_S<z<0$) is obtained from equation (5) of Sassa et al. (2001) as follows:

$$u_e^{(1)} = \frac{\rho_2\omega^2[\cosh(\kappa z) - \sinh(\kappa z)\tanh(\kappa z_S)]}{\rho_2\omega^2 + (\rho_2 - \rho_1)Ng\kappa\tanh(\kappa z_S)}u_0 \qquad (for\ z_S < z < 0) \tag{3.30}$$

The amplitude of fluid pressure fluctuation, u_S, at the level of the solidification front is obtained from equation (6) of Sassa et al. (2001) as follows:

$$u_S = \frac{\rho_2\omega^2}{\rho_2\omega^2\cosh(\kappa z_S) + (\rho_2 - \rho_1)Ng\kappa\sinh(\kappa z_S)}u_0 \tag{3.31}$$

The amplitude of oscillatory pore pressure $u_e^{(1)}$ and the maximum cyclic shear stress τ at a given horizon z in the elestoplastic soil ($-d < z < z_S$) below the two-layer fluid are related to the amplitude of fluid pressure fluctuation, u_S, at the solidification front. These relations are obtained from equations (12) and (13) of Sassa et al. (2001) as follows:

$$u_e^{(1)} = u_S\exp[\kappa(z - z_S)] \qquad (for\ -d < z < z_S) \tag{3.32}$$

$$\tau = -\kappa u_S(z - z_S)\exp[\kappa(z - z_S)] \quad (for\ -d < z < z_S) \tag{3.33}$$

The wave number κ appearing in equations (3.26) and (3.28)-(3.33) should satisfy the dispersion relationship for the two-layer fluid in equation (3.24).

APPENDIX 2. DERIVATION OF EQUATION (3.8)

Consider the soil body considering one-dimensionally in the course of wave loading (Fig. 3.4). An soil element lying $\zeta(Z)$ is considered. The total stress rate at the soil element is expressed as follows with the time average of a wave cycles being considered:

$$\dot{\sigma}_v = \frac{D}{Dt}\int_{\zeta(Z)}^{-S} \gamma' d\zeta + \frac{D}{Dt}\int_{\zeta(Z)}^{H} \gamma_f d\zeta \tag{3.34}$$

Note here that the first term on the right hand side of equation (3.34) is zero since the mass of the solid phase of the region from $\zeta(Z)$ to the soil surface is conserved. The second term becomes $-\gamma_f \dot{\zeta}$. That is to say,

$$\dot{\sigma}_v = -\gamma_f \dot{\zeta} \tag{3.35}$$

The total stress in the soil element is the sum of the effective stress and the pore pressure. The pore pressure consists of the hydrostatic pressure, $\gamma_f(H\text{-}z)$, and the excess pore pressure. Therefore, total stress rate is expressed as

$$\dot{\sigma}_v = \dot{\sigma}_v' + \dot{u}_e^{(2)} + \left\{\gamma_f (H-\zeta)\right\}^{\cdot} = \dot{\sigma}_v' + \dot{u}_e^{(2)} - \gamma_f \dot{\zeta} \tag{3.36}$$

From equations (3.35) and (3.36),

$$\dot{\sigma}_v' + \dot{u}_e^{(2)} = 0 \tag{3.37}$$

APPENDIX 3. FINITE-DIFFERENCE REPRESENTATIONS WITH RESPECT TO EQUATION (12)

We used the following finite-difference representations with respect to equation (3.12):

$$\frac{U(Z,\xi+\Delta\xi)-U(Z,\xi)}{\Delta\xi}$$
$$= 2\pi\frac{M(Z,\xi)\cdot\alpha(Z,\xi)}{\gamma_f\omega}\kappa_0^2\left[\frac{k(Z+\Delta Z,\xi)-k(Z-\Delta Z,\xi)}{2\Delta Z}\cdot\frac{U(Z+\Delta Z,\xi+\Delta\xi)-U(Z-\Delta Z,\xi+\Delta\xi)}{2\Delta Z}\cdot\alpha(Z,\xi)\right.$$
$$+k(Z,\xi)\cdot\alpha(Z,\xi)\cdot\frac{U(Z+\Delta Z,\xi+\Delta\xi)-2U(Z,\xi+\Delta\xi)+U(Z-\Delta Z,\xi+\Delta\xi)}{\Delta Z^2}$$
$$\left.+k(Z,\xi)\cdot\frac{U(Z+\Delta Z,\xi+\Delta\xi)-U(Z-\Delta Z,\xi+\Delta\xi)}{2\Delta Z}\cdot\frac{\alpha(Z+\Delta Z,\xi)-\alpha(Z-\Delta Z,\xi)}{2\Delta Z}\right]$$
$$+M(Z,\xi)\frac{\partial v^p}{\partial\xi} \tag{3.38}$$

where $\alpha(Z,\xi)=\{1-n(Z,0)\}/\{1-n(Z,\xi)\}$. We represent $u_e^{(2)}$ by U and $\kappa_0 Z$ by Z.

References

Carter, J. P., Booker, J. R. & Small, J. C. (1979). The analysis of finite elasto-plastic consolidation, *International Journal for Numerical and Analytical Methods in Geomechanics*, **3**, 107-129.

Florin, V. A. & Ivanov, P. L. (1961). Liquefaction of saturated sandy soils, *Proceedings of the 5th International Conference on Soil Mechanics and Foundation Engineering*, **1**, 107-111.

Gomyo, W., Sakai, K., Takayama, T., Terauchi, K. & Takahashi, S. (1995). Site investigation on the stability of rubble-mound breakwaters. *Proceedings of Coastal Engineering, JSCE,* **42**, No.2, 901-905 (*in Japanese*).

Ishihara, K. (1993). Liquefaction and flow failure during earthquake. Rankine lecture, *Geotechnique*, **43**, No. 3, 351-415.

Lee, K. L., & Albaisa, A. A. (1974). Earthquake induced settlements in saturated sand, *Journal of the Geotechnical engineering division, ASCE*, **100**, GT4, 387-406.

Lamb, H. (1932). *Hydrodynamics*, Cambridge University Press, p. 738.

Miyamoto, J., Sassa, S. & Sekiguchi, H. (2002). Solidification and consolidation in liquefied sand with contractancy due to wave loading. *Proceedings of Coastal*

Engineering, JSCE, **49**, No.2, 846-850 (*in Japanese*).

Nagase, H. & Ishihara, K. (1988). Liquefaction-induced compaction and settlement of sand during earthquake. *Soils Fdns*, **28**, No. 1, 65-76.

Sassa, S. & Sekiguchi, H. (1999). Wave-induced liquefaction of beds of sand in a centrifuge. *Geotechnique,* **49**, No.5, 621-638.

Sassa, S. & Sekiguchi, H. (2001). Analysis of wave-induced liquefaction of sand beds. *Geotechnique,* **51**, No.2, 115-126.

Sassa, S., Sekiguchi, H. and Miyamoto, J. (2001). Analysis of progressive liquefaction as a moving-boundary problem. *Geotechnique,* **51**, No.10, 847-857.

Scott R. F. (1986). Solidification and consolidation of a liquefied sand column, *Soils Fdns*, **26**, No. 4, 23-31.

Sumer, B. M., Fredsoe, J., Christensen, S. & Lind, M. T. (1999). Sinking/floatation of pipelines and other objects in liquefied soil under waves. *Coastal Engineering*, **38**, 53-90.

Sumer, B. M. & Fredsoe, J. (2002). *The mechanics of scour in the marine environment*, World Scientific, 445.

Taylor, D. W. (1948). *Fundamentals of Soil Mechanics*, John Wiley & Sons. 111-112.

Yoshida, N., Yasuda, S., Kiku, M., Masuda, T. & Finn, W. D. L., (1994) Behavior of sand after liquefaction, *Proceedings of the 5th U.S.-Japan Workshop on Earthquake Resistant Design of Lifeline Facilities and Countermeasures against Soil Liquefaction, Salt Lake City, Technical Report NCEER-94-006, National Center for Earthquake Engineering Research,* USA, pp. 181-198.

Yoshimi, Y., Kuwabara, F. & Tokimatsu, K., (1975). One-dimensional volume change characteristics of sands under very low confining stresses, *Soils Fdns*, **15**, No. 3, 51-59.

Table 3.1 Wave conditions and soil parameters for analysis

Wave conditions	
Wave frequency f ($\omega/2\pi$): Hz	8
Fluid depth H: mm	80
$u_{\xi 0}$: kPa	3
Soil bed conditions	
Sand	Silica sand #7(A)
Specific gravity Gs	2.69
Maximum void ratio e_{max}	1.15
Minimum void ratio e_{min}	0.69
Mean grain size D_{50}: mm	0.14
Soil depth D: mm	80
Void ratio	0.995
Relative density Dr: %	34
Permeability coefficient k: mm/s	0.19
Parameter C_f: mm/s	0.35
γ': kN/m^3	249
Thickness of transition layer: mm	0.4
Reference stress σ_{VR}: kPa	0.12
Parameters for source term	
A	7.47
B	12
β	0.12

Table 3.2 Cases of calculations using proposed model

Case	Wave loading cycles
A-9	9
A-25	25
A-50	50
A-100	100
A-200	200
A-280	280
A-400	400
A-500	500
A-600	600
A-700	700
A-800	800
A-1000	1000

Table 3.3 Wave conditions and soil parameters for analyses

Wave conditions	
Wave frequency f ($\omega/2\pi$): Hz	8
Fluid depth H: mm	80
$u_{\xi 0}$: kPa	3
Soil bed conditions	
Sand	Silica sand #7(B)
Specific gravity Gs	2.69
Maximum void ratio e_{max}	1.18
Minimum void ratio e_{min}	0.69
Mean grain size D_{50}: mm	0.14
Soil depth D: mm	85
Void ratio	1.033
Relative density Dr: %	30
Permeability coefficient k: mm/s	0.19
Parameter C_f: mm/s	0.35
γ': kN/m^3	244
Thickness of transition layer: mm	0.4
Reference stress σ_{VR}: kPa	0.12
Parameters for source term	
A	7.47
B	12
β	0.12

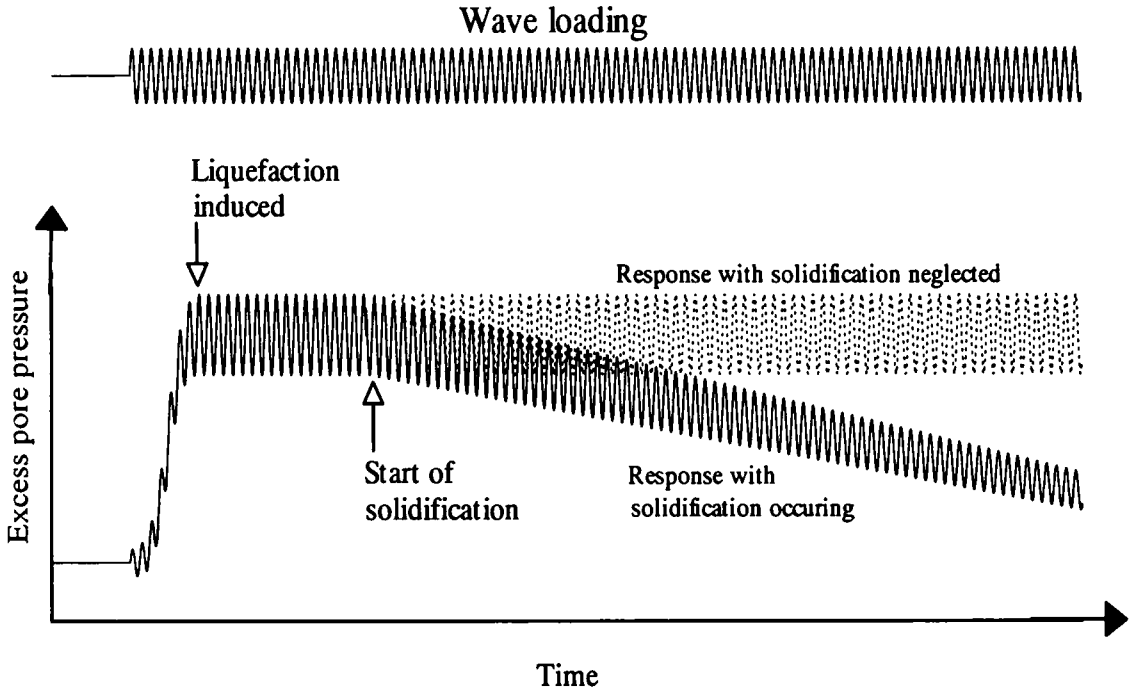

Fig. 3.1 Schematic evolution of excess pore pressures during prolonged wave loading, illustrating the importance of solidification process

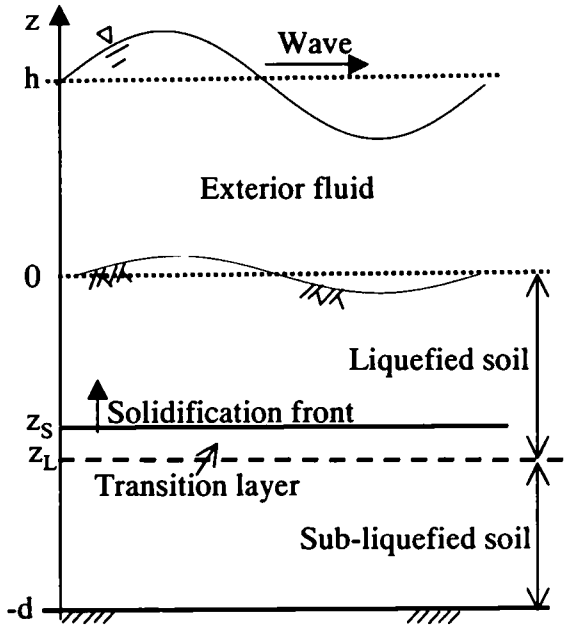

Fig. 3.2 Problem definition for describing progressive solidification in liquefied sand during wave loading

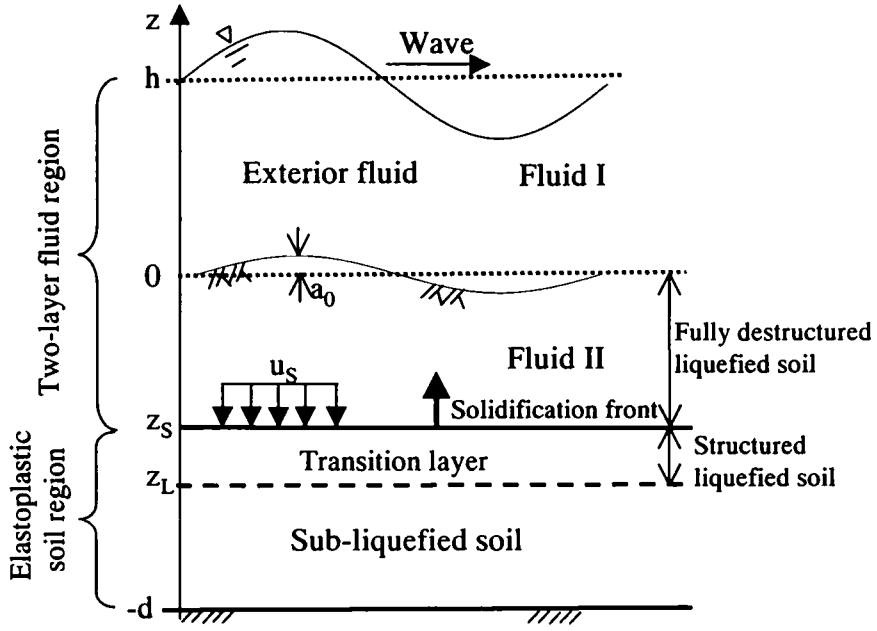

Fig. 3.3 Elastoplastic soil region and overlying two-layer fluid region

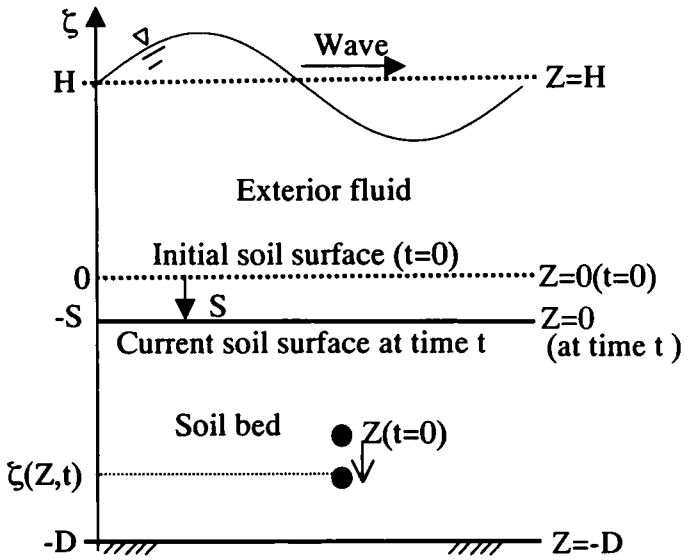

Fig. 3. 4 Configuration of soil body under one-dimensional consolidation

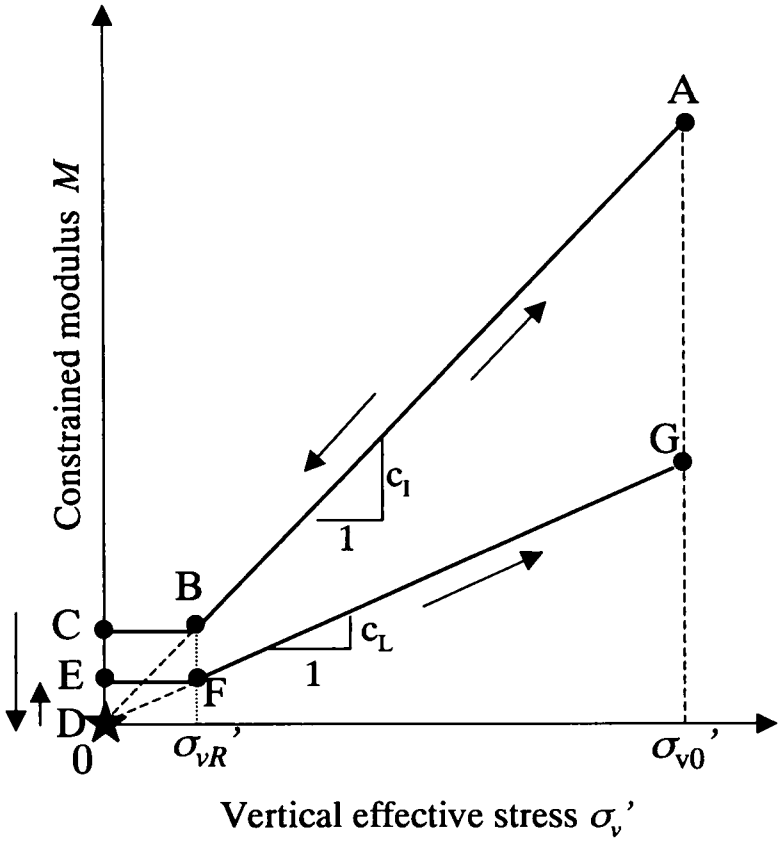

Fig. 3. 5 Proposed relation between constrained modulus M and vertical effective stress σ_v'.

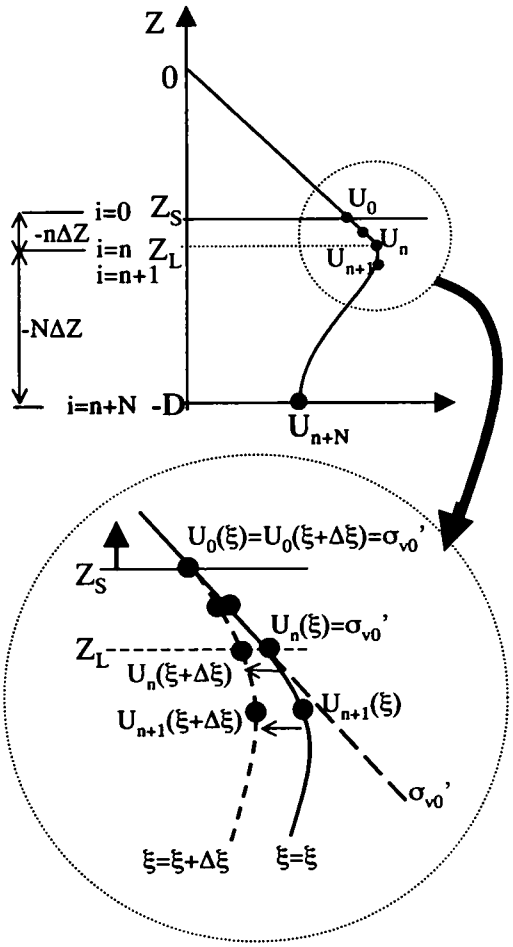

Fig. 3.6 Sketch illustrating the changes in the residual pore pressure profile at the transition layer and the uppermost layer of the sub-liquefied soil.

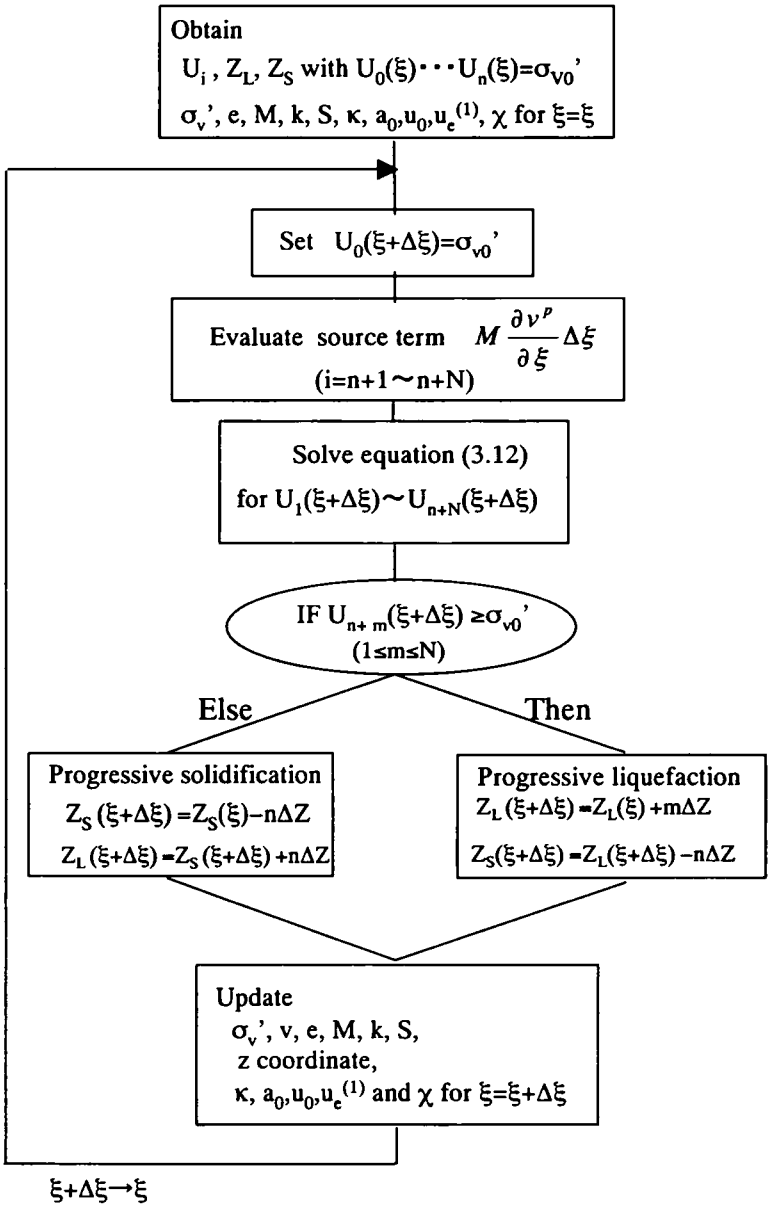

Fig. 3. 7 Flow chart for the identification of liquefaction or solidification fronts

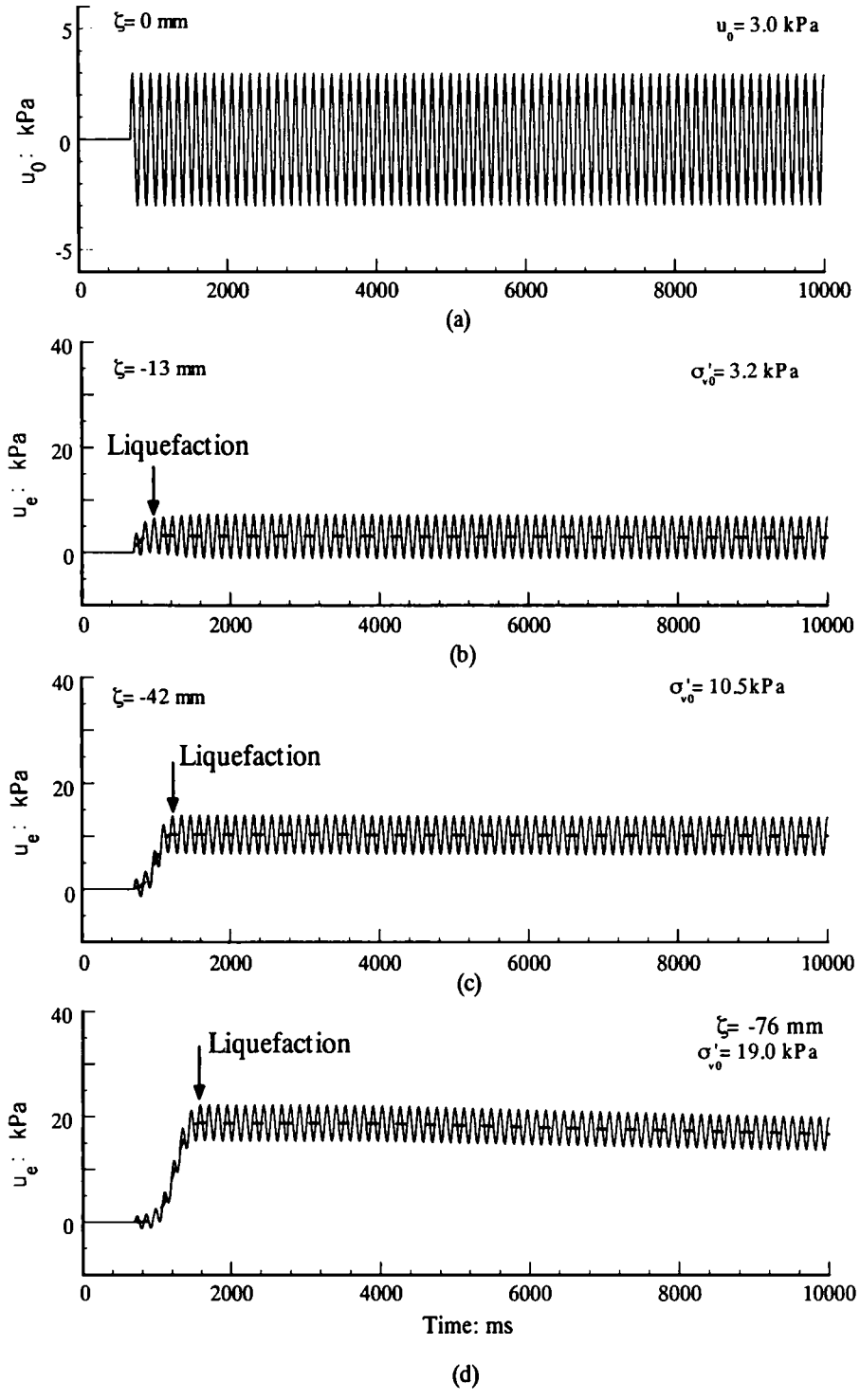

Fig. 3.8 Predicted waveforms : Time histories of (a) wave pressure acting on the soil surface and (b), (c) and (d) excess pore pressures

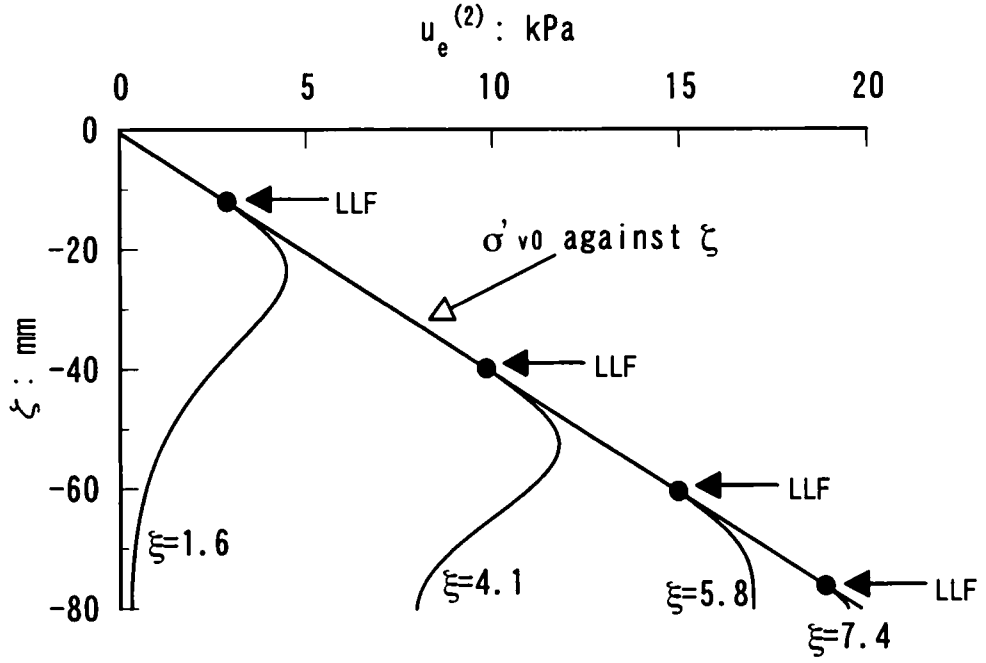

LLF: Location of liquefaction front

Fig. 3.9 Predicted temporal changes in the profile of $u_e^{(2)}$ against ζ

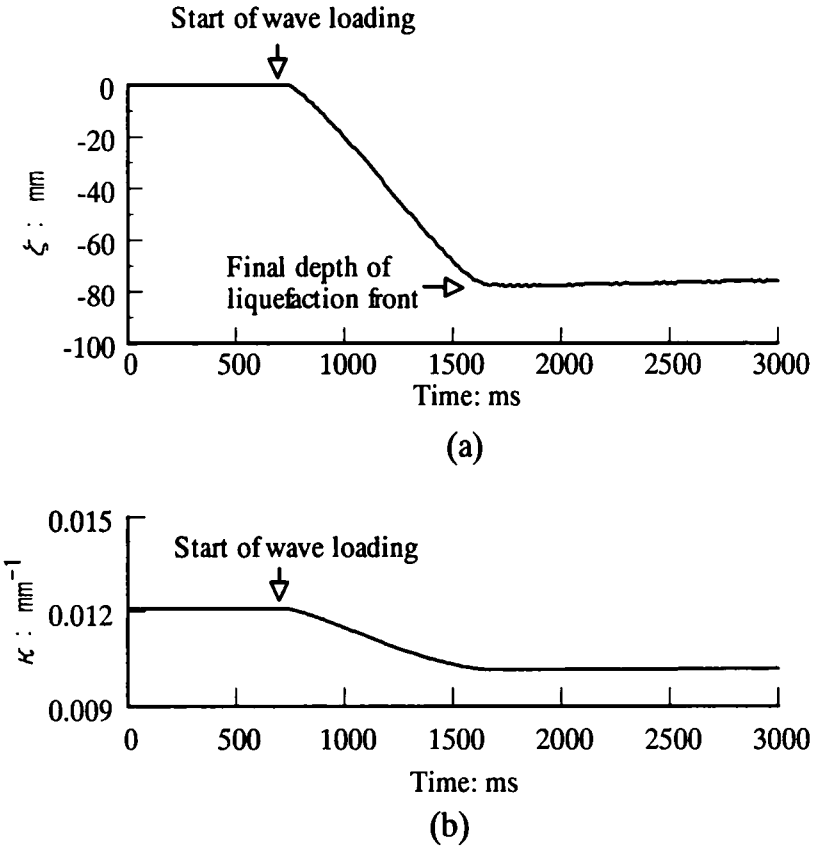

Fig. 3.10 Predicted temporal change of (a) the location of the liquefaction front and (b) the wave number, κ

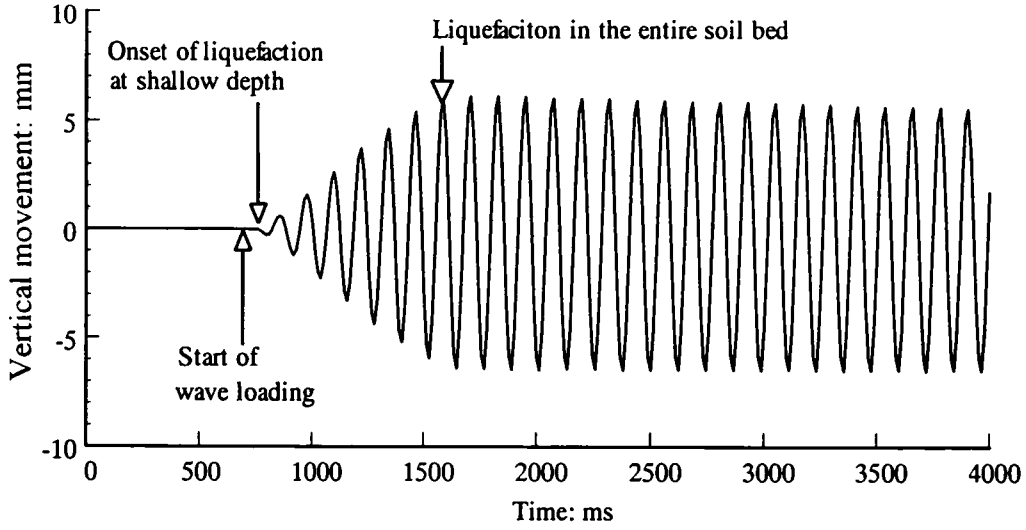

Fig. 3.11 Predicted vertical movement of the soil surface

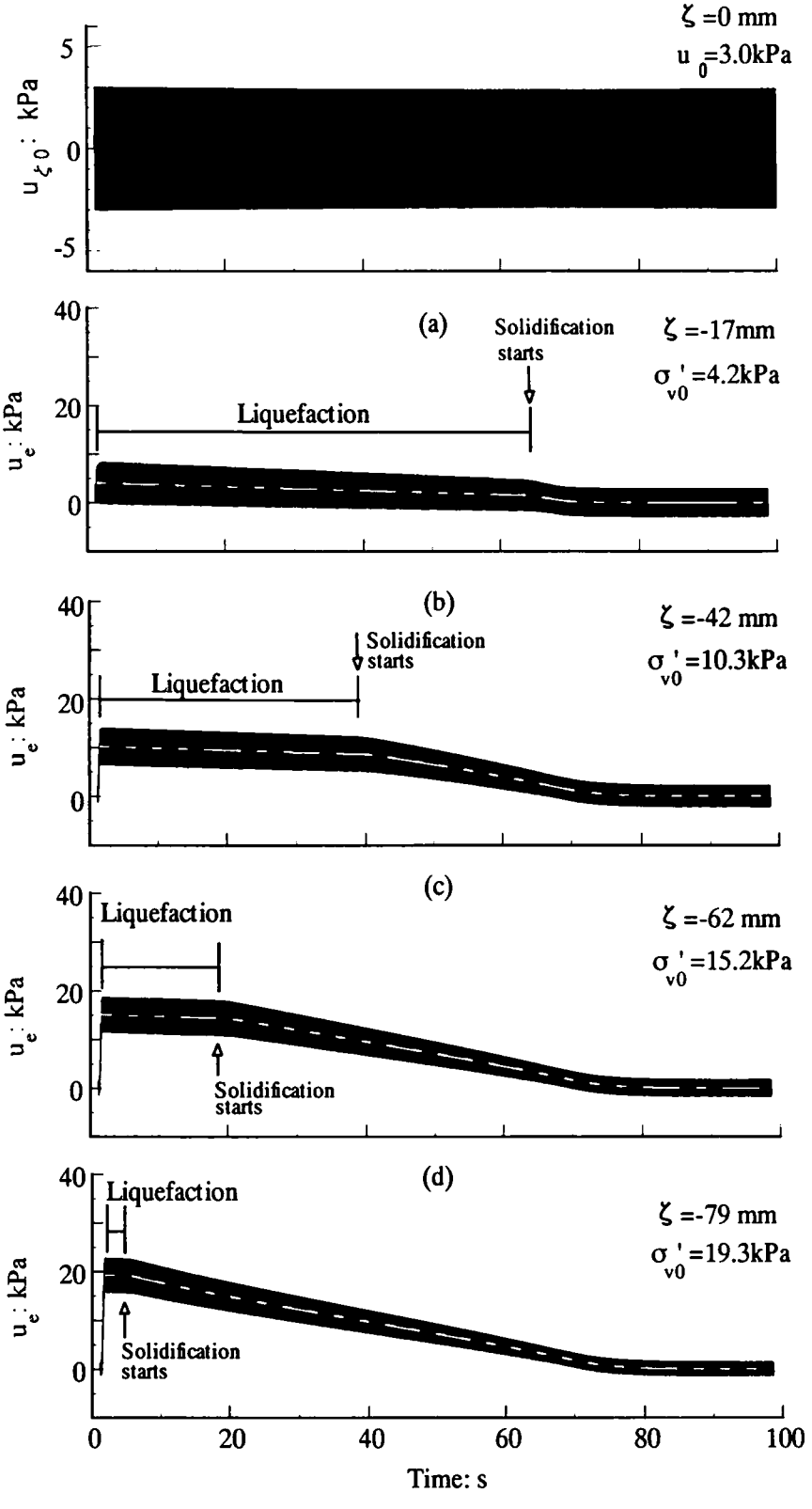

Fig. 3.12 Predicted waveforms in case A-800: time histories of (a) wave pressure acting on the location of the initial soil surface and (b), (c), (d) and (e) excess pore pressures at different spatial points.

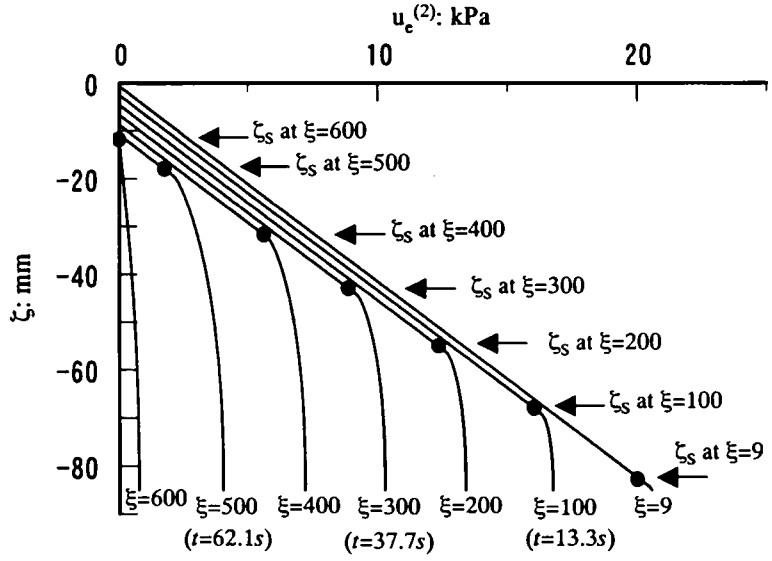

Fig. 3.13 Predicted temporal changes in the profile of $u_e^{(2)}$ against ζ for case A-800

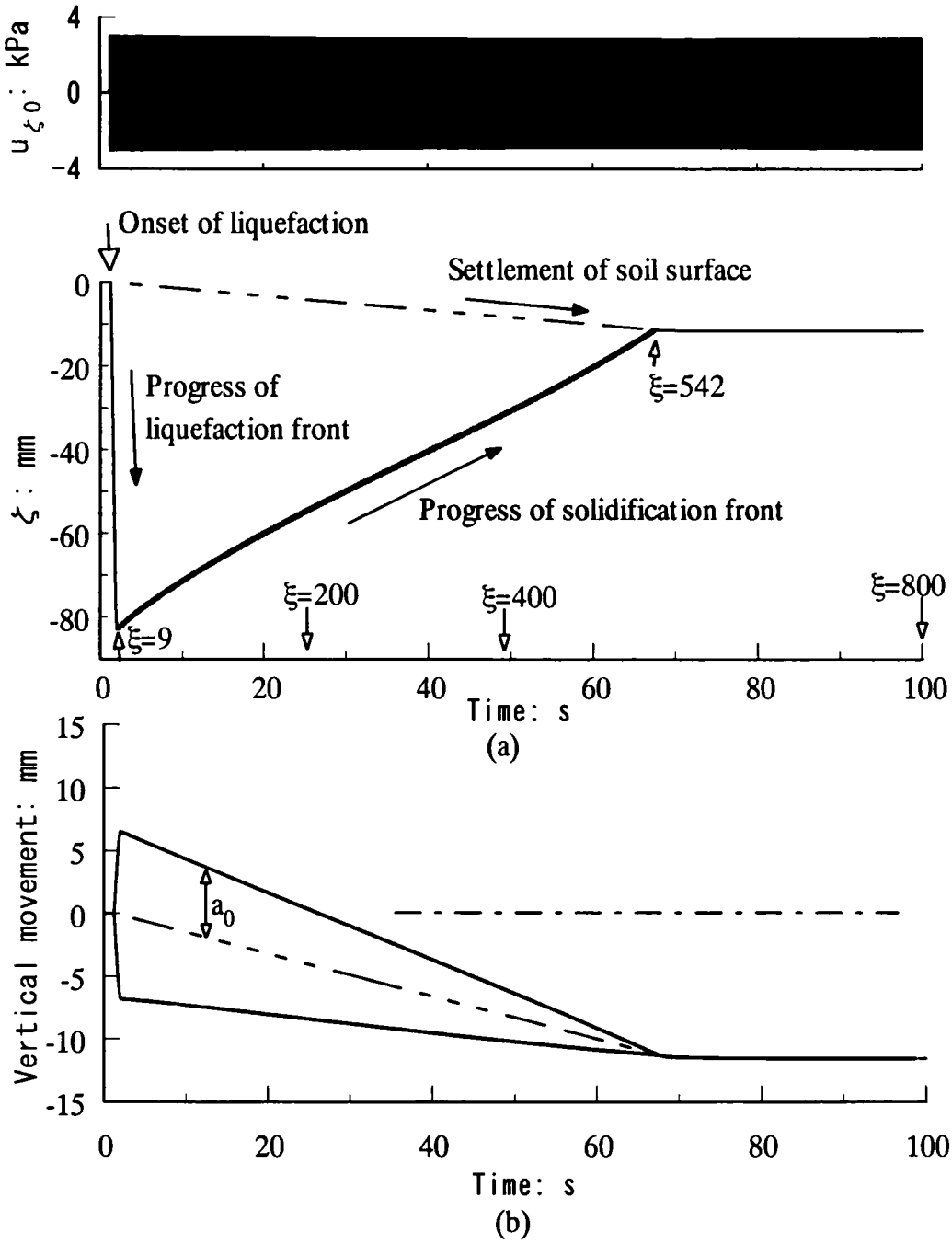

Fig. 3.14 (a) Predicted temporal changes in the locations of liquefaction and solidification fronts in case A-800, and (b) the associated, predicted vertical movements of the soil surface

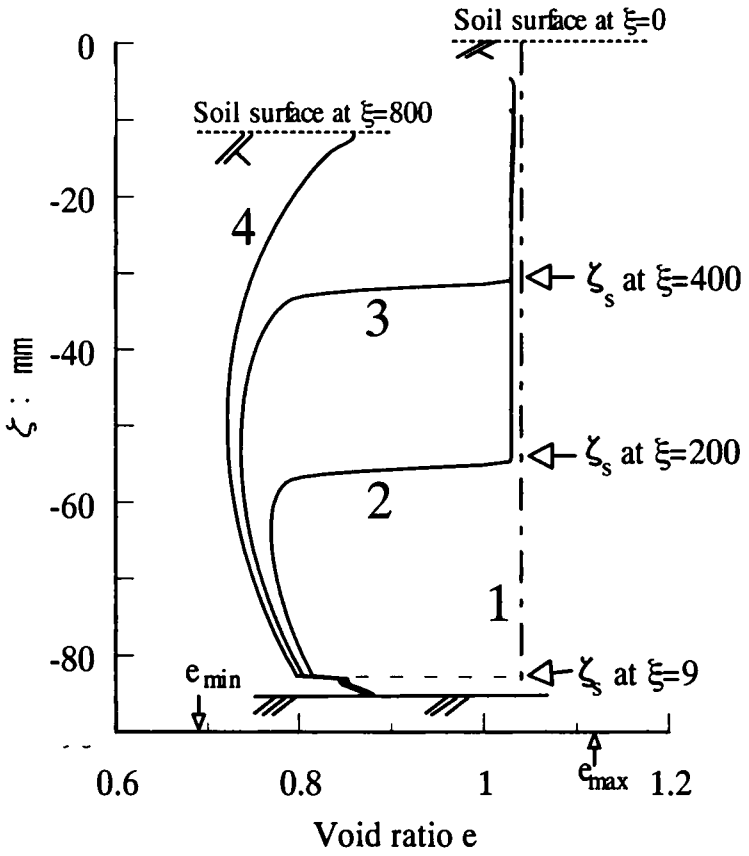

Legend

1: Initial profile
2: Profile after 200 cycles of wave loading
3: Profile after 400 cycles of wave loading
4: Profile after 800 cycles of wave loading

Fig. 3.15 Predicted pattern of the change in void ratio profile of sand bed in case A-800: significant densification in association with progressive solidification

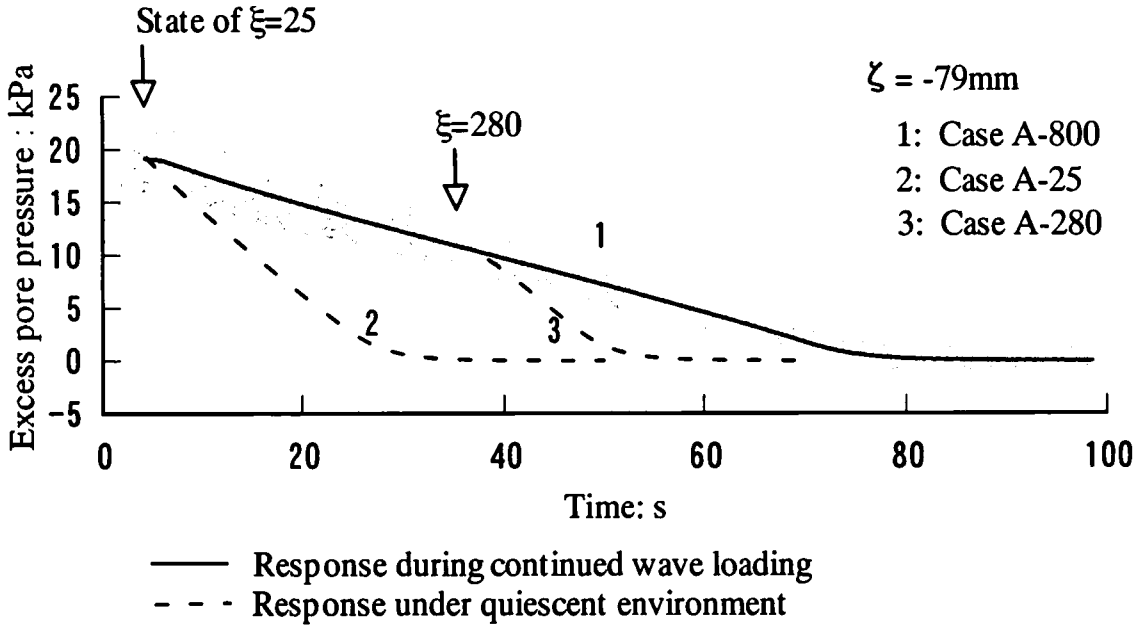

Fig. 3.16 Comparison between predicted rates of excess pore-pressure dissipation at a spatial point ζ=-79mm during continued wave loading and under quiescent environment

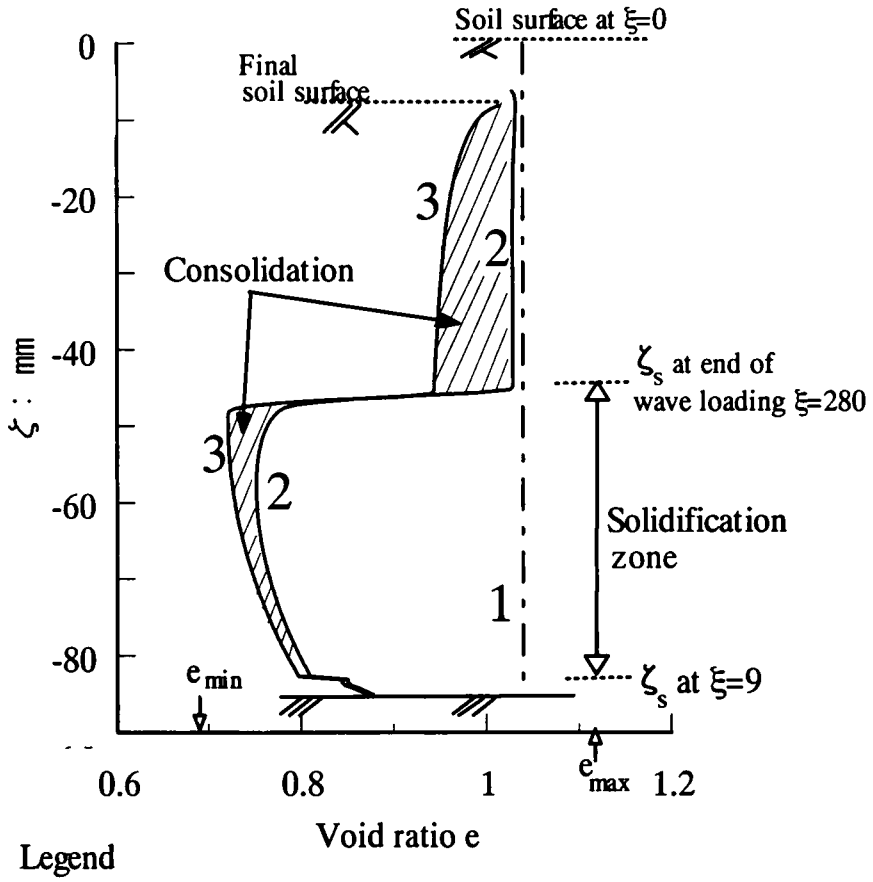

Fig. 3.17 Predicted pattern of the change in void ratio profile of sand bed in case A-280: Comparison between the amount of densification during consolidation in the soil region where the solidification has undergone and that where the solidification has not done.

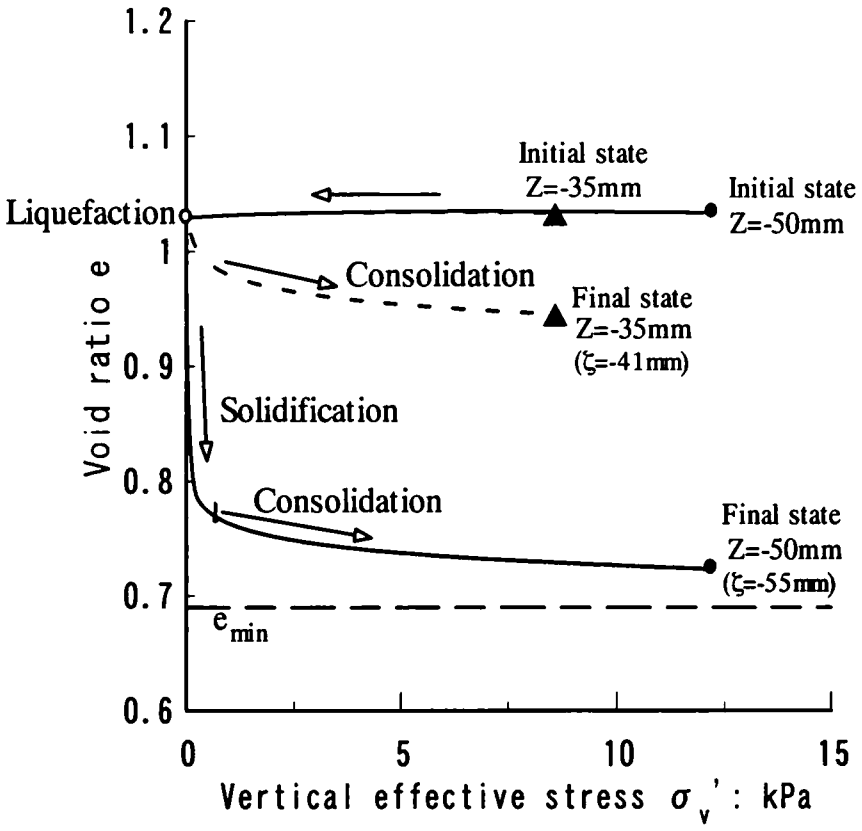

Fig. 3.18 Predicted σ_v'-e relation in case A-280: significant densification caused by contractancy due to wave loading in the solidification process

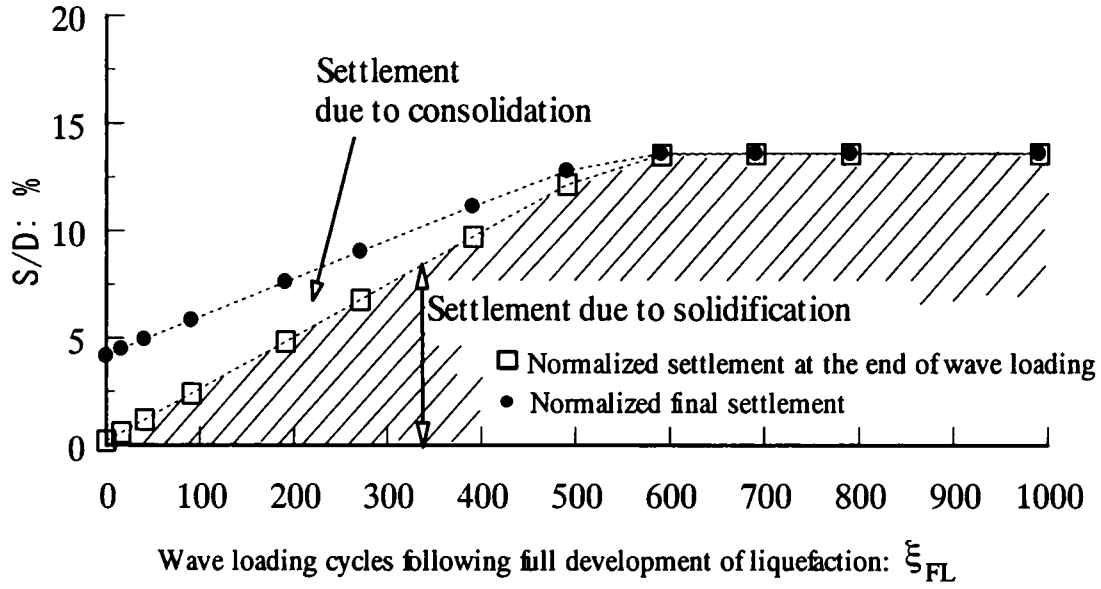

Fig. 3.19 Predicted increases in normalized settlement *S/D* with wave loading cycles following the full development of liquefaction zone

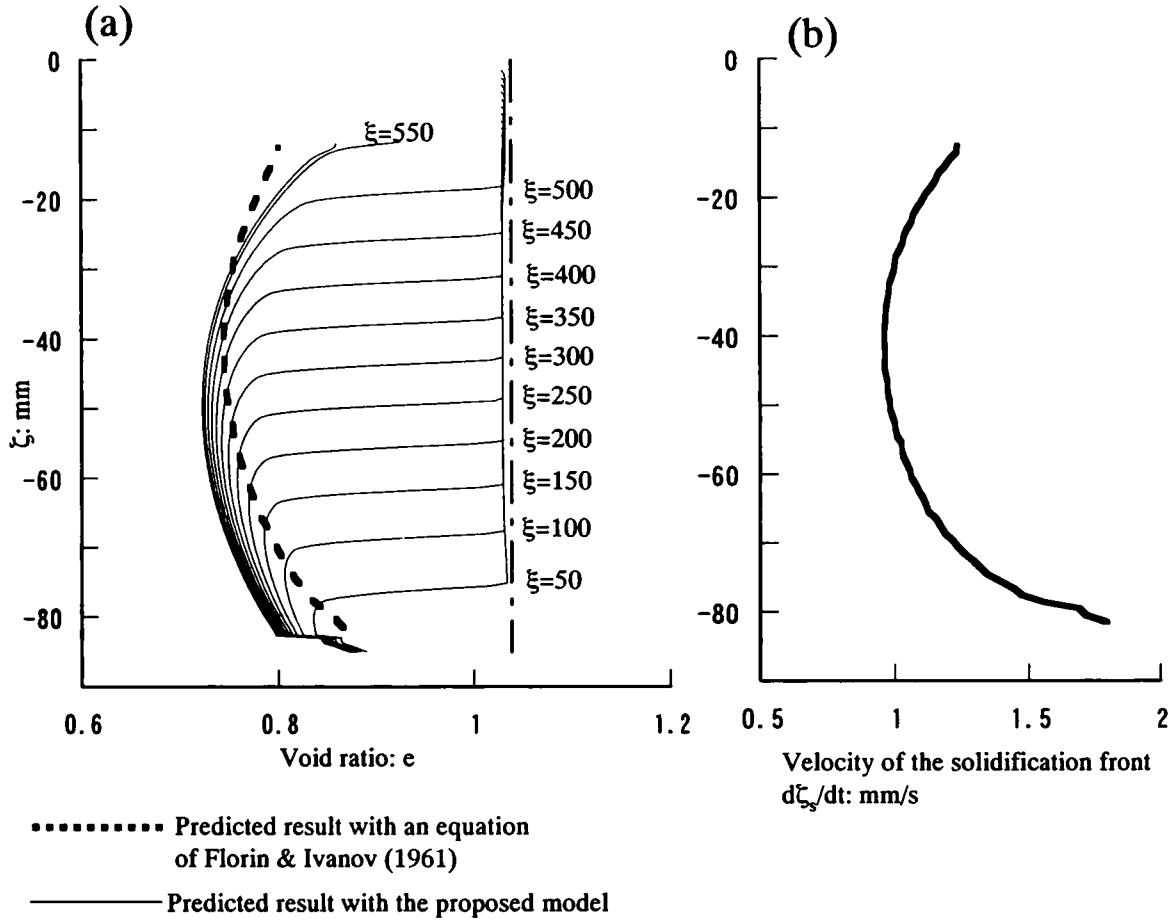

Fig. 3. 20 (a) Predicted temporal changes in void ratio profile in case A-800 and predicted void ratio profile obtained following an expression of Florin and Ivanov (1961), and (b) predicted changes in the velocity of the solidification front under advancement in case A-800

Chapter 4

Experimental studies of progressive liquefaction and solidification of sand beds in a centrifuge

4.1 INTRODUCTION

This chapter examines the progressive liquefaction and progressive solidification in liquefied sand on the basis of centrifugal wave-tank testing with viscous scaling. The experimental program included the following: (1) measurements of pore pressure responses indicating the progress of liquefaction and solidification fronts; (2) observing vibratory soil movements associated with the progress of the liquefaction and solidification fronts; and (3) assessing the degree of densification from changes in void ratio profiles with depth. Note that the changes in void ratio profiles of a given sand bed were estimated from results of the centrifuge upward seepage flow tests that were performed before and after a wave test. This methodology is based on correlation between the coefficient of permeability and the void ratio of a given sand (which is typified by equation (4.1)). For details of the procedure, refer to Appendix of this chapter.

This chapter is organized as follows. The experimental program and test procedure will first be described. The characteristics of progressive liquefaction will then be presented, focusing on the development of the vertical deformation of the liquefied soil in association with the advance of the liquefaction front. This will be followed by a discussion of solidification and densification in liquefied sand in the course of wave loading.

4.2 CENTRIFUGE WAVE TESTING AND EXPERIMENTAL PROGRAM

Seven wave tests were performed on the seven identical sand beds (test Nos. WJ09, WJ12, WJ16, WJ23, WJ40, WJ41, WJ42). All of the tests were carried out under a centrifuge acceleration of 30 g. Silicone oil with a viscosity of 30 cSt was used as the

pore fluid as well as the exterior fluid, in order to match the time scaling laws of soil consolidation and fluid-wave propagation. The number of wave loading cycles imposed, ξ_T, ranged from 23 to 1100 (Table 4.1). This allowed variations in the thickness of the soil region which experienced solidification.

The cross section of a wave tank used in the centrifuge wave testing is shown in Fig. 4.1. The wave tank is equipped with a reservoir that is connected to the base of the sediment trench through a solenoidal valve. An upward steady-state seepage flow test could be performed by opening the solenoidal valve, with a total head of the fluid in the reservoir being higher than that in the wave tank. The solenoidal valve was closed in wave loading stages in such a way that no fluid flow occurred through the base of the sand bed. The sand used in tests WJ09-WJ23 was Silica sand #7-Batch A (G_s=2.69, e_{max}=1.15, e_{min}=0.69 and D_{50}=0.14*mm*) and the sand used in tests WJ40-WJ42 was Silica sand #7-Batch B (G_s=2.69, e_{max}=1.18, e_{min}=0.69 and D_{50}=0.14*mm*). The sand beds formed had relative densities D_r of 29-41% and the initial soil depth D of 80-86*mm*. The fluid depth, H, was kept at 80*mm*. The wave paddle was excited at a frequency of 8*Hz*. The slotted partition was equipped for wave absorption purposes (Sekiguchi et al. 1998). The performance of the wave absorber when the dead-space length was 110*mm* was assessed by conducting a separate series of centrifuge wave tests with fluids overlying a rigid base. The measured reflection coefficient was equal to 0.16 (Miyamoto, 2000). Therefore, it can be said that essentially progressive waves were generated in the wave channel. The stroke of the wave paddle was selected so that the wave-induced cyclic stress ratios at the level of the soil surface χ_0 ($=\kappa_0 u_0/\gamma'$) were 0.13-0.16 and exceeded a critical value χ_{cr} beyond which liquefaction occurs (Sassa & Sekiguchi, 1999). For the Silica sand #7, the value χ_{cr} was equal to 0.11 (Miyamoto & Sekiguchi, 2001).

The wave-induced fluid pressures at the soil surface and the pore pressures in the soil bed were measured with pore-pressure transducers (PPTs). The PPTs were fixed in the sediment trench of the wave tank. Soil movements were captured using a high-speed CCD camera. Recently, observations of soil behaviour using high-speed CCD camera have been a useful technique in centrifugal dynamic tests (Miyamoto et al., 2000; Okamura et al., 2001).

4.3 PROGRESSIVE LIQUFACTION AND VERTICAL VIBRATION OF LIQUEFIED SAND

A typical set of experimental results from test WJ12 are discussed here. The measured time histories of the excess pore pressures at three different soil depths are shown in Fig.

4.2, together with the input waveform. Let us first look at the response at a shallow soil depth (ζ=-13*mm*) as shown in Fig. 4.2 (b). After 3 cycles of wave loading, the residual pore pressure reached the level of the initial vertical effective stress σ_{v0}', indicating the occurrence of liquefaction at this soil depth. In the course of wave loading, the liquefaction front advanced downwards (Figs. 4.2 (c) and (d)). A close observation of the waveform at ζ=-76*mm* for instance shows that the oscillatory pore pressure exhibited a significant amplification in association with the progress of the liquefaction front. The residual pore pressure at ζ=-76*mm* started dissipating from t=4000*ms* or so, indicating the occurrence of solidification at this soil depth. It is seen from the measured results in Fig. 4.2 and the predicted results in Fig. 3.8 in chapter 3 that the measured patterns of developments in residual as well as oscillatory pore pressures are consistent with the predicted ones.

The vertical movements of the soil surface in test WJ12 were recorded in flight by using the high-speed CCD camera at an image rate of 250 frames/s. The developments of the vertical displacement with time at three representative locations of the soil surface depicted in Fig. 4.3. Let us first look at Fig. 4.3 (a) for the x=-40*mm* location. No significant movement occurred before the soil bed underwent liquefaction. However, upon the occurrence of liquefaction at the shallow soil depth, the surface of the soil bed exhibited a significant vibratory motion. The amplitude of the vibratory motion increased markedly in association with the progress of the liquefaction front. After the end of progressive liquefaction, the amplitude of the soil vibration remained practically constant in the recording period. Essentially the same patterns of vertical soil movements were observed at the other two locations, as shown in Figs 4.3 (b) and (c), although the amplitudes of the soil vibratory movements were somewhat different from each other.

The vibratory motion of the soil surface was a consequence of liquefaction. Indeed, an idea of the fluidity of the liquefied soil can readily be obtained from Fig. 4.4. In these figures the images of the wavy motion of the fluid-soil interface at three different phases are shown. The averaged value of the measured amplitudes of vertical movements at these locations, a_0, was equal to 4.4*mm*. This provides a measure of shear strain amplitude equal to $2a_0/L$=1.7%, where L is the wavelength.

The measured consequence of vertical vibration of liquefied sand described above conforms well to the predicted results that were plotted in Fig. 3.11 in chapter 3. The measured shear strain amplitude of 1.7% in the entirely liquefied soil bed is consistent with the predicted value of 2.4%, emphasizing the high fluidity of liquefied soil.

4.4 PROGRESSIVE SOLIDIFICATION AND DENSIFICATION IN LIQUEFIED SAND

A typical set of experimental results from test WJ40 are discussed here. The measured time histories of the wave-induced pore pressure fluctuations at different depths in test WJ40 are shown in Fig. 4.5, together with the input waveform. At 7 cycles of wave loading (t=1.9s), liquefaction extended to the bottom layer of the soil bed (Fig. 4.5 (e)). The residual pore pressure at the bottom of the soil bed started dissipating at the 36th wave loading cycle (t=6 s) or so, indicating the start of the solidification process. In the course of continued wave loading, the solidification front advanced upward (See Fig. 4.5 (d), (c) and (b)). It is of interest to mention that the advance of the solidification front was accompanied by gradual reduction in the amplitudes of the oscillatory pore pressures, $u_e^{(1)}$. The measured responses of pore pressure are consistent with the predicted results, with respect to both the residual and oscillatory pore pressures.

The measured progress of liquefaction and solidification fronts in test WJ40 is shown in Fig. 4.6 (a). Following the occurrence of liquefaction at the shallow soil depth, the liquefaction front rapidly advanced downwards and reached the deepest level at ζ=-82mm. Note that with the continued wave loading, the solidification front advanced upward to a final level of the soil surface indicated by an asterisk. Here S_f represents the magnitude of the final surface settlement that was determined by a surveying after the stopping of the centrifuge.

The vibratory movements of the soil surface during wave loading in test WJ40 were recorded in flight by using the CCD camera at a recording rate of 60 frames/s. The measured envelop of vertical movements of the soil surface during the wave loading are shown in Fig. 4.6 (b). It can be noted that the soil surface started vibrating upon the occurrence of liquefaction at the shallow soil depth and the amplitude of it, a_0, grew with increasing extent of the liquefied zone. After the full developments of the liquefied zone, the amplitude a_0 decreased in association with the progress of the solidification front. The settlement of the soil surface gradually occurred with the advance of the solidification front. The measured consequence of progressive solidification conforms well to the predicted results that were plotted in Fig. 3.14 in chapter 3.

The void ratio profiles in the soil bed determined before and after wave test WJ40 are compared in Fig. 4.7. As mentioned earlier, these profiles obtained by processing the results of the two upward seepage flow tests that were performed before and after the wave test. It is important to note that the difference between the two profiles at a given

depth ζ represents the degree of densification which was brought about at that depth in the given wave loading history. Remember that the solidification front in test WJ40 reached the soil surface during wave loading period. It is evident that the region which experienced solidification underwent a significant densification. In the light of the theoretical prediction described in chapter 3, the measured significant densification is associated to the contribution of the contractancy of the sand.

Let us compare the measured rate of the excess pore-pressure dissipation in test WJ40 during continued wave loading with those under quiescent environment in wave tests WJ41and WJ42 (Fig. 4.8). In this figure, the time histories of the excess pore-pressures at the soil depth ζ=-82*mm* are depicted. In tests WJ41, the wave loading was stopped at ξ=23, allowing the excess pore-pressure to dissipate under a quiescent environment. This process was nothing but a well-known consolidation process. In test WJ42, the wave loading was stopped at ξ=285, permitting consolidation to occur. It is seen that the excess pore pressure dissipation due to consolidation took place much faster than that associated with solidification. This observed trend is consistent with what has been predicted in Fig. 3.16 in chapter 3.

Let us examine the degrees of densification which were brought about during and after the cessation of wave loading. The void ratio profiles in the soil bed in test WJ42 determined before and after the wave test are shown in Fig. 4.9. In test WJ42, the solidification extended from the bottom of the soil bed to the middle soil depth. It is evident that a marked densification was brought about in the solidification zone. The region above the solidification zone underwent densification, but the degree of the densification was only 1/3～1/4 of the densification that took place in the solidification zone. The difference between the degree of densification due to the solidification and that due to the consolidation has been captured by the prediction (Fig. 3.17 in chapter 3).

All the wave tests performed indicate that the final surface settlements S_f tend to increase with increasing wave loading cycle ξ_T. A close examination of this trend led us to plot the normalized surface settlement S_f/D against ξ_{FL} (Fig. 4.10). Here ξ_{FL} is wave loading cycles following the full development of the liquefied zone. In this figure, the predicted results with D_{r0} being varied between 29% and 41% are also shown for comparison purposes. It is seen that the experimental data points plot in a manner which is in general agreement with the predicted pattern. It is important in this respect to note that (1) when the value of ξ_{FL} is smaller than 600 or so, the normalized final settlement S_f/D is nearly proportional to ξ_{FL} and that (2) when ξ_{FL} is larger than about 600, S_f/D is nearly constant. In the light of theoretical prediction, the final settlement varies

depending on the relative importance of solidification and consolidation. Namely, as the settlement due to solidification is more dominant with increasing ξ_{FL} than that due to consolidation, the final settlement is more marked. Note that, if the value of ξ_{FL} is large enough for the solidification zone to extend to the soil surface, the final settlement corresponds to the settlement due to solidification and levels off irrespective of ξ_{FL}.

4.5 CONCLUSIONS

The characteristics of progressive liquefaction and progressive solidification in liquefied sand have been discussed based on the centrifugal wave testing with viscous scaling. The principal conclusions obtained from the present study may be summarized as follows:

(a) The progressive nature of liquefaction was observed in detail with the application of a high-speed CCD camera to centrifuge wave testing, as well as with pore pressure measurements. The progressive liquefaction was well reflected in the vertical vibration of the liquefied soil. In fact, when liquefaction occurred, the sand surface started vibrating and the amplitude of the soil vibration increased markedly with the downward advance of the liquefaction front. These measured features of progressive liquefaction conforms well to the predicted results presented in chapter 3, which emphasizes the high fluidity of liquefied soil.

(b) The advance of the solidification front in the course of wave loading was observed in the cases where the liquefied sand layer continued to be subjected to severe wave loading. In fact, after the progressive liquefaction, the residual pore pressure at the bottom of the liquefied sand started dissipating and the solidification front advanced to the soil surface in the course of wave loading.

(c) The observation of the soil surface with CCD camera showed that the vibratory movement of the soil surface decreased in association with the progressive solidification. This observation emphasizes the relation between the depth of liquefaction and the vertical vibration of the liquefied soil.

(d) The degrees of densification in sand beds were estimated from results of the centrifuge upward seepage flow tests that were performed before and after a wave test. It was observed that the densification due to the solidification was more significant than the densification due to the consolidation following liquefaction under a quiescent environment.

APPENDIX PROCEDURE FOR ESTIMATING VOID RATIO PROFILES FROM UPWARD SEEPAGE FLOW

It is known that the coefficient of permeability of sand, k, depends on the void ratio e, and that the following form of correlation holds true (Taylor, 1948).

$$k = C_f \frac{e^3}{1+e} \tag{4.1}$$

where C_f is a parameter which depends on the grain size, the viscosity of pore fluid and the arrangement of sand grains. Equation (4.1) tells us that if the values of k and C_f are known, then one can evaluate the corresponding value of the void ratio e.

Consider a soil bed subjected to upward seepage flow under steady-state conditions. It then follows that

$$q = k \cdot i \cdot A_t \tag{4.2}$$

where q is the fluid discharge, i is the hydraulic gradient and A_t is the area of the sand bed which is perpendicular to the direction of the fluid flow. The fluid discharge may be directly determined by measuring the rate of drop in the level of the fluid in the reservoir. Namely,

$$q = \frac{1}{\gamma_f} \cdot \frac{du_r}{dt} \cdot A_r \tag{4.3}$$

where γ_f is the unit weight of the fluid, u_r the static hydraulic pressure in the reservoir and A_r is the area of the reservoir. If the steady-state pore pressures are measured at two different soil depths, then the hydraulic gradient, i, at the midpoint reads

$$i = \frac{1}{\gamma_f} \cdot \frac{u_{us}(j) - u_{us}(j-1)}{\Delta l} \tag{4.4}$$

where $u_{us}(j)$ stands for the excess pore pressure measured at the jth soil depth and Δl is the vertical distance between the jth and (j-1)th depths of measurement.

Note that the measurement of the settlement of the soil surface gives rise to the value

of the average void ratio, e_{ave} in the soil bed. The value of e_{ave} may be related to the local void ratios, e_j, in the following form:

$$e_{ave} = \frac{\sum l_j}{\sum \{l_j/(1+e_j)\}} - 1 \tag{4.5}$$

By noting that equation (4.1) holds true for each soil layer and by solving equations (4.1) and equation (4.5) simultaneously, one can determine a profile of void ratios together with the value of C_f.

References

Okamura, M., Matsuo, O. & Tamoto, S. (2001). A high frame rate image acquisition system for dynamic centrifuge tests. *Internatinal Journal of Physical Modelling in Geotechnics*, **1**, No. 1, 71-76.

Miyamoto, J. (2000). *Studies of wave-induced liquefaction and flow deformation of sand beds*. MEng. Thesis, Kyoto University (*in Japanese*).

Miyamoto, J., Sassa, S. & Sekiguchi, H. (2000). Wave-induced liquefaction and flow deformation in sand beds. *Proceedings of Coastal Engineering, JSCE,* **47**, No.2, 921-925 (*in Japanese*).

Miyamoto, J. & Sekiguchi, H. (2001). Effect of wave loading history on the initiation and development of liquefaction in sand beds. *Proceedings of the 4th International Conference on Micromechanics of Granular Media, Powders and Grains 2001*, Sendai, 259-262.

Sassa, S. & Sekiguchi, H. (1999). Wave-induced liquefaction of beds of sand in a centrifuge. *Geotechnique,* **49**, No.5, 621-638.

Sekiguchi, H., Kita, K., Sassa, S. & Shimamura, T. (1998). Generation of progressive fluid waves in a geo-centrifuge. *Geotechnical Testing Journal*, **21**, No. 2, 95-101.

Taylor, D. W. (1948). *Fundamentals of Soil Mechanics*, John Wiley & Sons. 111-112.

Table 4.1 Details of centrifuge wave tests on loose deposits of sand

Test number	ξ_T	Dr: %	χ_0	D: mm
WJ09	86	33	0.13	85
WJ12	96	34	0.15	80
WJ16	90	33	0.16	85
WJ23	1100	41	0.15	85
WJ40	800	29	0.15	85
WJ41	23	40	0.15	85
WJ42	285	37	0.15	86

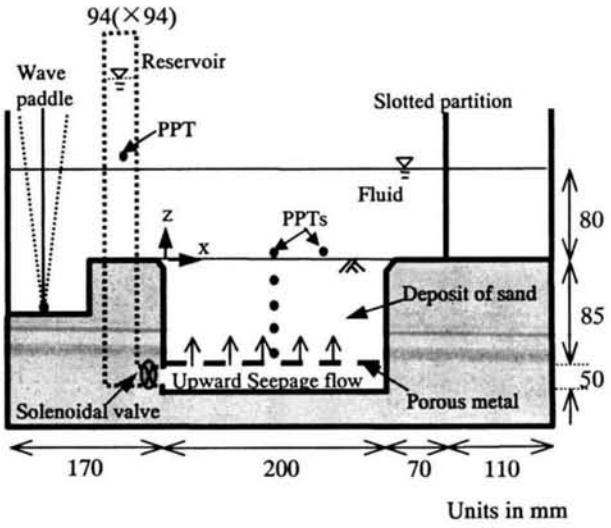

Fig. 4.1 Cross section through a wave tank for use in a geo-centrifuge

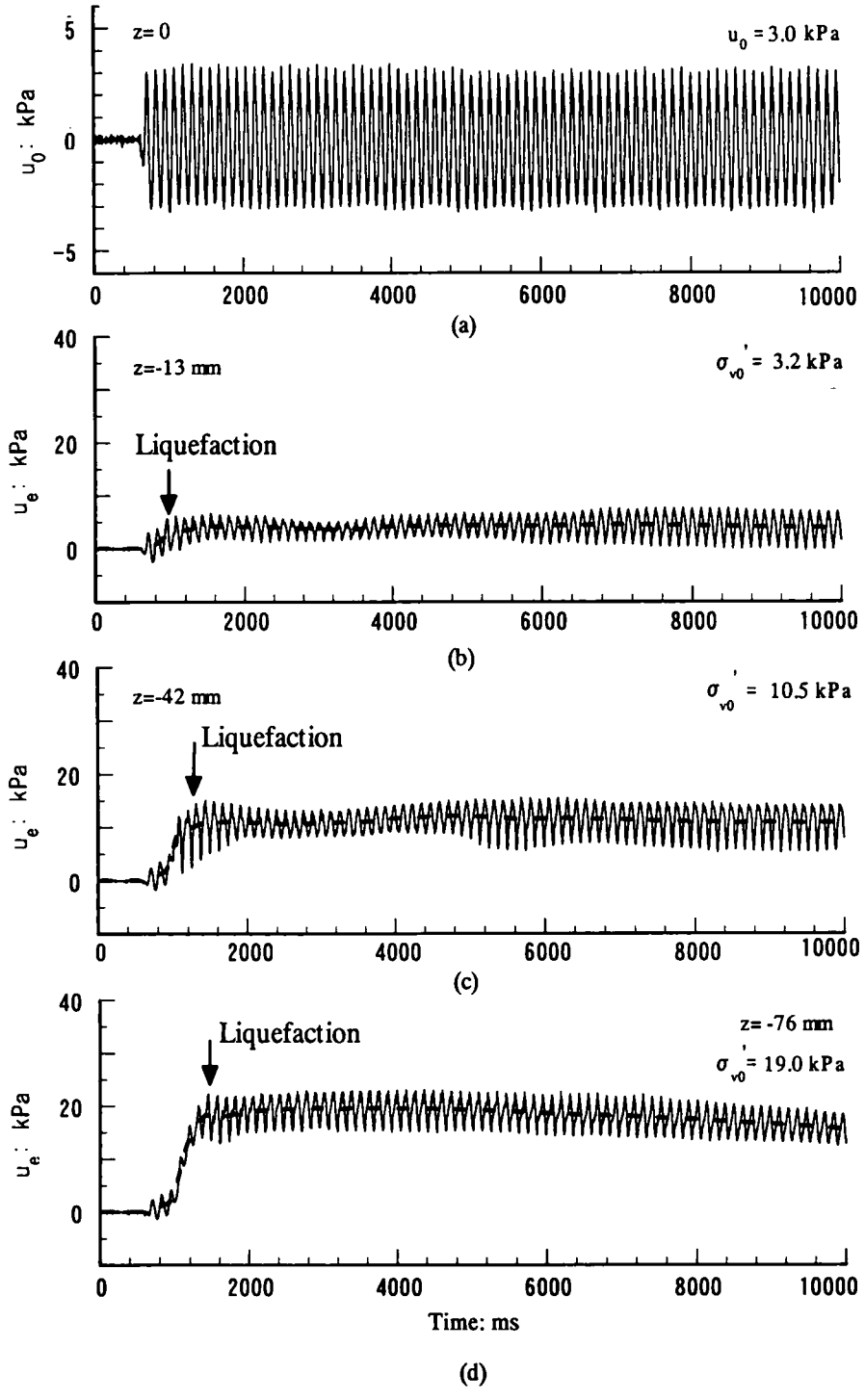

Fig. 4.2 Measured waveforms in wave test WJ12: time histories of (a) wave pressure acting on the location of initial soil surface; and (b), (c) and (d) excess pore pressures at different spatial points.

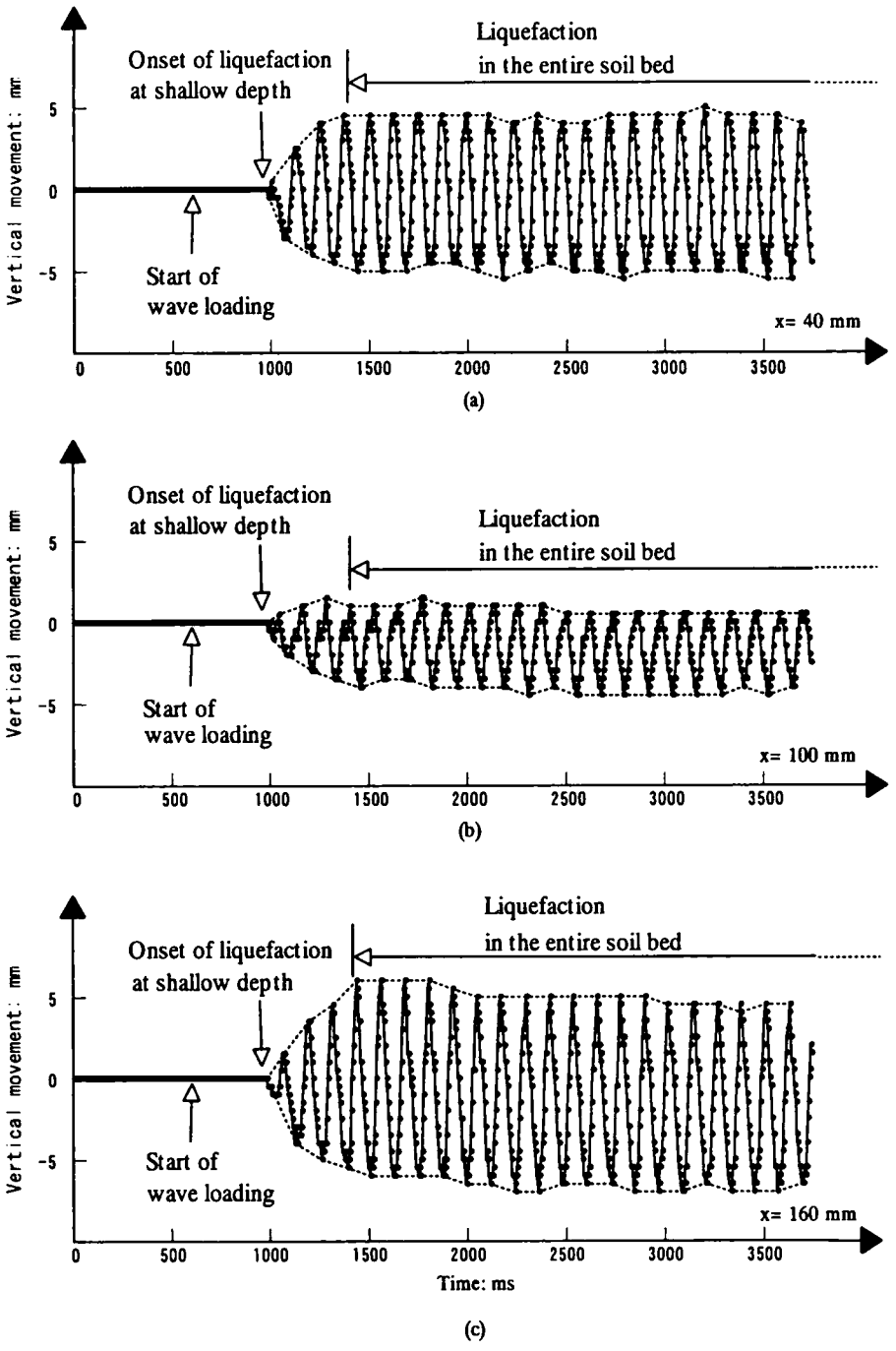

Fig. 4.3 Measured time histories of vertical movement of soil surface in wave test WJ12

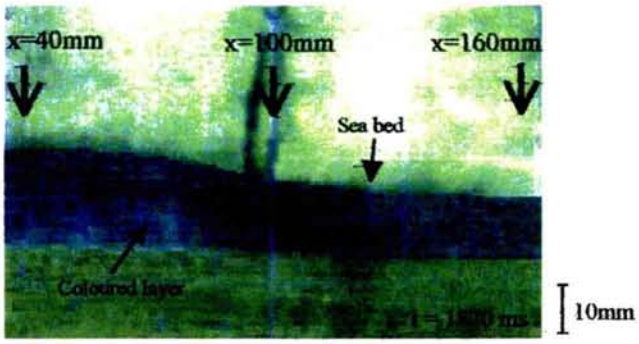

(a)

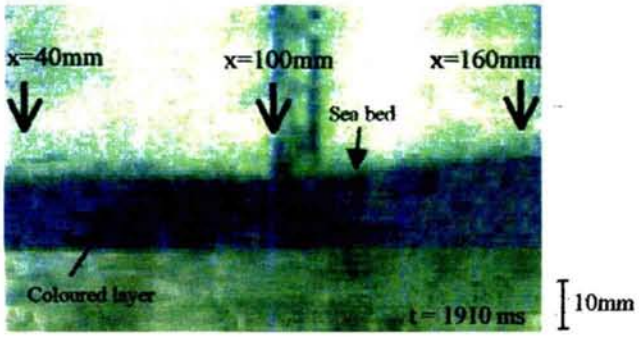

(b)

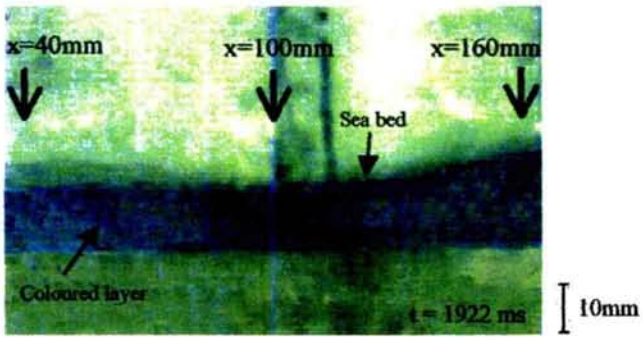

(c)

Fig. 4.4 Surface profiles of entirely liquefied soil bed observed at three different phases

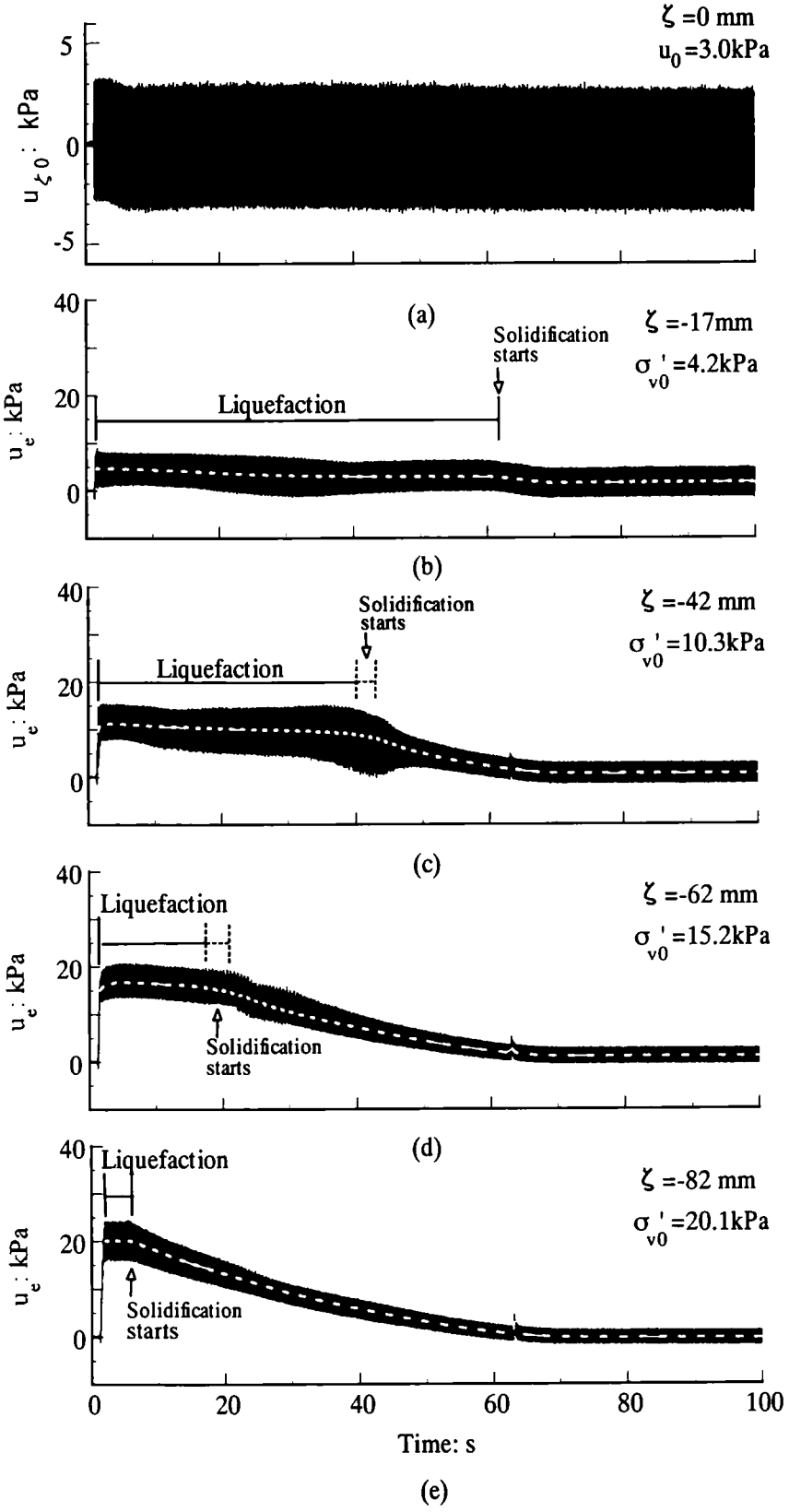

Fig. 4.5 Measured waveforms in wave test WJ40: time histories of (a) wave pressure acting on the location of initial soil surface; and (b), (c), (d) and (e) excess pore pressures at different spatial points.

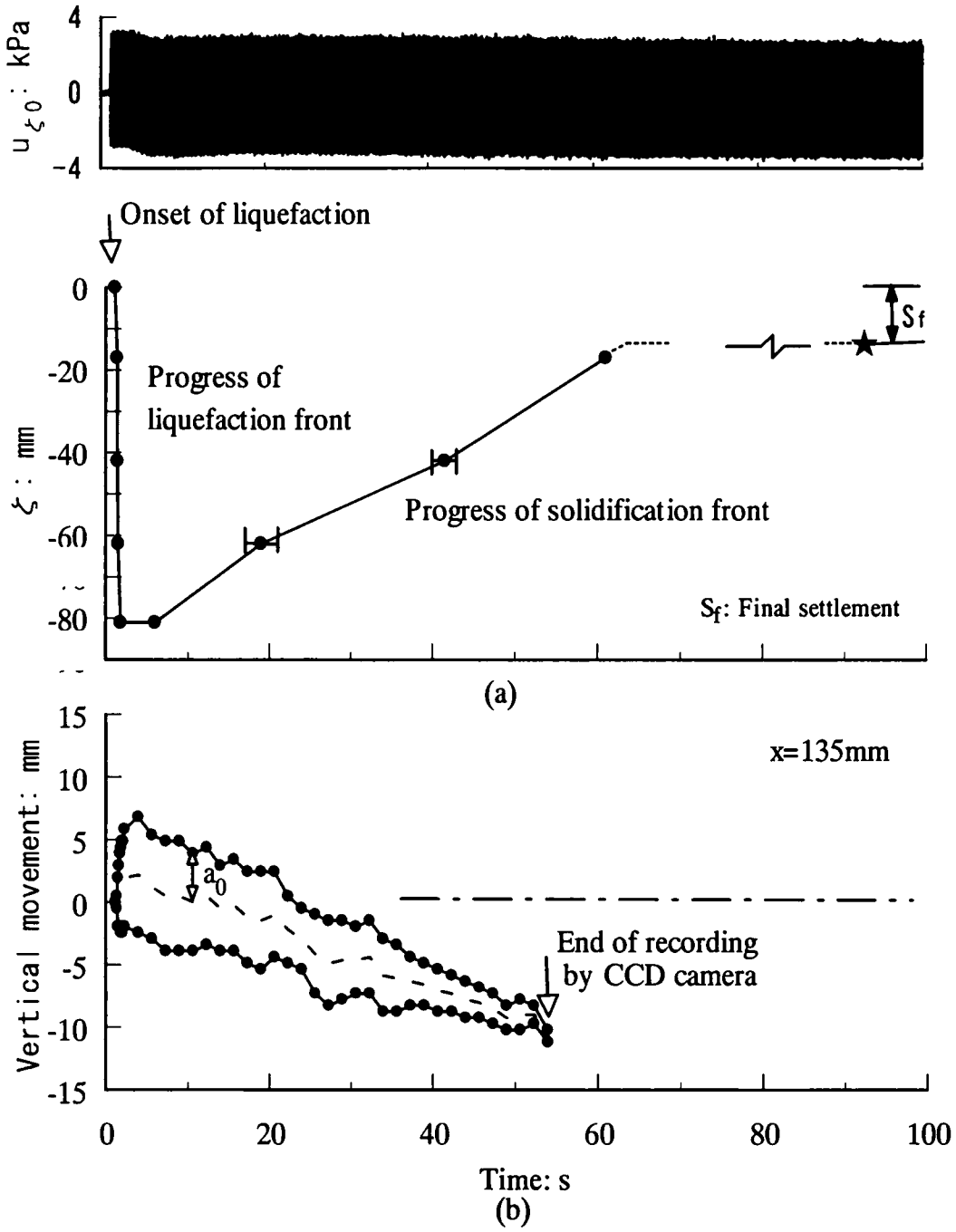

Fig. 4.6 (a) Measured progresses in liquefaction and solidification fronts in wave test WJ40 and (b) associated, measured vertical movements of the soil surface

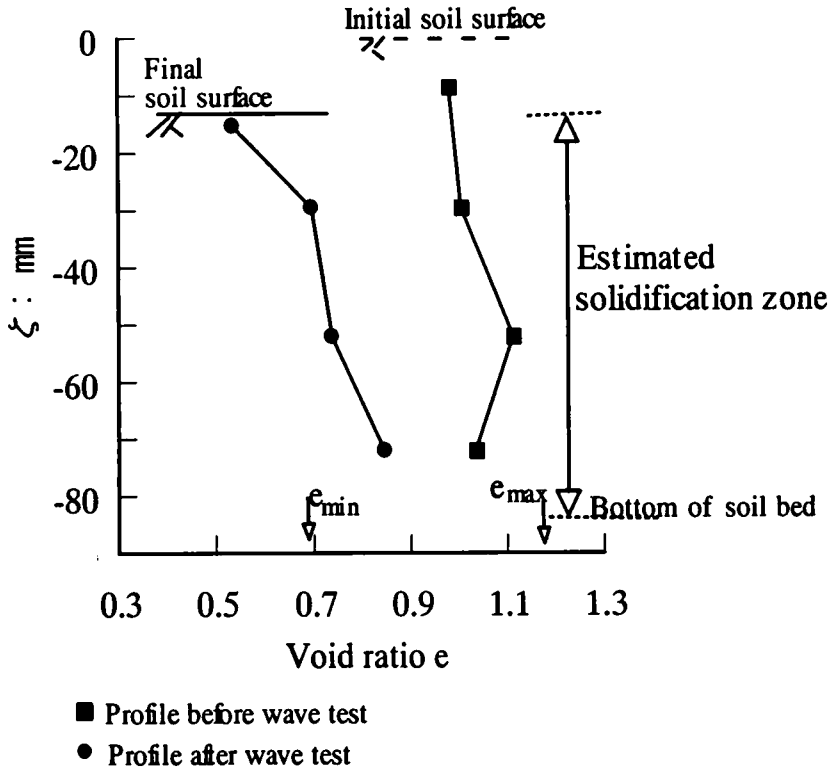

Fig. 4.7 Measured changes in void ratio profile of sand bed in test WJ40: significant densification brought about in solidification zone

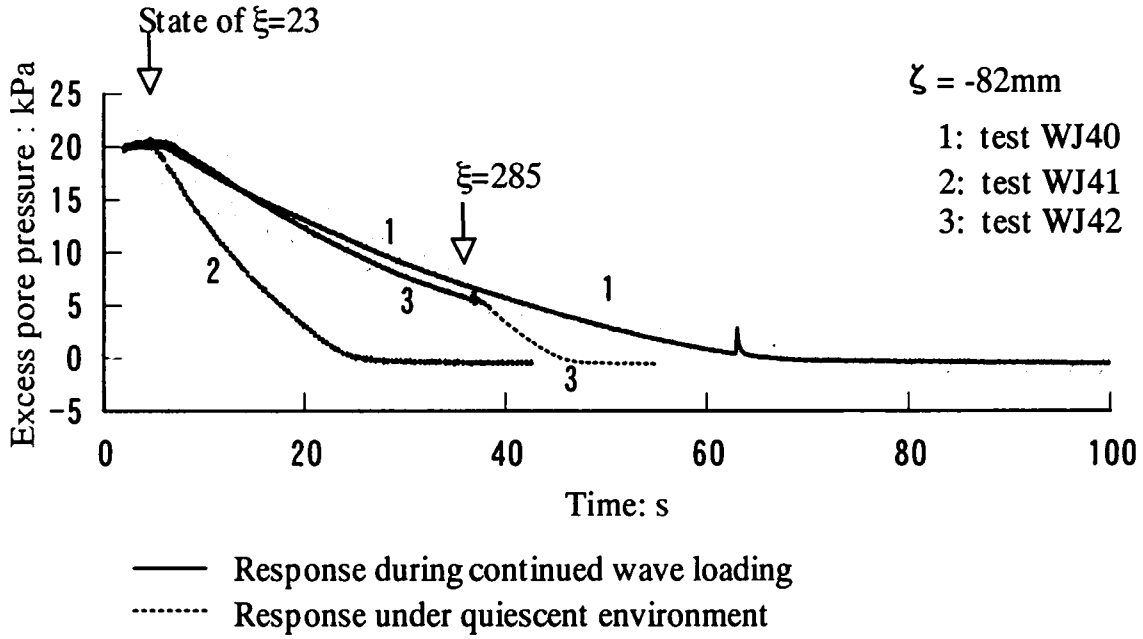

Fig. 4.8 Comparison between measured rates of excess pore-pressure dissipation at a spatial point ζ=-82mm during continued wave loading and under quiescent environment

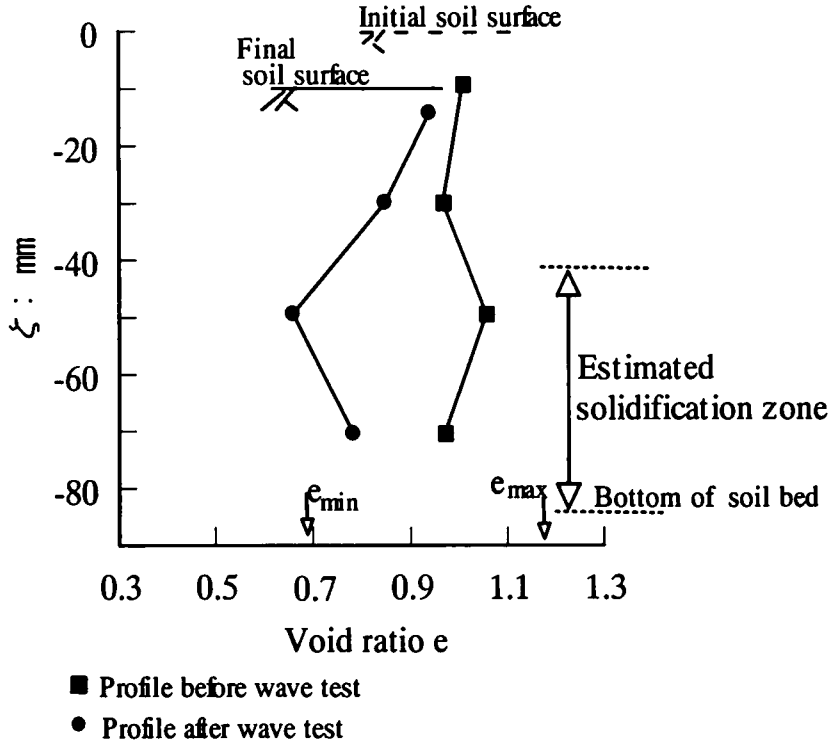

Fig. 4.9 Measured changes in void ratio profile of sand bed in test WJ42: comparison between densification in solidification zone and in the region which did not experience solidification

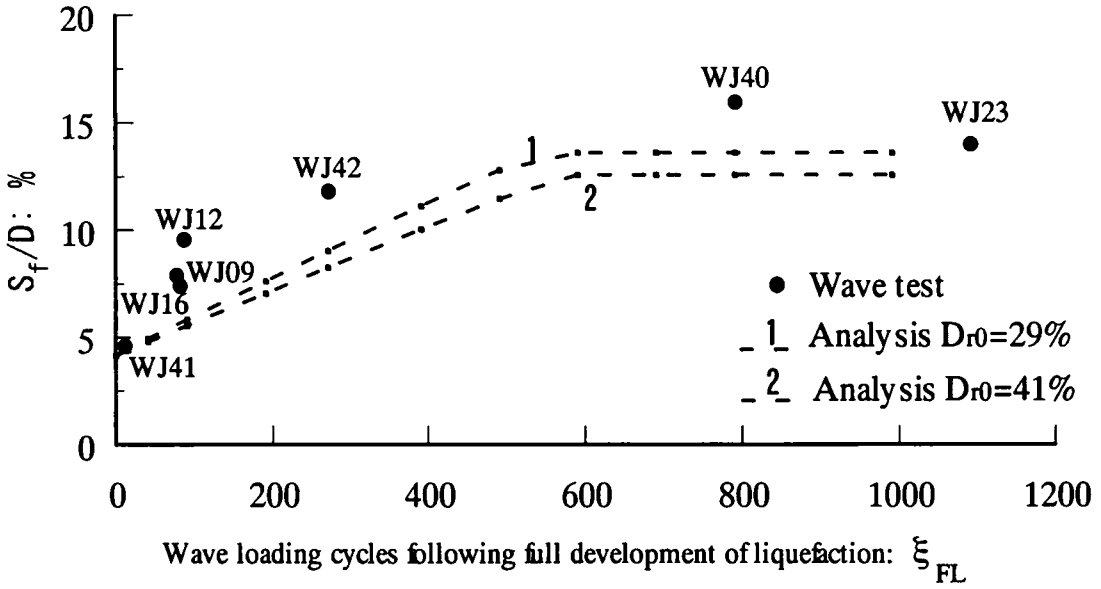

Fig. 4.10 Measured variations of normalized settlement S_f/D at the end of consolidation with wave loading cycles following the full development of liquefaction zone

Chapter 5

Effects of wave loading history on liquefaction in sand beds

5.1 INTRODUCTION

The behaviour of beds of sand under fluid wave trains takes a variety of forms, depending on the shear resistance of the soil, on the wave severity and on the duration of wave loading. The characteristics of liquefaction in loosely packed, fresh deposits of sand under fluid waves were discussed by Sassa & Sekiguchi (1999) based on results from centrifugal wave-tank testing, and it was found that there exists a critical cyclic stress ratio, χ_{cr}, beyond which liquefaction occurs.

The shearing resistance of soil is in general history-dependent. Thus any preshearing due to wave loading may influence the behaviour of a soil bed under the subsequent wave loading. The preshearing effect may bring about the variations in the critical cyclic stress ratio or in the extent of liquefaction. The effect of loading history on seismic liquefaction of sands has been investigated many investigators (Finn et al., 1970; Seed et al., 1977 among others). However, more development is necessary to achieve a full understanding of wave-loading history effect.

This chapter will discuss the effects of wave loading history upon the performance of sand beds at the subsequent wave loading stage. The organization of this chapter is as follows. The effect of severity of wave loading acted as preshearing on the liquefaction resistance of sand beds at subsequent wave loading stage will first be discussed on the basis of centrifugal wave testing, focusing on distinguishing preshering effect into low-level preshearing and high-level preshearing. Then, the influence of number of wave loading cycles on resistance to liquefaction at subsequent wave loading stage will be investigated using centrifuge modelling as well as a simple yet workable model. This will be followed by predictions regarding the behaviour of a sand bed that is subjected to a complex wave loading history that consists of groups of severe wave loading.

5.2 INFLUENCE OF SEVERITY OF WAVE LOADING ON RESISTANCE TO LIQUEFACTION AT SUBSEQUENT WAVE LOADING STAGE

5.2.1 Experimental program and test procedure

A wave tank used in centrifuge wave tests is shown in Fig. 5.1. Waves were generated by using a quasi-flap type wavemaker that was driven by an AC servo-motor. The wave-generating system used by Sekiguchi et al. (1998) and Saasa & Sekiguchi (1999) permitted a soil bed to be subjected to regular waves of constant amplitude. However, waves of varying amplitude were unable to be generated. This limitation has been overcome by introducing a feedback system where the data from a laser-type displacement transducer (designated LDT1) was utilized to continuously vary the stroke of the wave paddle without stopping the centrifuge. This allowed the reproduction of a sequence of storm waves starting from relatively small waves and incrementing to very intense ones.

Three sets of centrifuge wave tests were performed on fresh deposits of fine-grained sand (Table 5.1-5.3). All of the tests were carried out under a centrifuge acceleration of 30 g. Silicone oil with a viscosity of 30 cSt was used as the pore fluid as well as the exterior fluid over the soil surface, in order to match the time scaling laws of soil consolidation and fluid-wave propagation. The sand used was Silica sand #7-Batch C (G_s=2.69, e_{max}=1.28, e_{min}=0.76, D_{50}=0.14*mm*). The sand beds formed had relative densities D_r of 34-42% and the initial soil depths D of 84-86*mm*. The fluid depth, H, was kept at 80*mm*. The wave paddle was excited at a frequency of 8*Hz*. The slotted vertical partition was installed for wave absorption purposes, and essentially progressive waves were generated in the wave tank. Wave pressures at the soil surface and wave-induced pore pressures in the soil bed were measured with pore pressure transducers (PPTs). Elevations of the soil surface were continuously measured using LDT2.

The first set of wave tests (Series I) included three separate tests in which the sand beds were subjected to wave trains of constant amplitude (Table 5.1). Series I examined critical cyclic stress ratio for the fresh deposits of Silica sand #7, χ_{cr}, beyond which liquefaction occurs. In these wave tests, the amplitude of fluid pressure acting on a soil surface, u_0, varied as listed in Table 5.1. In this table, χ_0 is defined as $\kappa_0 u_0/\gamma'$ in which κ_0 is the wave number and γ' represents the submerged unit weight of the soil.

The second set of wave tests (Series II) consisted of two separate tests with wave

trains of different rates of increasing amplitude (Table 5.2). Series II examined the effect of rate of increase in wave amplitude on the soil response. Time histories of wave-induced pressure fluctuations at the soil surface, u_0, in these tests are shown in Fig. 5.2. In each test, wave loading consisted of two phases: a linearly increasing amplitude phase and a constant-amplitude phase. The rates of increase in wave amplitude were different in these tests.

The third set of wave tests (Series III) included four separate tests in which sand beds were subjected to two stage wave loading with an intervening quiescent phase (Table 5.3). Series III investigated the effect of preshearing on the soil response. Time histories of wave induced pressure fluctuations at the soil surface, u_0, in these tests are shown in Fig. 5.3. The sequence of wave loading in tests WJ36, WJ39 and WJ34 consisted of two wave loading stages and an intervening quiescent stage. The loading stage 1 acted as preshearing relative to the subsequent wave loading (loading stage 2). The rates of increase in wave amplitude in loading stage 2 of these tests were selected to be the same as that in test WJ32, which was a reference test with no preshearing. Note that in loading stage 1 in tests WJ36 (or WJ39) and WJ34, where constant-amplitude waves were generated, the amplitudes of wave pressure at the soil surface, u_0, are different (u_0=1.1 kPa in WJ 36; u_0=2.2 kPa in WJ 34). The corresponding responses of pore pressure in wave loading stage 1 are typified in Fig. 5.4. In test WJ36, liquefaction did not occur, but in test WJ34 liquefaction did. For the convenience of later discussion, cases where the cyclic stress ratio, χ_0, remained below the critical stress ratio χ_{cr} ($\chi_0<\chi_{cr}$) in loading stage 1, such as in test WJ36, are referred to as low-level preshearing. Cases with $\chi_0>\chi_{cr}$, such as in test WJ34, are referred to as high-level preshearing.

5.2.2 Effect of rate of increase in wave amplitude on soil response

The effects of the rate of increase in wave amplitude on soil behaviour can be seen from Fig. 5.5. It is seen from the results of constant-amplitude cases that critical cyclic stress ratio, χ_{cr}, for the fresh deposits of Silica sand #7 is equal to 0.11. Note here that the state of u_e/σ_{v0}'=1.0 indicates the occurrence of liquefaction at a soil depth under discussion. It is seen that in test WJ31 where the wave amplitude was slowly increased with time, liquefaction occurred under a significantly larger level of wave severity than in test WJ32 where the wave amplitude was increased rapidly. This difference in liquefaction resistance may be ascribed to the partial drainage effect during wave loading.

The value of χ_{cr} obtained from test WJ32 is the same as that obtained from constant-amplitude cases. It is instructive to mention that the liquefaction resistance of

fresh deposits of sand could be assessed by only one wave test if the wave amplitude is increased in the same rate as that in WJ32.

Developments of residual pore pressure at two different soil depths in test WJ 32 are seen in Fig. 5.6. It is seen that upon the occurrence of liquefaction at shallow soil depth, residual pore pressure at deeper soil depth started to build up markedly, leading up to liquefaction. Note that in the process concerned, the rate of increase in wave-amplitude was kept constant. This phenomena is closely linked with the downward propagation of the liquefaction front (chapters 3 and 4).

5.2.3 Effect of preshearing on the liquefaction resistance

The effect of low-level preshearing on the behaviour of soil at shallow depth will be discussed first. In Fig. 5.7, the developments of pore pressure ratios in wave loading stage 2 in tests WJ36 and WJ 39 are compared with that of test WJ32 which had not been subjected to preshearing. It is noteworthy that the liquefaction resistance of the soil bed was significantly improved by the low-level preshearing.

The measured results of the soil surface elevation using LDT2, expressed in terms of relative density, fluctuated between 33-36 % before wave loading stage 1 in test WJ 36, and after loading stage 1, the measured relative densities fluctuated in the range of 32-37 %. Considering that the resolution of LDT2 was ± 2.5 % in terms of relative density, it may be concluded that the densification in the sand bed due to the low-level preshearing was of a marginally discernible extent, if any.

The development of pore pressure ratio in wave loading stage 2 of test WJ34 is shown in Fig. 5.8. In this figure the performance in wave test WJ32 with no preshearing is also plotted. It is seen that the development of u_e/σ_{v0}' against χ_0 in wave test WJ34 is almost the same as that in wave test WJ32.

The results of measurement of the soil surface elevation by means of LDT2 are shown in Fig. 5.9, where D_0 represents the original thickness of the sand bed and s is settlement of soil surface. It is evident that the high-level preshearing gave rise to a significant densification in the soil bed prior to the commencement of loading stage 2. However, this appreciable overall densification in the soil bed did not improve the liquefaction resistance, as discussed in Fig. 5.8.

5.2.4 Discussion

The consequences of preshearing effects observed from Series III are summarized in Fig. 5.10. The low-level preshearing yielded very little or no densification at the following consolidation phase. However, the observed increase in the resistance to liquefaction under the subsequent wave loading was marked. In contrast, the high-level preshearing gave rise to little or no increase in the liquefaction resistance, even though the overall relative density of the sand bed had increased from 34% to 55% during a consolidation phase prior to the wave reloading stage.

The relation between the liquefaction resistance and relative density, D_r, of the sand was presented by Tatsuoka et al. (1986) (Fig. 5.11). It is of interest to mention that when D_r of sand is less than 75%, the increase in the liquefaction resistance is small, and that the liquefaction resistance of sand significantly increases beyond D_r=77% or so.

However, a set of centrifuge wave tank tests with high-level presheairng applied (Sassa & Sekiguchi, 1998; Sassa & Sekiguchi, 1999) showed that a liquefied soil bed repeatedly underwent liquefaction in the wave reloading stages, although the overall relative density of the soil bed became larger than 80% (Fig. 5.12).

In order to gain a better understanding of the effect of high-level preshearing on the liquefaction resistance, the associated changes in relative density profile of sand beds due to high-level presheairng need to be investigated. In the next section, the effect of hifg-level preshearing is investigated in view of changes in void ratio profile.

5.3 INFLUENCE OF NUMBER OF WAVE LOADING CYCLES ON RESISTANCE TO LIQUEFACTION AT SUBSEQUENT WAVE LOADING STAGE

This section will discuss the effect of varying the duration of high-level preshearing in sand beds upon their performance at the subsequent wave loading stage. For this purpose, results from a range of centrifugal wave tank tests on sand deposits will first be discussed. Then, the analytical model proposed in chapter 3 will be applied in order to reproduce the observed performance of high-level presheairng.

5.3.1 Experimental program and test procedure

Three sets of centrifuge tests (Nos. WJ40, 41, 42) were performed on initially loosely packed deposits of sand. All of the tests were carried out under a centrifugal

acceleration of 30 g. Silicone oil with a viscosity of 30 cSt was used as the pore fluid as well as the exterior fluid, in order to match the time scaling laws of soil consolidation and fluid-wave propagation. Each set of the centrifuge tests comprised two upward seepage flow tests and two wave loading tests. Specifically, these four tests were performed on the same bed of sand in order of the first seepage flow test, the first wave loading test (FW-test), the second seepage flow test and the second wave loading test (SW-test). The wave loading in FW-test acted as preshearing relative to the subsequent wave loading in SW-test. The number of wave loading cycles in such FW-tests was varied as listed in Table 5.4. Note that the seepage flow tests performed before and after a FW-test permitted the estimation of the changes in void ratio profiles of a given sand bed due to the preshearing, from directly measured profiles of the coefficient of permeability in the sand bed. This methodology uses the correlation between the coefficient of permeability and void ratio for a given sand. For details of the procedure, refer to chapter 4.

The cross section of a wave tank used in the centrifugal wave testing is shown in Fig. 5.13. The base of the sediment trench was connected to a reservoir through a solenoidal valve. When performing an upward steady-state seepage flow test, the solenoidal valve was opened, with a total head of the fluid in the reservoir being higher than that in the wave tank. The solenoidal valve was closed in the wave loading testing so that no fluid flow occurred through the base of the sand bed. The sand used was Silica sand #7-Batch B (G_s=2.69, e_{max}=1.18, e_{min}=0.69 and D_{50}=0.14*mm*). The sand beds formed had relative densities D_r of 29-40% and the initial soil depths D of 85-86*mm*. The fluid depth, H, was kept at 80*mm*. The wave paddle was excited at a frequency of 8*Hz*. The slotted vertical partition was installed for wave absorption purposes, and essentially progressive waves were generated in the wave tank. In each of the three FW-tests, the stroke of the wave paddle was selected so that the wave-induced cyclic stress ratio at the level of the soil surface χ_0 were equal to 0.15 and exceeded a critical value χ_{cr} for liquefaction to occur. Note that for the fresh deposits of Silica sand #7, the critical value χ_{cr} was equal to 0.11 (section 5.2). Thus, the FW-tests may be understood as being high-level preshearing for the corresponding SW-tests. Although the same stroke of the wave paddle was specified in the three SW-tests, the resulting χ_0-values ranged 0.13-0.14 with consideration of the increased γ'-value due to the preshearing.

5.3.2 Experimental results

Let us take up test WJ42-FW to begin with. The measured time histories of pore

pressure fluctuations at four different depths are shown in Fig. 5.14, together with the input waveform. At 6 cycles of wave loading (t=3.0s), the liquefaction zone extended to the bottom of the soil bed (Fig. 5.14(e)). In fact the residual pore pressure there reached the level of initial vertical effective stress, σ_{v0}'. Interestingly, during the continued wave loading, the residual pore pressure at the bottom of the soil bed started dissipating, indicating the start of a solidification process. It is evident that in the course of continued wave loading, the solidification front advanced upwards. The wave loading was stopped at ξ=285 (t=37s), allowing the excess pore-pressures in the soil bed to dissipate under a quiescent environment. The process following the cessation of wave loading was nothing but a well-known process of consolidation.

The void ratio profiles in the soil bed determined before and after the wave test WJ42-FW are shown in Fig. 5.15 (a). Remember that in test WJ42-FW the solidification extended from the bottom of the soil bed to the middle soil depth. It is evident from Fig. 5.15(a) that a marked densification was brought about in the solidification zone. The region above the solidification zone also underwent densification. However, this was solely due to consolidation and the degree of the densification was only 1/3-1/4 of the densification that was effected in the zone undergoing solidification.

The effect of high-level preshearing on the behaviour of a soil bed under the subsequent wave loading depends on the way in which the soil bed has undergone solidification. This aspect is illustrated in Fig. 5.15 (b). Here the profile of the maximum residual pore pressures, $u_e^{(2)}{}_{\text{-max}}$, in test WJ42-SW are plotted, together with the σ_{v0}' versus ζ line. It is seen that re-liquefaction occurred in the region from the soil surface to the middle soil depth, where no solidification had developed in the previous wave test. In contrast, the soil in the region below underwent a moderate build-up of residual pore pressure, but remained far from the state of liquefaction. These observations indicate that the solidification improved the liquefaction resistance in a significant degree.

The improvement of liquefaction resistance due to solidification was observed also in test WJ 40. In wave test WJ40-FW the solidification front advanced upwards from the bottom of the soil bed to the soil surface, having brought about marked densification in the entire soil bed (Fig.5.16 (a)). The profile of the maximum residual pore pressures, $u_e^{(2)}{}_{\text{-max}}$, in the wave reloading stage (WJ40-SW) are shown in Fig. 5.16 (b). It is seen that except for the very shallow soil depth, the $u_e^{(2)}{}_{\text{-max}}$ profile plots well away from the σ_{v0}' versus ζ line, emphasizing the effect of solidification regarding the improvement in liquefaction resistance.

In fact, the extent of liquefaction in SW-test became shallower than that in FW-test because of the solidification. This observation led to the following inference. If the

wave loading was stopped before the solidification developed, then the extent of re-liquefaction at the subsequent wave loading stage would be essentially the same as the extent of liquefaction in the previous wave loading stage. This inference can be examined against the performance of test WJ41. In wave test WJ41-FW the wave loading duration was selected so that no visible sign of solidification occurred in the entire soil bed which underwent liquefaction. Thus, the densification that occurred was solely due to the consolidation process following liquefaction (Fig. 5.17 (a)). The void ratios in the soil bed after the consolidation ranged 0.78-0.95. The profile of the maximum residual pore pressures, $u_e^{(2)}{}_{\text{-max}}$, in test WJ41-SW are shown in Fig. 5.17(b). It is seen that the soil bed underwent re-liquefaction to nearly the same extent as the liquefaction which occurred in test WJ41-FW.

5.3.3 An analytical model for describing the effect of preshearing

The proposed analytical model for progressive liquefaction/ solidification in chapter 3 has proven capable of predicting the pore-pressure responses and the related changes in void ratio profiles in the sand beds in the course of the wave loading histories imposed. In this sub-section, I will describe a representative set of predictions, with the wave loading history corresponding to test WJ42. For the convenience of discussion, the wave loading stage which corresponds to WJ42-FW will be referred to as the first wave loading stage and the wave loading stage corresponding to WJ42-SW will be referred to as the second wave loading stage.

In the first wave loading stage, the solidification front started advancing upwards following the full development of liquefaction in the sand bed and reached a soil depth ζ=-44*mm* at the end of the wave loading (ξ=285). Upon the cessation of wave loading, consolidation started occurring and developed in the entire soil bed. The predicted changes in void ratio profiles in this case is shown in Fig. 5.18 (a). It is evident that a marked densification was brought about in the solidification zone. This is a manifestation of the contractancy of the soil under many cycles of shearing.

In the second wave loading stage, the liquefied zone extended down to a soil depth ζ=-43*mm* (Fig. 5.18 (b)). It should be noted that the maximum depth of liquefaction was very close to the final level of the solidification front that was reached at end of the first wave-loading stage (Figs. 5.18 (a) and (b)). It should also be noted that the predicted profile of the residual pore pressure at the second wave loading stage (Fig. 5.18 (b)) is consistent with the measured one which is shown in Fig. 5.15 (b).

5.4 PREDICTIONS REGARDING BEHAVIOUR OF A SAND BED UNDER COMPLEX WAVE LOADING HISTORY

The proposed analytical model in chapter 3 can predict the behaviour of sand beds with complex wave loading histories. In order to demonstrate this aspect, a discussion will subsequently be made of a case where an initially loosely fresh deposit of sand is subjected to four groups of severe wave loading in sequence (Fig. 5.19 (a)). The wave conditions adopted are as follows: centrifugal acceleration 30g; fluid depth H=80mm; wave frequency f=8Hz.

The predicted temporal changes in the location of the interface between the liquefied soil and the sub-liquefied soil in the course of the imposed wave loading history is shown in Fig. 5.19 (b). Upon the onset of liquefaction at shallow soil depth, the liquefaction front rapidly advanced downwards and came to a final level of ζ=-82mm. With the continued severe wave loading, the solidification front advanced upwards while the severe wave loading was maintained. When the severity of the wave loading became smaller, the solidification front rose at much faster rates. When the severity of the wave loading was increased again, the re-liquefaction occurred and the liquefied zone extended down to a depth ζ=-66mm. The maximum depth of the liquefaction front was very close to the uppermost level (ζ=-69mm) of the soil which had experienced solidification during the preceding group of waves. Essentially the same pattern of the changes in the location of the interface between the liquefied and sub-liquefied zones of sand was repeated in the third and fourth groups of waves.

The predicted changes in void ratio profile of the sand bed are shown in Fig. 5.20. After the passage of the first group of waves (ξ=176), marked densification was brought about in the deeper part of soil (profile 2), where the soil experienced solidification. Due to the loading from the subsequent groups of waves, the markedly densified region became larger as the solidification developed (profiles 3 and 4). Thus, the extent of the re-liquefaction became successively smaller in the course of wave loading history imposed.

From the final profile of the void ratio (profile 5), it is seen that there were three regions marked asterisks where the degrees of densification were appreciably smaller than those of the neighboring regions. Each region marked an asterisk was located slightly above the final level of the solidification front in each group of wave loading. Remember that the re-liquefaction developed down to a horizon slightly above the final level of the solidification front in the previous group of wave loading. Thus, the regions

marked with asterisks did not experience solidification, resulting in the bands of less densification.

5.5 CONCLUSIONS

The effects of wave loading history on liquefaction in sand beds have been discussed based on the centrifuge wave testing with viscous scaling and on the analytical model for progressive liquefaction/solidification. The principal results obtained may be summarized as follows.

(a) The rate of increase in wave amplitude significantly affected the resistance to liquefaction of the sand beds. That is, in the case where the wave amplitude was increased rapidly with time, liquefaction occurred at a lower cyclic stress ratio than in the case where the wave amplitude was increased slowly with time. This difference in liquefaction resistance may be ascribed to the partial drainage effect during wave loading.

(b) It is important to distinguish preshearing effect into that due to low-level preshearing and that due to high-level preshearing. The low-level preshearing with $\chi_0<\chi_{cr}$, which was accompanied by a marginally discernible densification, significantly increased the resistance to liquefaction.

(c) The high-level preshearing with $\chi_0>\chi_{cr}$, which brought about an appreciable densification, did not improve the liquefaction resistance.

(d) These observations suggest that the resistance to wave-induced liquefaction is not entirely governed by the overall relative density of a soil bed. Important factors to be taken into consideration are (1) highly non-linear relation between soil resistance and relative density and (2) changes in relative density profile.

(e) In the course of continued wave loading, the residual pore pressure at the bottom of the liquefied zone of sand started dissipating, indicating the start of a solidification process. The solidification front advanced upward during the continued wave loading, with significant densification being accompanied.

(f) The solidification front extends upwards to a shallower soil level as the number of wave loading cycles is increased. Such a prolonged high-level preshearing makes the resistance to re-liquefaction in the solidified zone significantly larger than the liquefaction resistance of the fresh deposits of the sand.

(g) The proposed model for progressive liquefaction/solidification can reproduce the observed effects of high-level preshearing in a consistent fashion.

(h)The proposed analytical model is also capable of predicting the behaviour of sand beds under complex wave loading histories. It is demonstrated that in each of the imposed groups of waves, the re-liquefaction extended down to a horizon slightly above the previously solidified zone, forming the alternating bands of markedly densified and less densified soil.

References

Finn, W. D. L., Brasby, P. L. & Pickering, D. J. (1970). Effects of strain history on liquefaction of sand. *J. Soil Mech. & Found. Div., ASCE,* **96**-6, 1917-1934.

Sassa, S. & Sekiguchi, H. (1998). Wave-induced liquefaction, densification and re-liquefaction of sand beds. *Proceedings of the International Conference Centrifuge 98,* Tokyo, **1**, 391-396.

Sassa, S. & Sekiguchi, H. (1999). Wave-induced liquefaction of beds of sand in a centrifuge. *Geotechnique,* **49**, No.5, 621-638.

Seed, H. B., Mori, K. & Chan, C. K. 1977. Influence of seismic history on liquefaction of sands. *J. Geotech. Engng Div., ASCE, 103-4*: 257-270.

Sekiguchi, H., Kita, K., Sassa, S. & Shimamura, T. (1998). Generation of progressive fluid waves in a geo-centrifuge. *Geotechnical Testing Journal, ASTM, 21-2*: 95-101.

Tatsuoka, F., Maeda, S., Ochi, K. & Fujii, S. (1986). Prediction of cyclic undrained strength of sand subjected to irregular loading, *Soils & Foundations*, **26**, No.2, 73-90.

Table 5.1 Principal parameters in constant-amplitude cases (Series I)

Test number	χ_0	Dr: %	D: mm
WJ26	0.104	42	84
WJ34A	0.11	34	86
WJ36A	0.05	34	85

Table 5.2 Principal parameters in increasing-amplitude cases (Series II)

Test number	$\delta u_0/\delta\xi$: : kPa	Dr: %	D: mm
WJ31	0.02	39	85
WJ32	0.08	37	85

Table 5.3 Principal parameters in series III investigating the effects of presheairng

Test numbei	χ_0 (Stage I)	Dr: %	D: mm
WJ32	No	37	84
WJ34	0.11	34	86
WJ36	0.05	34	85
WJ39	0.05	39	85

Table 5.4 Principal parameters in tests investigating the effect of duration of high-level preshearing

	ξ_T [1)]	χ_0	Dr [2)]: %		χ_0	Dr [2)]: %
WJ40FW	800	0.15	29	WJ40SW	0.13	90
WJ41FW	23	0.15	40	WJ41SW	0.14	59
WJ42FW	285	0.15	37	WJ42SW	0.13	79

1) number of wave cycles imposed 2) overall relative density

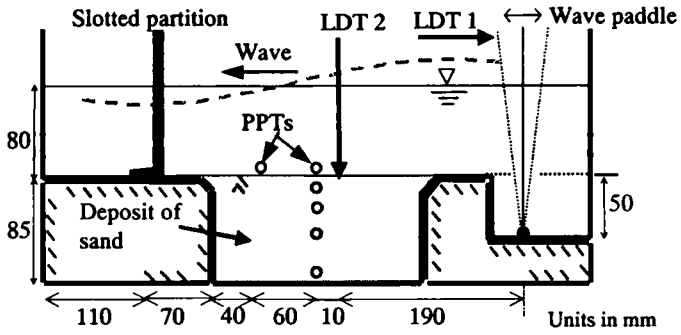

Fig. 5.1 Cross section of a wave tank for use in centrifuge wave testing on soil bed

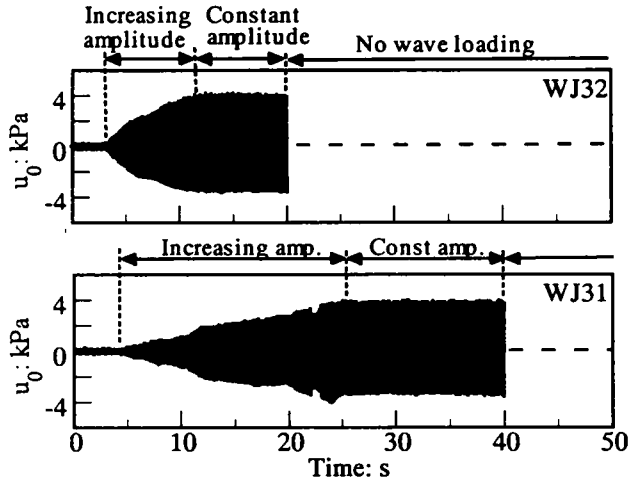

Fig. 5.2 Time histories of wave pressure corresponding to different rates of increase in wave amplitude

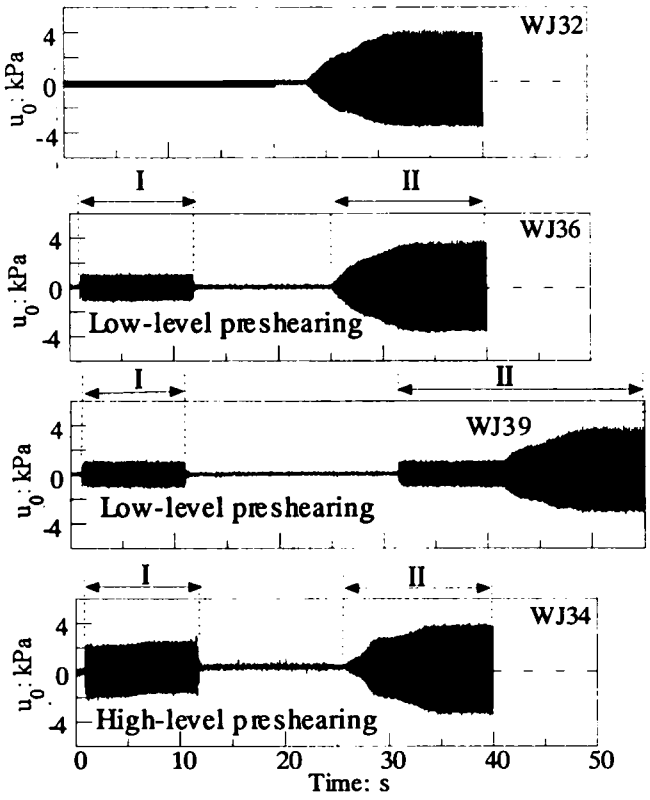

Fig. 5. 3 Time histories of wave-induced pressure fluctuations at the soil surface in the four wave tests designated

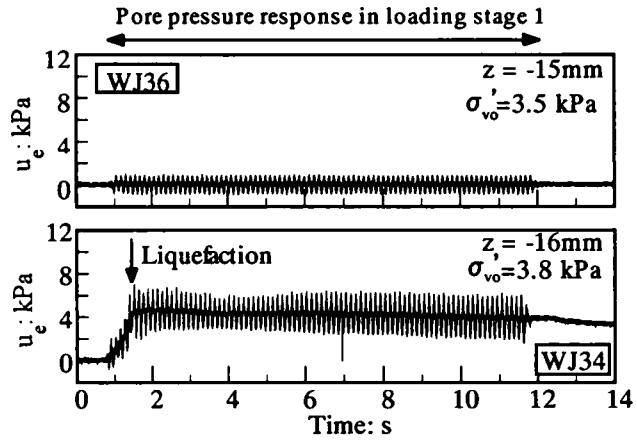

Fig. 5.4 Comparison of pore pressure in loading stage I to different levels of wave severity

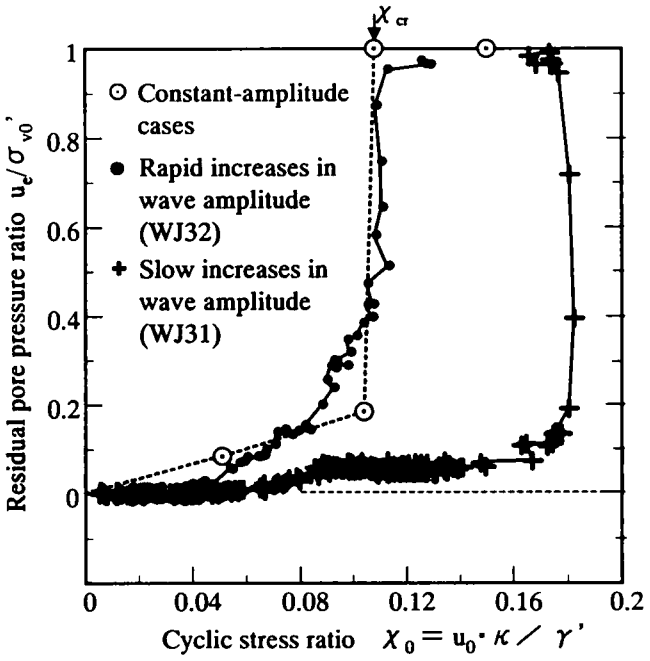

Fig. 5.5 Development of residual pore pressure ratio plotted against cyclic stress ratios.

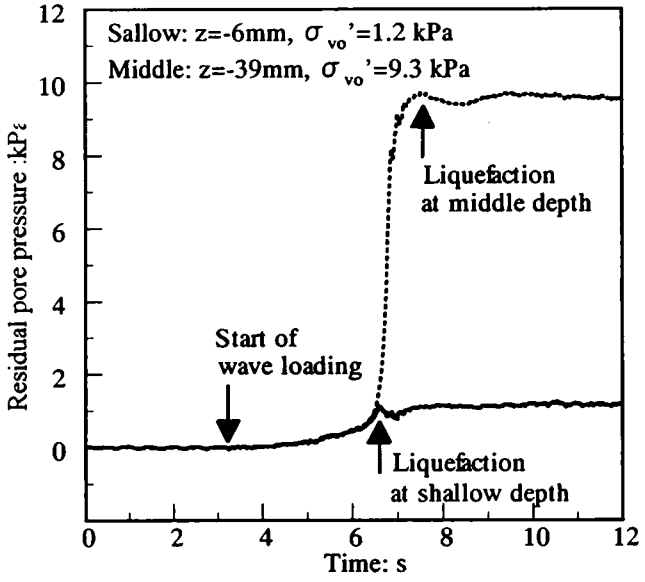

Fig. 5.6 Developments of residual pore pressures at two different soil depths indicating progressive nature of liquefaction

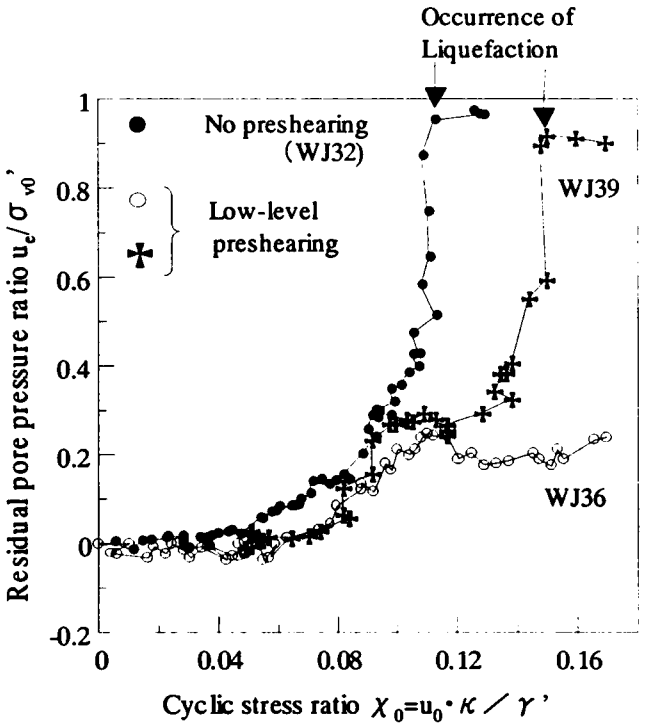

Fig. 5.7 Effects of low-level preshearing on the development of residual pore pressure ratio with cyclic stress ratio in wave loading stage II.

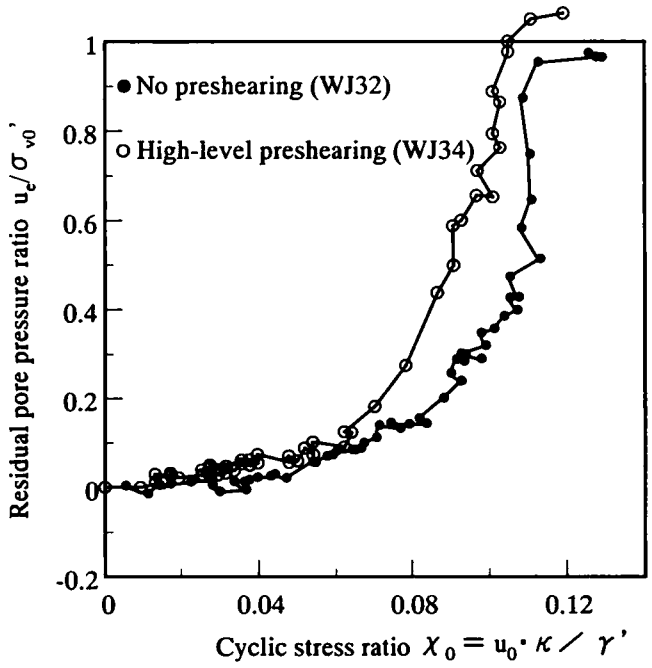

Fig. 5.8 Comparison of developments of residual pore pressure ratios in wave tests with either high-level presheairng or no preshearing

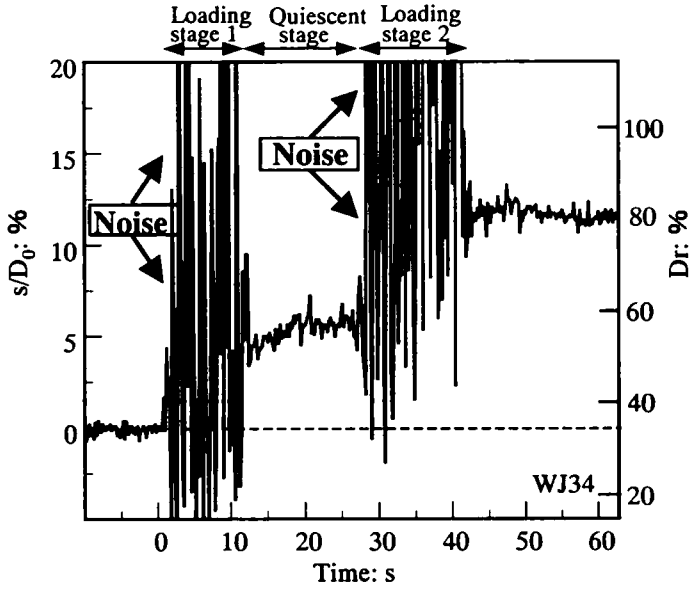

Fig. 5. 9 Time history of normalized settlement s/D_0 of the soil surface obtained from readings of LDT2

Description	Volume changes at the following consolidation phase	Liquefaction resistance to subsequent loading
Low-level preshearing	Very little or no densification	Significant increase in χ_{cr}
High-level preshearing	Significant densification	Little or no increase in χ_{cr}

Fig. 5.10 Summary of effects of preshearing on the performance of sand beds

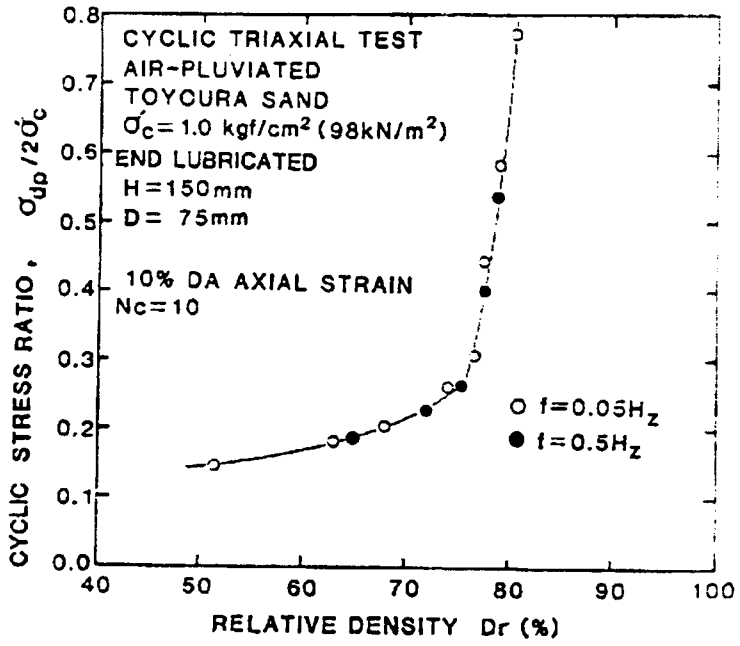

Fig. 5.11 Effects of relative density on cyclic triaxial test results (Tatsuoka et al. 1986)

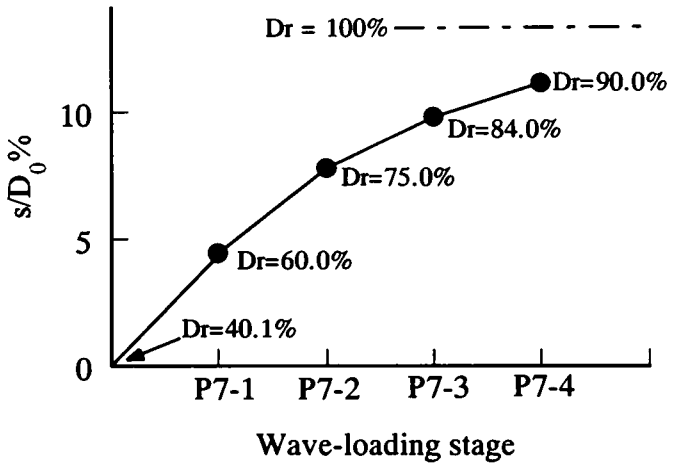

Fig. 5.12 Measured variations of overall relative density in the four tests performed in sequence; liquefaction occurred in each wave loading stage. (adapted from Sassa & Sekiguchi, 1999)

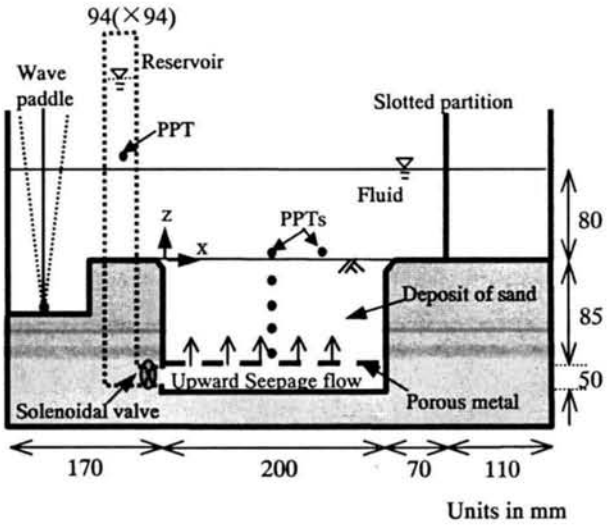

Fig. 5.13 Cross section through a wave tank for use in a geo-centrifuge

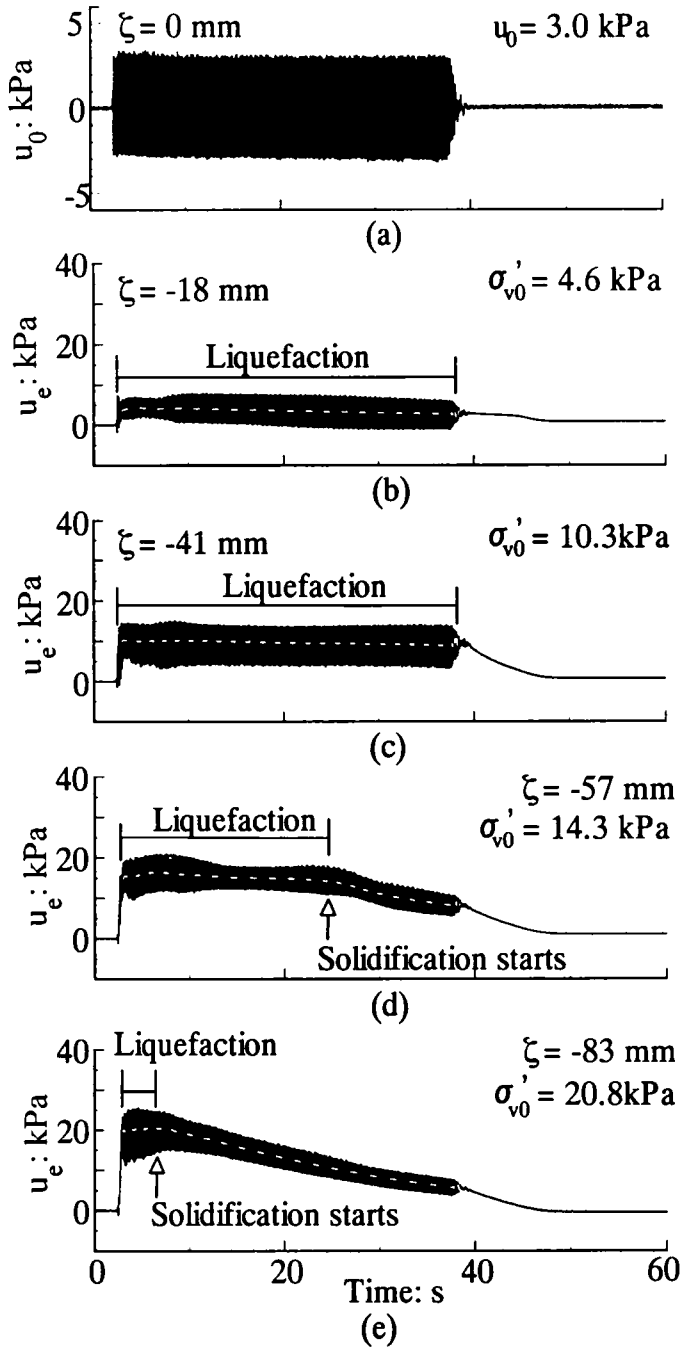

Fig. 5.14 . Measured waveforms in wave test WJ42-FW: time histories of (a) wave pressure acting on the location of initial soil surface; and (b), (c), (d) and (e) excess pore pressures at different spatial points.

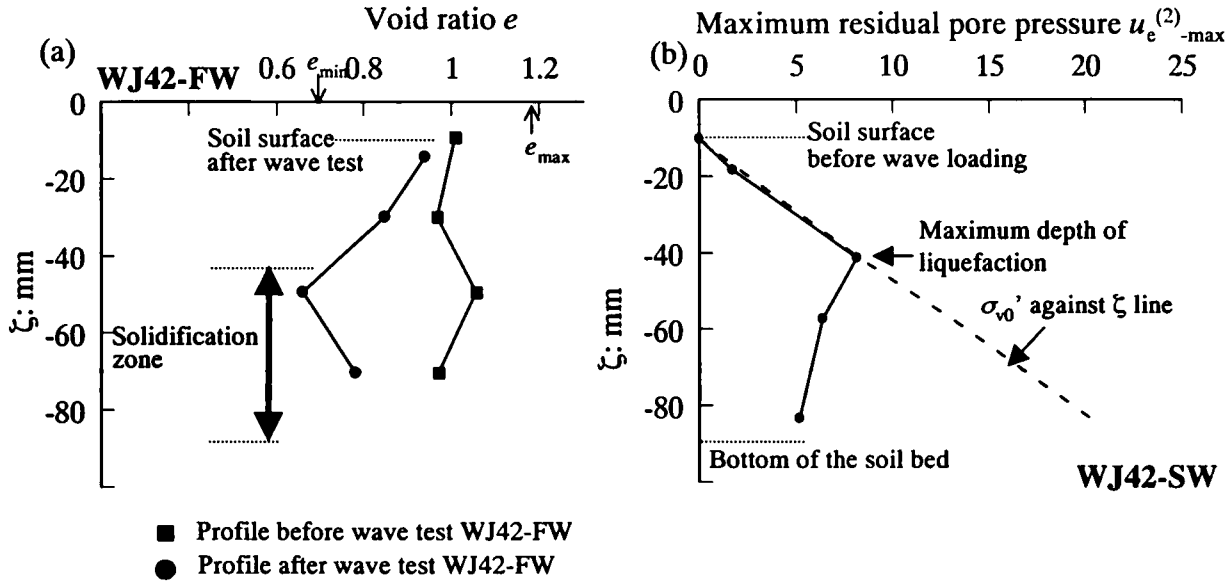

Fig. 5.15 (a) Measured changes in void ratio profile of sand bed in test WJ42-FW; (b) measured profile of $u_e^{(2)}{}_{-max}$ with ζ in test WJ42-SW

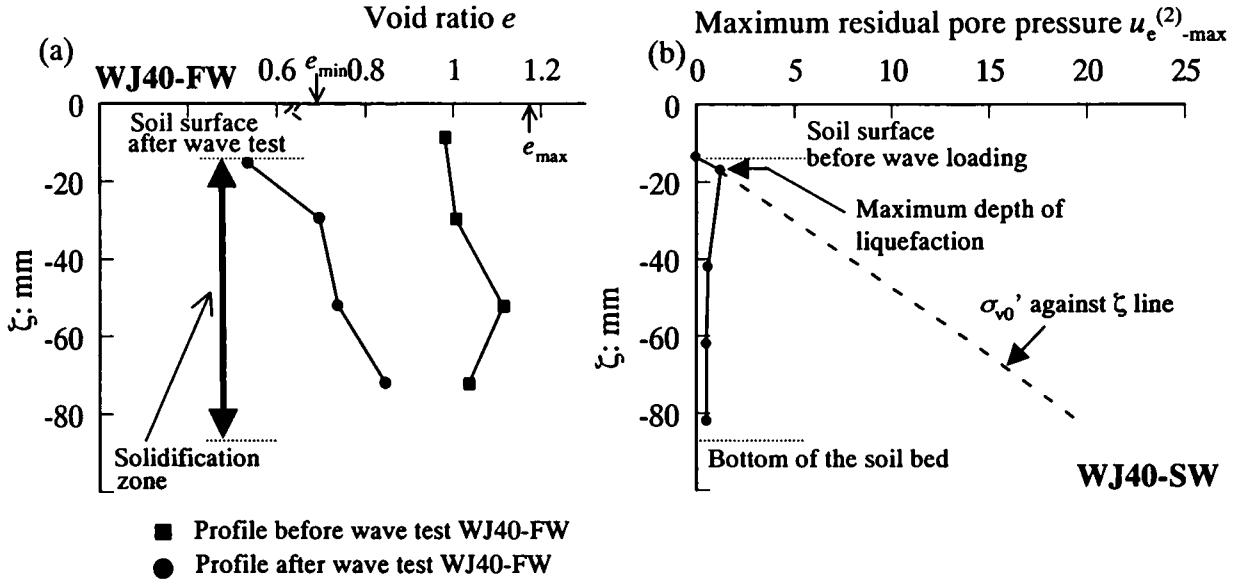

Fig.5.16 (a) Measured changes in void ratio profile of sand bed in test WJ40-FW; (b) measured profile of $u_e^{(2)}{}_{-max}$ with ζ in test WJ40-SW

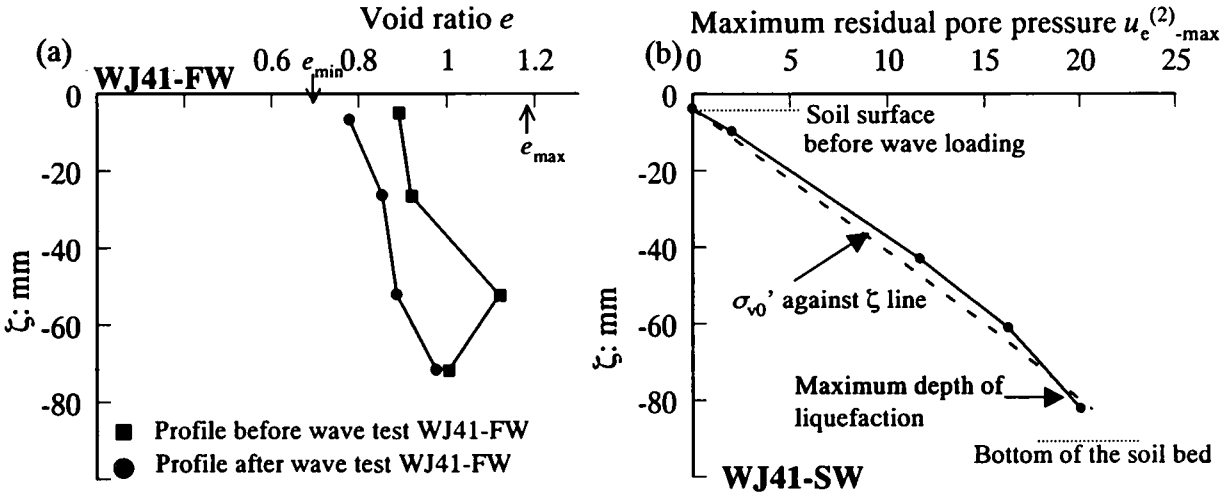

Fig. 5.17 (a) Measured changes in void ratio profile of sand bed in test WJ41-FW; (b) measured profile of $u_e^{(2)}{}_{-max}$ with ζ in test WJ41-SW

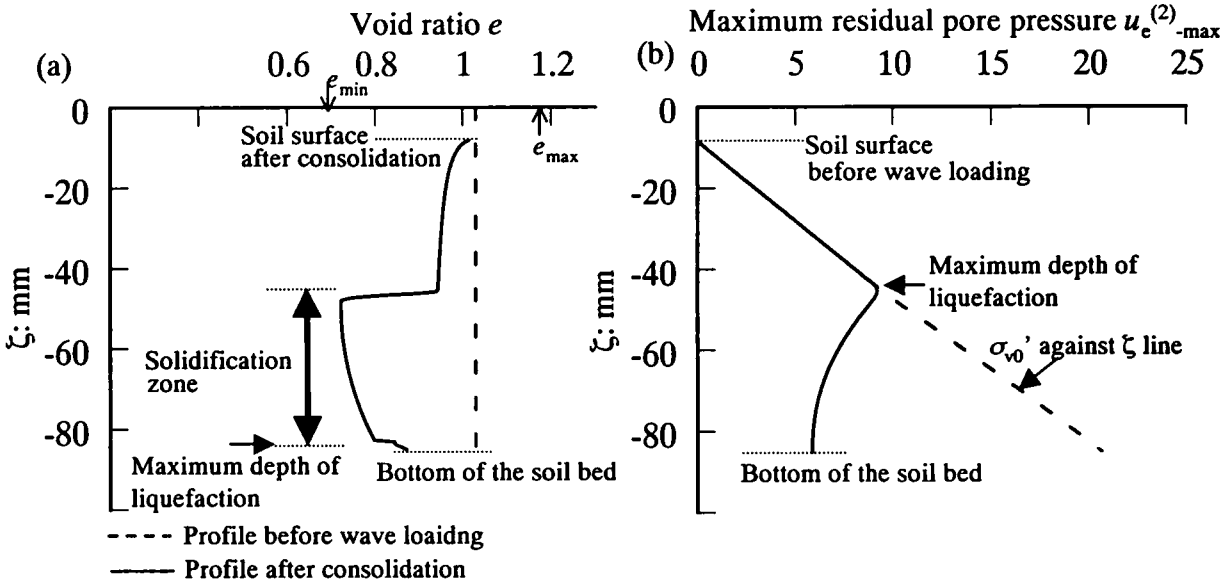

Fig.5.18 Predicted changes in void ratio profile of sand bed in the first wave loading stage, and (b) predicted profile of $u_e^{(2)}{}_{-max}$ with ζ in the subsequent wave loading stage

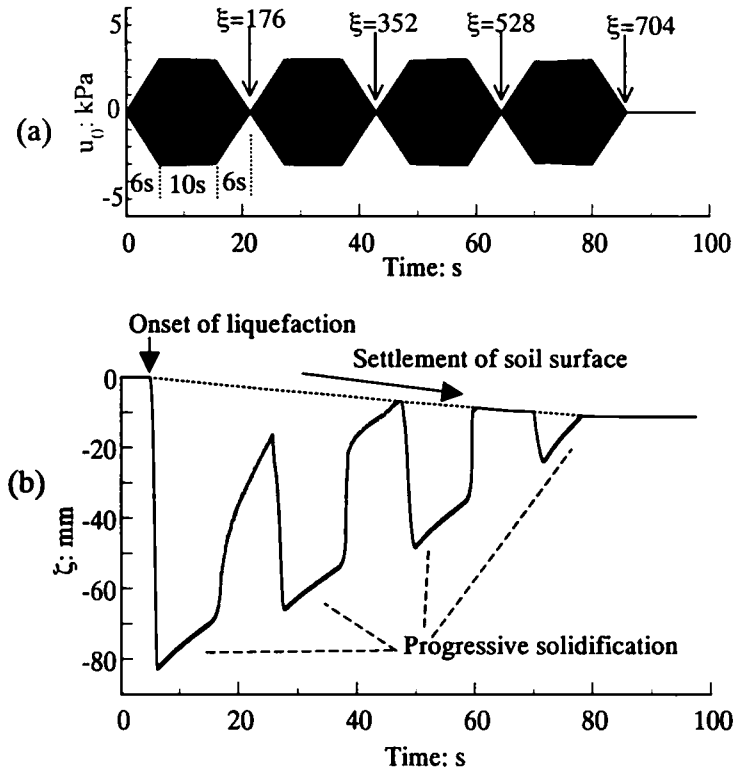

Fig. 5.19 (a) Time history of u_0 consisting of four groups of severe waves, and (b) predicted temporal changes in the location of the interface between the liquefied soil and the sub-liquefied soil

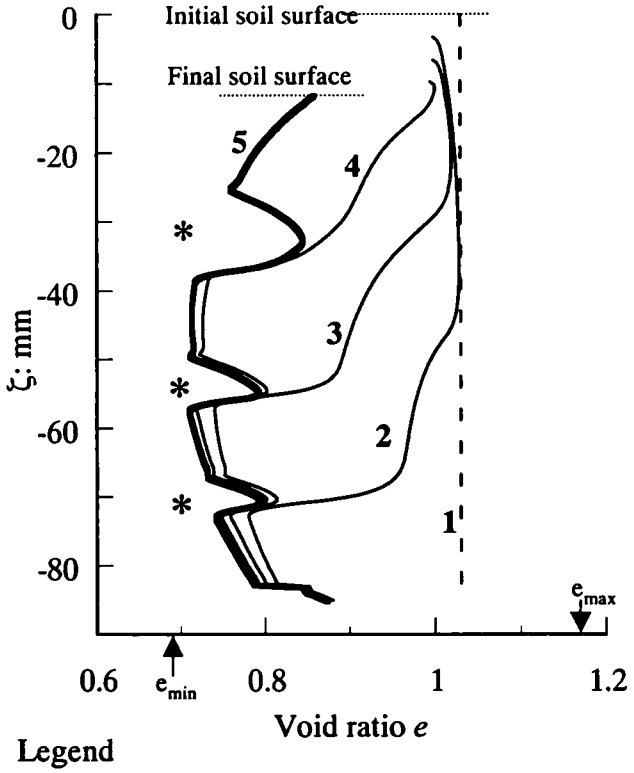

Legend

1: Initial profile
2: Profile after 176 cycles of wave loading
3: Profile after 352 cycles of wave loading
4: Profile after 528 cycles of wave loading
5: Final profile (t=100s)

Fig. 5.20 Predicted changes in void ratio profiles of the sand bed in the wave loading history consisting of four groups of sever waves

Chapter 6

Energy dissipation in liquefied sand during wave loading

6.1 INTRODUCTION

This chapter discusses energy dissipation in a system consisting of exterior fluid, liquefied sand and sub-liquefied sand under wave loading. In this discussion, it is important to distinguish liquefied sand into *fully destructured liquefied soil* and *structured liquefied soil*. This distinction was introduced in chapter 3 in order to describe the progressive liquefaction/solidification during wave loading. The fully destructured liquefied soil has no stiffness, and the structured liquefied soil has a marginally discernible stiffness while the effective stress is zero. In chapter 3, the importance of structured liquefied sand for solidification in liquefied sand was emphasized. In this chapter, it is shown that the structured liquefied soil plays a vital role for dissipating wave energy.

This chapter is organized as follows. The degrees of energy dissipation in the fully destructured liquefied soil, in the structured liquefied soil and in the sub-liquefied soil will be discussed respectively first from the previous studies. The dissipation of energy in the structured liquefied sand layer will then be estimated and it will be compared to the energy dissipation in the liquefied soil obtained from an experimental result of Takahashi et al. (1994).

6.2 ENERGY DISSIPATIONS IN LIQUEFIED SAND AND SUB-LIQUEFIED SAND

Consider a situation where fluid wave trains propagate over a bed of cohesionless soil, causing the soil bed to liquefy. The liquefaction front advances downwards in the course of wave loading. After the advance of the liquefaction front, solidification occurs at the bottom of the liquefied soil layer. The solidification front advances to the soil surface during the wave loading. Let us consider the situation under the progressive solidification. The entire system under consideration consists of exterior fluid, fully destructured liquefied soil, structured liquefied soil and sub-liquefied soil (Fig. 6.1).

The energy dissipation occurs in each layer in the entire system due to the solid-to-solid friction, fluid-solid friction, viscosity of the fluid and so on. In what follows, the degrees of energy dissipation in the fully destructured liquefied soil, in the structured liquefied soil and in the sub-liquefied soil are discussed from previous studies.

6.2.1 Energy dissipation in fully destructured liquefied sand

The marked fluidity of the fully destructured liquefied soil was observed and discussed in chapter 4 in the present thesis. The energy dissipation in the very soft sediments having marked fluidity was examined theoretically (Gade, 1958; Dalrymple & Liu, 1978). Here, the very soft sediment was assumed to be a viscous fluid. Note here that Gade (1958) and Dalrymple & Liu (1978) treated the soft sediments classified as clay or mud, not liquefied sand. The clay or mud can be considered as practically impermeable to water in the time scale of water waves. In addition, they have cohesion. Therefore, treating soft clay or mud as a viscous fluid may be approved.

However, it may be difficult to consider the energy dissipation in liquefied sand, by assuming the fully destructured liquefied soil as a viscous fluid. The reason for this difficulty is that whether the liquefied sand has viscosity is not clear (Kokeguchi et al., 2001). In addition, the measured or estimated values of viscosity in liquefied sand are various in many investigations (Hamada & Wakamatsu; 1998, Towhata et al., 1999; Towhata & Kawasaki, 1999). In Hamada & Wakamatsu (1998), the viscosity of liquefied sand is order of 10^0 Pa ·s. In Towhata et al. (1999) it is order of 10^2 Pa ·s. In Towhata & Kawasaki (1999) it is order of 10^6 Pa ·s. One reason for the wide dispersion of measured or estimated viscosity of liquefied sand may be that liquefied sand was treated, with the distinction between fully destructured liquefied soil and structured liquefied soil not being considered. The degree of the spread of structured liquefied soil might be different in their experiments.

The wave damping by liquefied sand was examined using small or mid-scaling wave channel (Takahashi, et al. 1994; Kang et al. 1997). In the experiments, the sand beds were under conditions of steady state seepage flow. It was shown that the degree of wave damping relates to the degree of the spread of the boiling zone in a sand bed. The degree of wave damping which was observed when the boiling occurred in the entire soil bed was smaller than the degree of damping observed when the boiling occurred partially. When the boiling occurred in the entire soil bed, the fully destructured liquefied soil might spread in the most part of the sand bed. In contrast, when the

boiling occurred partially, the structured liquefied sand might be in the most part of the sand bed. The experimental results indicate that the degree of energy dissipation in the structured liquefied sand is more significant than that in the fully destructured liquefied soil.

With no information on the viscosity of the fully destructured liquefied sand and the indication that the energy dissipation in the fully destructured liquefied soil is small compared to that in the structured liquefied soil, the energy dissipation in the fully destructured liquefied soil is not considered in the next section in this chapter.

6.2.2 Energy dissipation in structured liquefied sand

The structured liquefied soil retains a very small stiffness, not zero stiffness. The small stiffness of the sand may play a vital role in the energy dissipation. This aspect is shown in the results from the finite element analyses of a wave-soil system (Park et al. 1996; Kang et al. 1997) and the VOF-FEM analysis of it (Takahashi et al., 2002). Here, it was shown that the energy dissipation reached the maximum degree when the shear modulus of the sand was a certain small value. However, the values of the shear modulus at the maximum dissipation of energy were different between Park et al. (1996) or Kang et al. (1997) and Takahashi et al. (2002) (Table 6.1). One of the possible reasons is the difference of the scale of the problems for the analyses.

6.2.3 Energy dissipation in sub-liquefied sand

It was shown in chapter 3 that the sub-liquefied soil was densified markedly under the progressive solidification. From this aspect, the sub-liquefied sand may be classified as the sand having a large stiffness and supporting power. The wave damping by the sand having a large stiffness has been examined by many researchers. The energy dissipation by the bottom turbulence layer was investigated by Putnam & Johnson (1949). This energy dissipation could be considered to be due to the soil surface friction, since the damping coefficient is represented using the friction coefficient for the soil surface. The energy dissipation by the percolation of water through the sand bed was investigated by Putnum (1949), Reid & Kajiura (1957) and Takahashi et al. (2002). The effect of solid-to-solid friction (a Coulomb friction) at the points of contact between grains on the damping of water waves were theoretically examined by Yamamoto (1982, 1983) and Lee et al. (2002). Experimental approach of the wave attenuation by the coulomb damping was performed by Yamamoto et al. (1983) and Yamamoto &

Schuckman (1984). A summary of the energy dissipation due to the bottom friction, percolation and the coulomb friction is given by Yamamoto & Takahashi (1985).

From a VOF-FEM analysis (Takahashi et al. 2002), the effect of percolation on the energy dissipation is not important when the coefficient of permeability, k, is the same order as that of the sand in the present study (k=0.1 - 0.2 mm/s). Specifically, the damping ratio, ε, is 10^{-5} at k=0.1mm/s. Here, the damping ratio ε is expressed as

$$\varepsilon = \frac{L}{x}\ln\left(\frac{H_0}{H}\right) \tag{6.1}$$

where L is the wavelength, H_0 is the reference wave height at the origin and H is the wave height attenuated when the wave progresses in the distance x. For example, when ε =10^{-5}, the wave of H_0=1m is reduced to H=0.9 m after propagating no less than 10^4 wavelengths!

The coulomb friction in soils is important for clay or silts (Yamamoto & Takahashi, 1985). Yamamoto (1983) showed that the effect of the coulomb friction on wave damping is equally or more important than the wave-damping effect of percolation in the sandy seabeds. In the experiments, the damping of water waves by sand beds was too small to measure (Yamamoto et al. 1983).

It has been shown that the energy dissipation in the sand having a large stiffness is very small. Therefore, in the next section, energy dissipation in the sub-liquefied sand is not considered.

6.3 DISCUSSION ON EXPERIMENTAL RESULTS AND ESTIMATION OF ENERGY DISSIPATION IN STRUCTURED LIQUEFIED SAND

It has been shown in the previous section that the layer of structured liquefied sand plays a most important role in dissipation of wave energy in the all layers in the system shown in Fig. 6.1. In this section, it is shown that the layer of structured liquefied sand has ability to make the energy dissipation to an extent that can account for what has been observed in an experiment.

The wave attenuation by a liquefied sand bed was examined by Takahashi et al. (1994) with a two-dimensional small wave channel. In the experiment, liquefaction occurred in the sand bed due to the upward seepage flow and wave pressure fluctuations. The length of sand bed was 11.4m. However, the length of bed of liquefied sand was 4m,

because the water-supply pipes which generated the upward seepage flow were installed in the range of $4m$. Wave conditions and sand bed conditions were shown in Fig. 6.2. The soil depth is $0.4m$. It is assumed that the depth of liquefaction was $0.4m$. The variation in wave height, H, was measured. The wave height at x=0, H_0, was 0.08 m, and the one at x=$4m$ was $0.056m$.

Energy transport equation is expressed as follows:

$$\frac{dW}{dx} = -D_P \tag{6.2}$$

where W is the energy flux (= Ec_g: E is the time average of wave energy density; c_g is the group velocity) and D_p is the energy loss per area per time. In other words, D_p is the work that was done by the liquefied sand per area per time. The energy flux at x=0 or x=*4* is expressed as follows:

$$W = \frac{1}{8}\rho g H^2 \cdot \frac{\omega}{\kappa} \cdot \frac{1}{2}\left\{1 + \frac{2\kappa h}{\sinh(2\kappa h)}\right\} \tag{6.3}$$

where h is the depth of the exterior fluid, κ is the wave number, ρ is the density of the exterior fluid and ω is the angular frequency. The energy loss per cycle per wavelength, ΔE, is

$$\Delta E = D_p \cdot T \cdot L \tag{6.4}$$

where T is the wave period and L is the wavelength, which is obtained from a dispersion relationship. However, the dispersion relationship in the system consisting of exterior fluid and liquefied soil is difficult to derive. In this study, the following dispersion relationship is conveniently used in order to obtain L:

$$\left(\frac{2\pi}{T}\right)^2 = \frac{2\pi g}{L}\tanh\left(\frac{2\pi h}{L}\right) \tag{6.5}$$

From equation (6.3), the energy flux at x=0 and x=4 m are obtained as follows: $W(0)$ = 7.34 $N{\cdot}m/s$ /m, $W(4)$ = 3.59 $N{\cdot}m/s$ /m. From equation (6.2), the energy loss per area

per time is obtained as 0.94 $N{\cdot}m/s\ /m^2$. From equation (6.4), the energy loss per cycle per wavelength is obtained: ΔE=1.22 $N{\cdot}m$ / m. This is the work that was done by the liquefied sand per cycle per wavelength.

It is assumed that the layer of structured liquefied sand, whose thickness is δ, exists at the bottom of the liquefied soil, and that the liquefied soil overlying the layer of the structured liquefied soil is the fully destructured liquefied soil (Fig. 6.3). The boundary between the fully destructured liquefied soil and the structured liquefied soil is solidification front. As mentioned in the previous section, the energy dissipation in the fully destructured liquefied soil is negligible. In this chapter, the fully destructured liquefied soil is assumed to be an inviscid fluid. Therefore, the wave energy is dissipated in only the layer of structured liquefied soil.

Now, the possible highest dissipation of energy in the layer of the structured liquefied sand is estimated. This estimated energy dissipation in the structured liquefied soil is compared to the energy dissipation obtained from equation (6.4).

A relation between the shear stress, τ, and the shear strain, γ, of an element in the structured liquefied soil layer is assumed so that the energy loss in the element can be highest. The assumed relation between τ and γ of the structured liquefied sand is shown in Fig. 6.4. The hatched area represents the energy loss in the element of structured liquefied sand per cycle. The energy loss obtained from the τ-γ relation in Fig. 6.4 is the possible highest energy loss of the sand. The maximum cyclic stress ratio and the maximum shear strain is expressed as follows:

$$\tau_{\max} = -\kappa u_S(z - z_s)\cdot\exp[\kappa(z - z_s)] \qquad for \quad z<z_S \tag{6.6}$$

$$\gamma_{\max} = -\kappa u_S(z - z_s)/G\cdot\exp[\kappa(z - z_s)] \qquad for \quad z<z_S \tag{6.7}$$

where G is the shear modulus of the structured liquefied sand, u_s is the amplitude of the fluid pressure fluctuation at z_S. The amplitude u_s is obtained from a theory of wave propagation in a two-layer fluid. The concrete form of u_s is shown in chapter 3.

The energy loss per cycle per wavelength in the layer of the structured liquefied sand is expressed as follows:

$$\Delta E = \int_{z_s-\delta}^{z_s} 4\tau_{\max}\gamma_{\max} L dz \tag{6.8}$$

The energy loss ΔE is the function of the δ and G. Note that the shear modulus of the structured liquefied soil should be very small. The obtained ΔE is shown in Fig. 6.5. In this figure, the energy loss obtained from the experiment is also shown (ΔE=1.22 $N \cdot m$ / m). It is seen that when the thickness of the structured liquefied soil is 0.04m-0.08m and the shear modulus 100N/m^2-500N/m^2, the energy loss in the layer of structured liquefied sand is the same degree as that obtained from the experiment. This aspect indicates that the energy dissipation in the structured liquefied soil can account for the wave attenuation observed in the experiment.

6.4 CONCLUSIONS

The energy dissipation in a physical system involving liquefied sand has been discussed. It is important to distinguish liquefied sand into fully destructured liquefied soil and structured liquefied soil, when the energy dissipation in liquefied sand is discussed. From the previous studies, the energy dissipations in the fully destructured liquefied sand, in the structured liquefied sand and in the sub-liquefied soil are investigated respectively. It has shown that the structured liquefied soil could play a most important role in dissipating the wave energy in the system.

The energy loss that could occur in the layer of the structured liquefied sand was estimated, and then it was compared to the energy loss obtained from an experiment. It is shown that the structured liquefied sand has the ability to dissipate the energy to an extent that can account for the energy dissipated in the total system.

References

Dalrymple, R & Liu, P. L. F. (1978). Waves over soft muds: A two-layer fluid model, *J. Physical Oceanography*, **8**, 1121-1131

Gade, H. G. (1958). Effects of a nonrigid, impermeable bottom on plane surface waves in shallow water, *J. Marine Research*, 16-2, 61-82

Hamada, M. & Wakamatsu, K., (1998). A study on ground displacement caused by soil liquefaction, *J. Geothch. Engng. JSCE*, No. 596/III-43, 189-208 (*in Japanese*)

Kang, Y. K., Takahashi, S., Suzuki, K., Miura, H. & Park, W. S., (1997). Wave-absorbing effect of liquefied sand bed wave barrier, *Proc. Coastal Engng,*

JSCE **44**, No.1, 706-710 (*in Japanese*)

Kokeguchi, K., Shimokawa, A., Kohchi, J., Towhata, I. & Yoshikawa, A., (2001). Experimental study on strain-rate dependency in post-liquefaction behaviour of sand, *J. Geothch. Engng. JSCE*, No. 680/III-55, 97-108 (*in Japanese*)

Lee, T.L., Tsai, C. P. & Jeng, (2002). Ocean waves propagating over a Coulomb-damed poroelastic seabed of finite thickness: an analytical solution, *Computers and Geotechnics*, 29, 119-149

Park, W. S., Takahashi, S., Suzuki, K. & Kang, Y. K., (1996). Finite element analysis of interactions between wave, soil and structures, *Proc. Coastal Engng, JSCE* **43**, No.2, 1036-1040 (in Japanese)

Putnam, J. A., (1949). Loss of wave energy due to percolation in a permeable sea bottom, *Transactions, American Geophysical Union*, **30**, No. 3, 349-356

Putnam, J. A. & Johnson, J. W., (1949). The dissipation of wave energy by bottom friction, *Transactions, American Geophysical Union*, **30**, No. 1, 67-74

Reid, R. O., & Kajiura, K., (1957). On the damping of gravity waves over a permeable seabed, *Transactions, American Geophysical Union*, **38**, 662-666

Takahashi, S., Shimosako, K., Tamamoto, S. & Miura, H., (1994). Small-scale experiments on a boiling sand bed and its wave absorbing effects, *Proc. Coastal Engng, JSCE* **41**, No.1, 611-615 (*in Japanese*)

Takahashi, S., Suzuki, K., Muranishi, Y. & Isobe, M., (2002). U-π form VOF-FEM program simulating wave-soil interaction: CADMAS-GEO-SURF, *Proc. Coastal Engng, JSCE* **49**, No.2, 881-885 (*in Japanese*)

Towhata, I. & Kawasaki, K., (1999). Mechanism and prediction of sinking of shallow foundation due to liquefaction, *Symposium on mechanism of liquefaction, Japanese Geotechnical Society*, No. 113, 477-482 *(in Japanese)*

Towhata, I., Vargas-Monge, W., Orense, R. P., & Yao, M., (1999). Shaking Table tests

on subgrade reaction of pile embedded in sandy liquefied subsoil, *Soil Dynamics and Earthquake Engineering,* **18**, No. 5, 347-361

Yamamoto, T. (1982). Non-linear mechanics of ocean wave interactions with sediment beds, *Applied Ocean Research*, 4-2, 99-106

Yamamoto, T. (1983) On the response of a Coulomb-damped poroelastic bed to water waves, *Marine Geotechnology*, 5-2, 93-130

Yamamoto, T. & Schuckman, B. (1984). Experiments and theory of wave-soil interactions, *J. Engineering Mech. ASCE*, 110-1, 95-112

Yamamoto, T. & Takahashi, S. (1985). Wave damping by soil motion, *J. Waterway, Port, Coastal and Ocean Eng. ASCE*, 111-1, 62-77

Yamamoto, T., Takahashi, S. & Schuckman, B. (1983). Physical modeling of sea-seabed interactions, *J. Engineering Mech. ASCE*, 54-72

Table 6.1 Predicted shear modulus at the maximum wave damping and summary of the conditions of previous analyses

	Shear modulus at the maximum wave damping: kPa	Length of sand bed: m	Depth of sand bed: m	Depth of water: m	Wave period: s
Park et al. (1996)	1.1	4	0.4	0.25	1
Kang et al. (1997)	2	5	0.55	0.34	1.17
Takahashi et al. (2002)	58	280	15	10	8

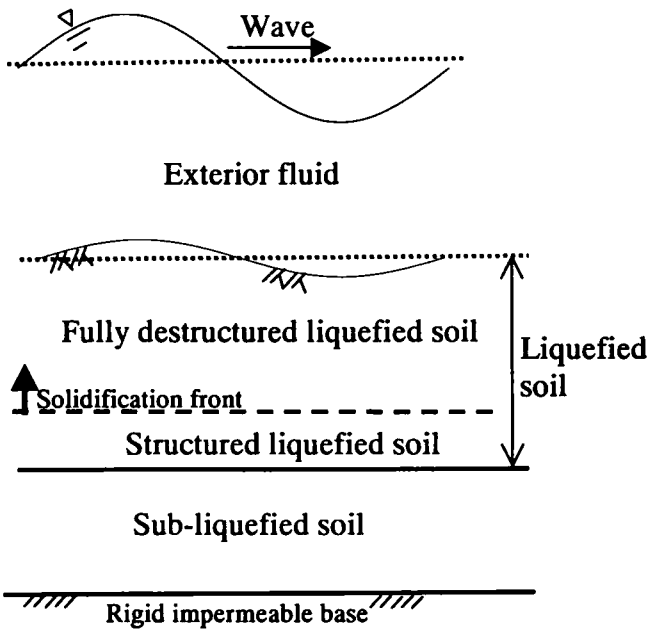

Fig. 6.1 Physical system involving liquefied soil

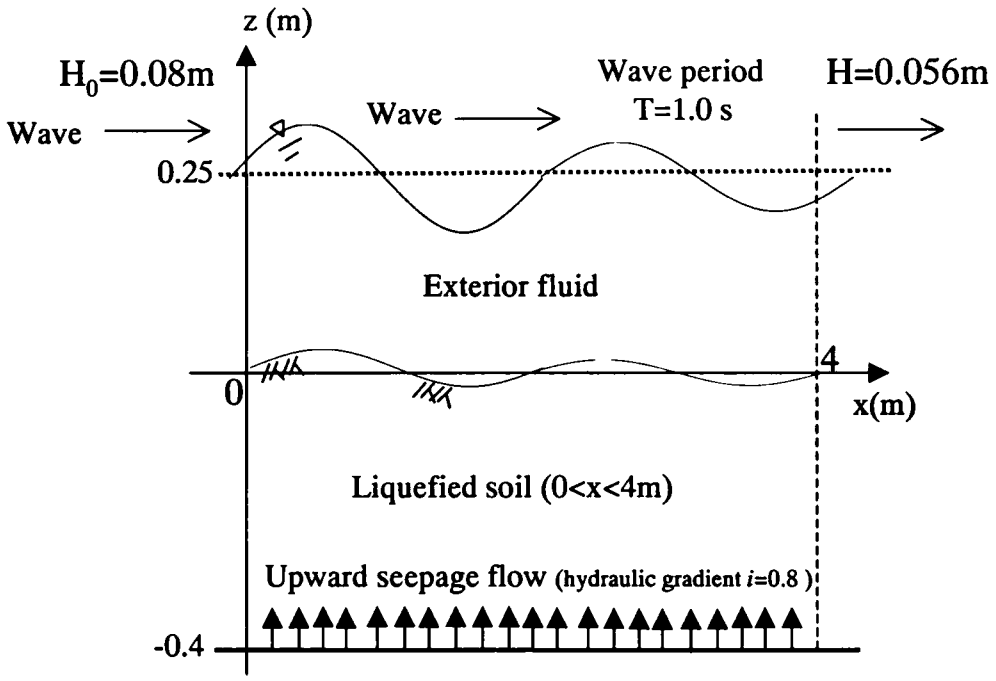

Fig. 6.2 Wave attenuation by liquefied sand in Takahashi (1994)

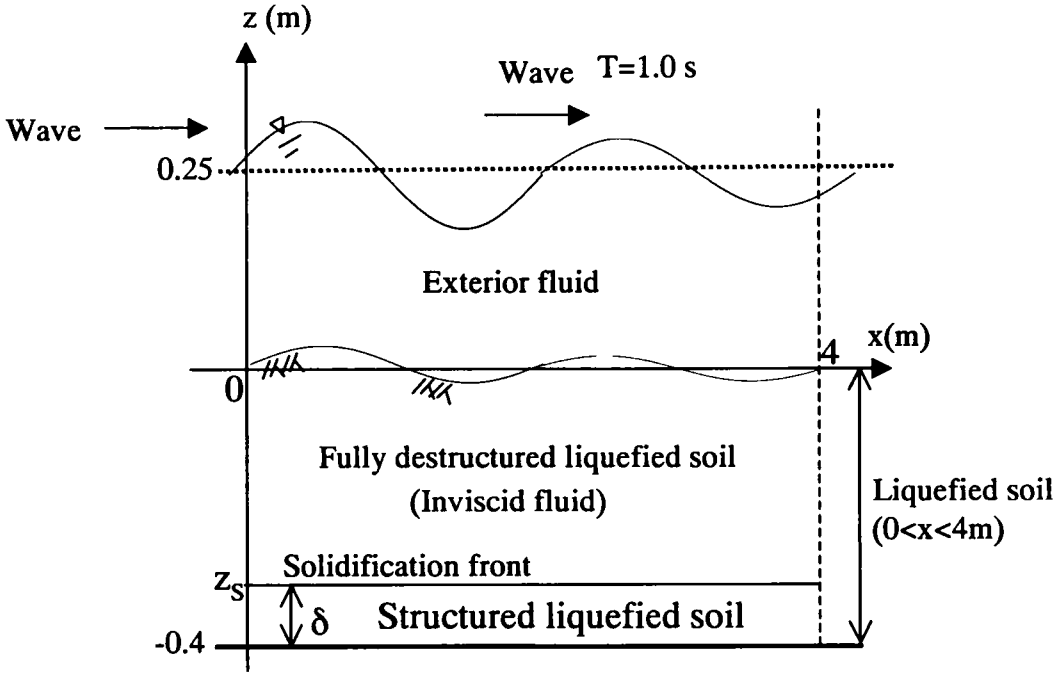

Fig. 6.3 Structured liquefied soil and fully destructured liquefied soil in the liquefied soil layer

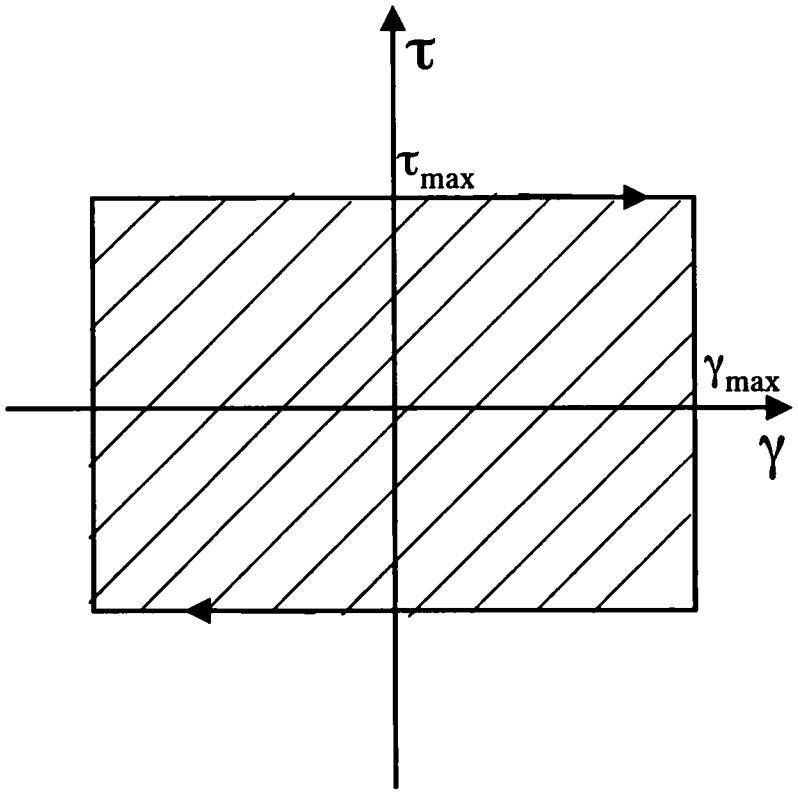

Fig. 6.4 The relation between τ and γ in the element of the structured liquefied sand, which is assumed so that the energy loss may be possible highest

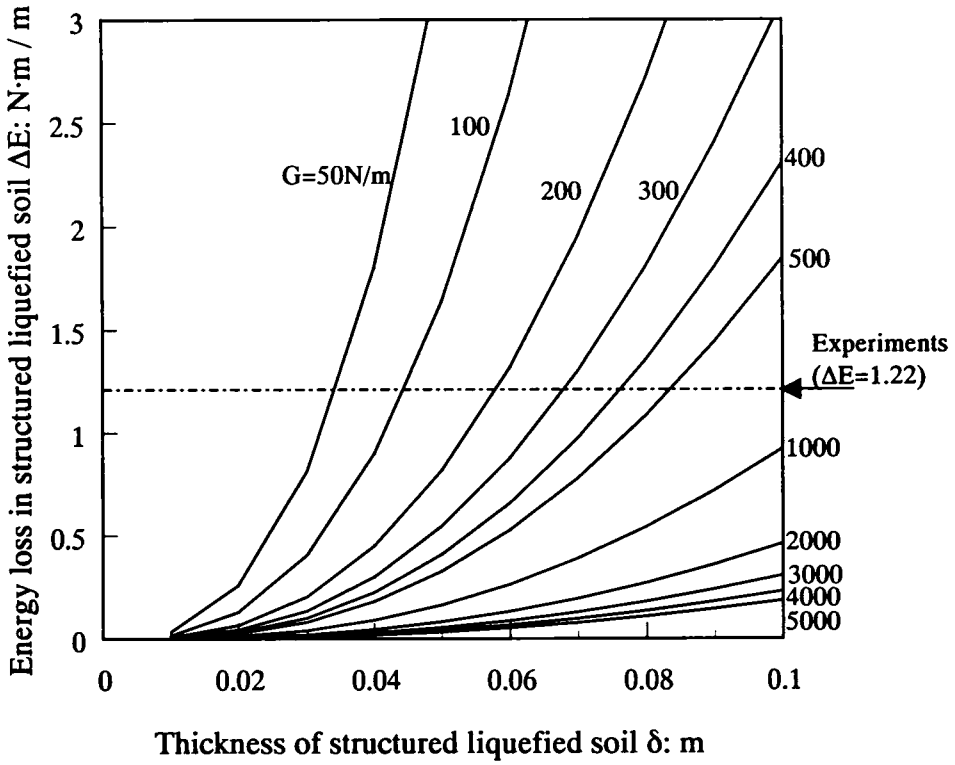

Fig. 6.5 Estimated energy loss in structured liquefied sand against the thickness of structured liquefied sand and the shear modulus of it

Chapter 7

Liquefaction and flow deformation in sand around coastal structures

7.1 INTRODUCTION

The performance of permeable granular systems such as detached breakwaters under storm waves has become an increasingly important subject of research in relation to the preservation of sand beaches as well as coastal environments (Isobe, 1994). The wave-induced instability of detached breakwaters on sandy seabeds is one of the long standing problems that needs closer examination (Fig. 7.1). For example, the detached breakwaters on the Niigata Coast of Japan settled by more than $10m$ due to wave attack over a period of several stormy seasons (Nishida et al., 1985). Possible factors that may be responsible for such a large settlement include wave pressures, oscillating flow through concrete blocks that compose the body of a detached breakwater and currents around the toe of the breakwater. These factors may trigger processes resulting in wave-induced liquefaction, scouring or sediment transport (Fig. 7.1). The question arises as to how these processes are linked with each other. In order to address this issue, it is important to achieve a full understanding of the wave-induced liquefaction of seabed soil near coastal structures and its consequences.

It has been observed in chapter 4 that the process of wave-induced liquefaction of a level bed is essentially of a progressive nature. The author performed a range of centrifuge wave tank tests on loosely packed level deposits of sand in order to investigate the relation between the progressive nature of liquefaction and the flow deformation in level beds of sand (chapter 4). The principal finding is that the progressive nature of liquefaction is well reflected in the flow deformation of the liquefied soil. In fact, when liquefaction occurred, the sand surface started vibrating and the amplitude of the soil vibration increased markedly with the downward advance of the liquefaction front.

With the above-mentioned in mind, this chapter examines the behaviour of granular slopes resting on liquefiable sand beds in a set of centrifuge wave tank tests. Comparison will be made of the wave-induced instability of level beds of sand with the performance of sand beds below much coarser granular slopes. The aim of the

experiments is to provide an insight into the wave-induced instability of detached breakwaters on sandy seabeds.

7.2 LIQUEFACTION-RELATED FLOW DEFORMATION IN SOIL BEDS BELOW GRANULAR SLOPES

The wave tank tests were performed under a centrifugal acceleration of 30 gravities. The cross section of the wave tank used is shown in Fig. 7.2. Silicon oil with a viscosity of 30 cSt was used in order to match the time scaling laws of soil consolidation and fluid-wave propagation. Four wave tests (test Nos. WJ11, WJ13, WJ14, WJ15) were performed on the four identical sand beds that were overlain by granular slopes (Table 7.1). The sand used was Silica sand #7-Batch A (G_s=2.69, e_{max}=1.15, e_{min}=0.69 and D_{50}=0.14*mm*). The sand beds on which the granular slopes rested were formed in the same way as in the wave tests on the level beds of sand described in chapter 4. The properties of gravel used to form a granular slope were as follows: G_s = 2.7, D_{50}= 3 *mm*. The gradient of the granular slope formed was 1: 2.7. The wave paddle was excited at a frequency of 8*Hz*.

The wave field with the presence of a granular slope was first investigated by conducting a separate series of centrifuge wave tests with the granular slope overlying a rigid base. The distributions of measured wave pressures on the rigid base are shown in Fig. 7.3 for two different phases. In these figures, the dotted lines represent wave pressures calculated using small-amplitude wave theory. It is seen that the measured results conform well to the theoretical lines in the range between x = 0 and x = 200 *mm*. The measured reflection coefficient of the granular slope was equal to 0.26. Considering these observations, it can be said that the wave field concerned approximates to a travelling-wave field.

Then, four wave tank tests with the same χ_0-value of 0.19 were performed on the sand beds that were overlain by granular slopes. The initial effective vertical stress, σ_{v0}', was estimated using elasticity theory (Poulos & Davis, 1974) with consideration of the effective weight of the granular slope. It is assumed that a vertical load acts on the surface of a semi-infinite body of elastic material. The vertical load increases linearly on an infinite strip (Fig. 7.4). The increments of the vertical effective stress, $\Delta\sigma_v$', due to the vertical surface loading is expressed as

$$\Delta\sigma_v' = \frac{p}{\pi}\left[\frac{(x-x_0)\cdot\alpha}{a} + \frac{\sin 2\delta}{2}\right] . \tag{7.1}$$

Here, with reference to Fig. 7.2, the following values were used: a=90mm, x_0=110mm, $p=\gamma'_g\, b$, in which γ'_g is the submerged unit weight of the granular slope. The initial effective vertical stress, σ_{v0}', was thus estimated from $\sigma_{v0}'=-\gamma' z+\Delta\sigma_v'$ (N.B. $z\leq 0$) .

The measured excess pore pressures in three of the four tests (WJ13, WJ14, WJ15) were compiled to give an idea as to the spread of the liquefied zone during the wave loading (Fig. 7.5). In this figure, the distribution of excess pore pressure ratios ($u_e^{(2)}/\sigma_{v0}'$) in the foundation soil is shown in terms of the gray levels indicated. It is seen from Figs. 7.5 (b), (c) and (d) that the process of liquefaction in the free field was essentially the same as that observed in the level beds of sand. In short, the liquefaction front advanced downward with increasing wave-loading cycle. However, in the sand bed below the granular slope, the liquefied zone spread two-dimensionally, except for the soil directly below the granular slope. This part of soil remained sub-liquefied due to the overburden effect that resulted from the effective weight of the granular slope. While wave loading was continued, the excess pore pressure started dissipating gradually in the soil directly below the granular slope, thereby reducing the extent of the liquefied zone (Fig. 7.5(e)).

The corresponding process of flow deformation in the foundation soil below a granular slope is shown in Fig. 7.6. This figure was constructed based on a typical set of deformation measurements in test WJ15. The dots marked on Fig. 7.6(a) represent the locations of the coloured sand markers that were used for visual observation. In Figs. 7.6(b), (c) and (d), it is noteworthy that the interface between the granular slope and the sand surface remained sharp. This observation indicates that essentially no transport of sand particles through the granular slope occurred. Therefore, the significant settlement of the granular slope as shown in Fig. 7.6(d) may be ascribed to the liquefaction-related flow deformation that occurred in the foundation sand.

It is important here to note that the flow deformation manifested itself in the form of two-dimensional, residual shear deformation. A closer examination of its development tells us that the residual shear deformation initially concentrated in the soil below the toe of the granular slope and then became severe in wider areas in association with the spread of the liquefied zone.

Interestingly, the rate of development of such flow deformation was much slower than the rate of development of the liquefied zone. This aspect is shown in Fig. 7.7. The time histories presented in this figure were constructed using a typical set of deformation measurements in test WJ11. The settlement of the granular slope continued following the end of propagation of the liquefied zone. Note that the settlement of the

toe of the granular slope started upon occurrence of liquefaction in the sand bed. This observation suggests the existence of a certain complex form of resistance of the liquefied soil to shearing, calling for future studies focusing on the physics of liquefied soil.

7.3 CONCLUSIONS

The characteristics of wave-induced instability of the level beds of sand with granular slopes have been discussed based on the centrifugal wave testing. The principal results obtained may be summarized as follows:

(a) The significant settlement of the granular slope was ascribed to the liquefaction-related flow deformation that occurred in the foundation sand. Specifically, the toe of the granular slopes started settling upon occurrence of liquefaction in the free field. The granular slopes then penetrated markedly in the foundation sand with significant flow deformation of the sand bed.
(b) The spread of the liquefied zone in the free field outside the toe of the granular slope was essentially the same as that observed for the level beds of sand without granular slopes. In the soil bed below the granular slope, however, the liquefied zone spread two-dimensionally.
(c) The residual shear deformation in the soil below the granular slope developed at much slower rates than the rates of spread of the liquefied zone. This observation may relate to a form of shear resistance of the liquefied soil undergoing plastic flow.

References

Isobe, M. (ed.) (1994). *Coastal and marine environments*. Asakura Press. 203. (*in Japanese*)

Nishida, H., Yamaguchi, Y., Kondo, T. & Shimizu, K., (1985). A study on sinking of blocks of detached breakwaters using elastic wave exploration. *Proceedings of Coastal Engineering, JSCE* 32, 365-369. (*in Japanese*)

Polus. H. G. & Davis. E. H. (1974). *Elastic solutions for soil and rock mechanics*, Series in soil engineering, John Wiley & Sons. 38.

Table 7.1 Details of centrifuge wave tests on loose deposits of sand that were overlain by granular slopes

Test number	χ_0	sand bed		granular slope
		γ': kN/m^3	Dr: %	γ'_g: kN/m^3
WJ11	0.19	250	35	no data
WJ13	0.19	252	39	247
WJ14	0.19	251	36	254
WJ15	0.19	250	36	264

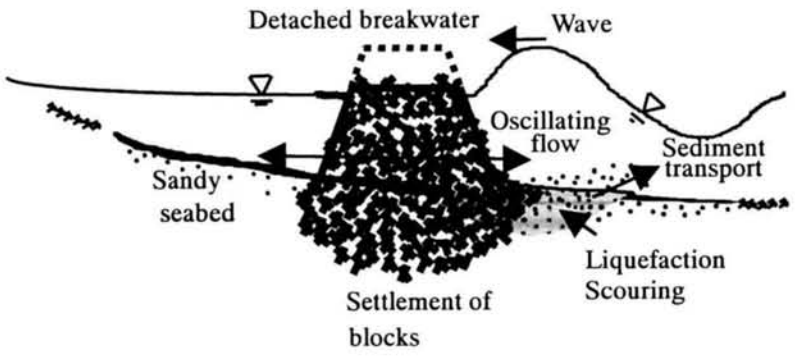

Fig. 7.1 Factors affecting stability of detached breakwater on sandy seabed

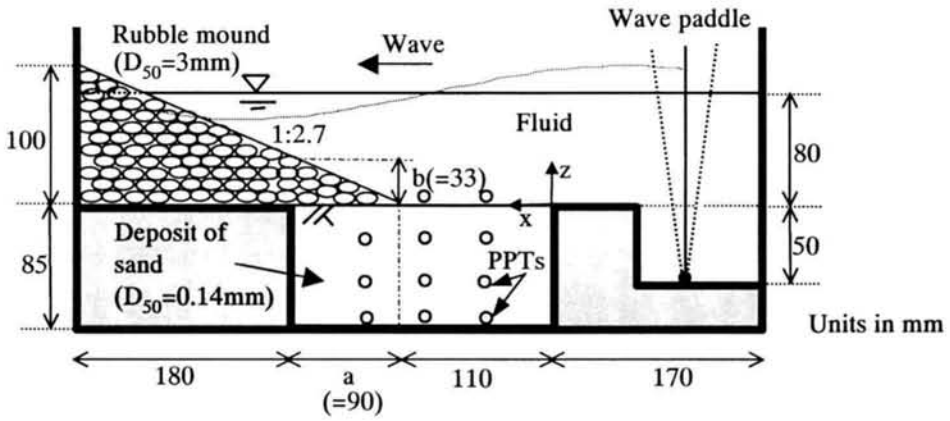

Fig.7.2 Cross section through granular slope model on liquefiable sand

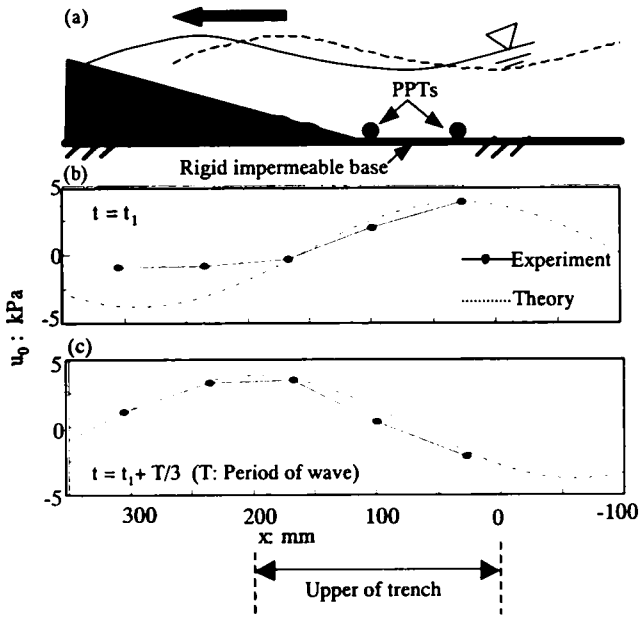

Fig. 7.3 Measured distributions of wave pressure on a rigid base outside and within a granular slope

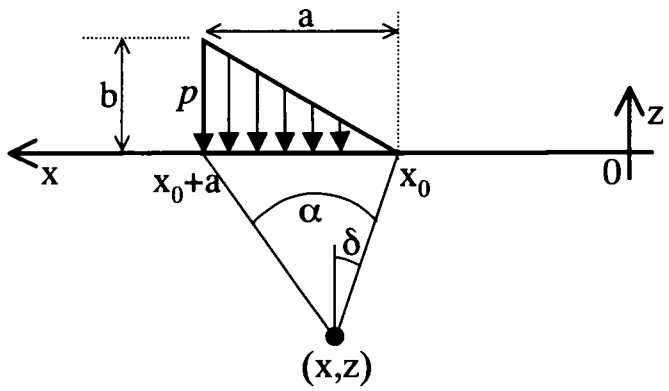

Fig. 7.4 Vertical loading increasing linearly on an infinite strip.

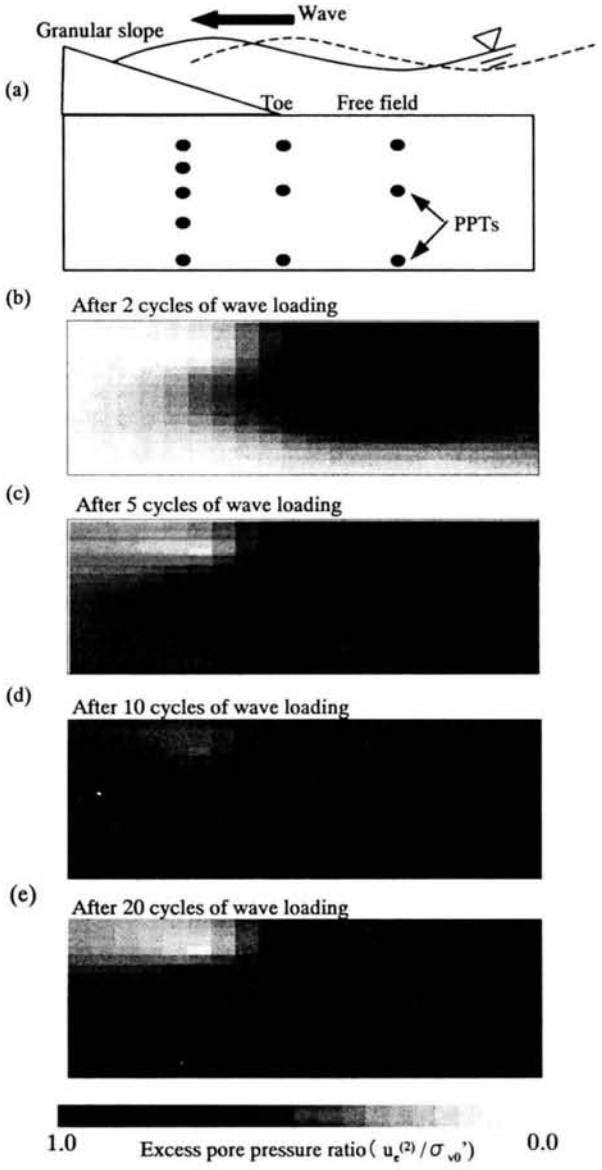

Fig.7.5 Measured spread of liquefied zone due to wave loading

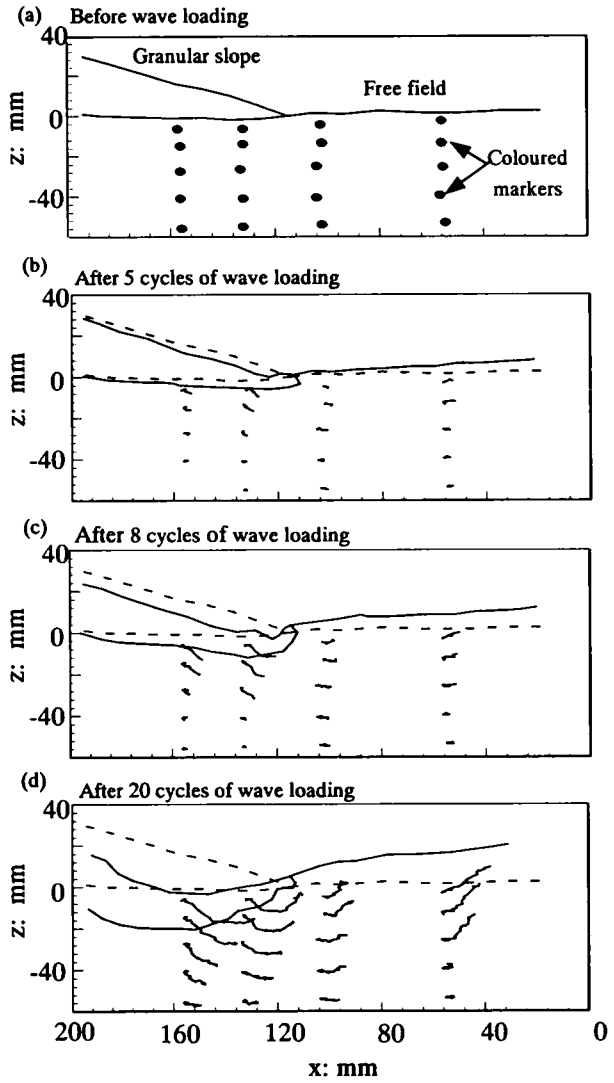

Fig. 7.6 Measured flow deformation of a sand bed below a granular slope due to wave loading

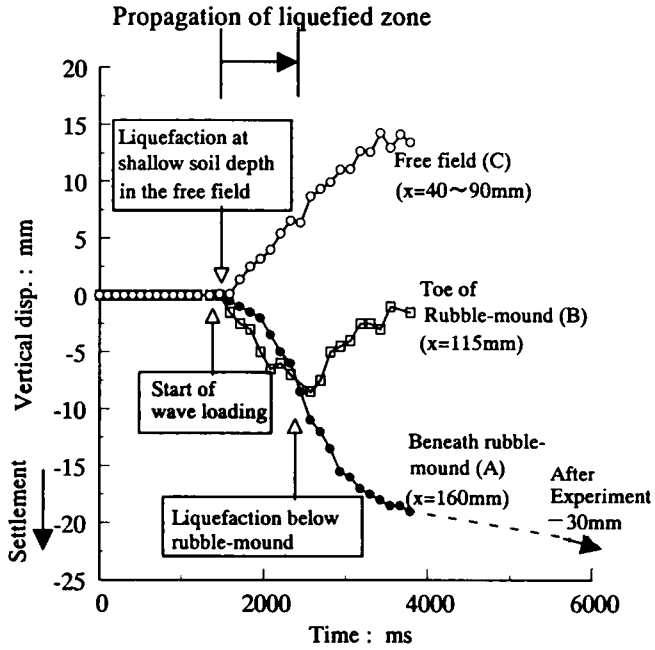

Fig. 7.7 Measured time histories of settlement of granular slope

Chapter 8

Conclusions

The dynamics of liquefied sand under severe wave loading has been discussed, emphasizing progressive liquefaction, solidification in liquefied sand during wave loading, re-liquefaction characteristics and flow deformation in liquefied sand through the integrated use of centrifuge wave tank testing and theoretical investigation. The wave damping by liquefied sand also has been discussed. The principal findings and conclusions obtained in the present thesis may be summarized as follows.

In chapter 2, previous studies on wave-induced liquefaction were reviewed. Importance of a sound framework for treating the behaviour of liquefied soil under wave loading was emphasized.

In chapter 3, the progressive liquefaction and solidification processes in liquefied sand during continued wave loading were discussed and a theoretical framework for describing them has been proposed. Namely, two levels of liquefied soil were introduced: *fully destructured liquefied soil* that has no stiffness; and *structured liquefied soil* that has a marginally discernible stiffness while the effective stress is zero. The principal findings may be summarized as follows.

(a) After the full development of the liquefied zone due to the progressive liquefaction, in the course of continued wave loading, the residual pore pressure at the bottom of the liquefied sand started dissipating, triggering the start of solidification. The solidification front advanced upward to the soil surface during the continued wave loading.

(b) The vibratory movements of the soil surface developed in association with the advance of the liquefaction front and decreased in association with the advance of the solidification front.

(c) The advance of the solidification front brought about marked densification in the region behind the front. This densification was caused by the contractancy due to cyclic loading. The degree of densification due to the solidification process was more significant than that brought about by the consolidation under quiescent environment after the cessation of the wave loading.

(d) The relation between the velocity of the solidification front and the degree of

densification due to the solidification is approximately represented by a simple expression that had been proposed by Florin & Ivanov (1961).

In chapter 4, the characteristics of progressive liquefaction and progressive solidification in liquefied sand were examined using centrifugal wave tank testing with viscous scaling. The progressive nature of liquefaction and solidification were observed in detail with the application of a high-speed CCD camera to centrifuge wave testing, as well as with pore pressure measurements. The degrees of densification in sand beds were estimated from results of the centrifuge upward seepage flow tests that were performed before and after a wave test. The measured consequences of progressive liquefaction/solidification conformed well to the predicted results from the theoretical model proposed in chapter 3.

The effects of wave loading history on liquefaction in sand beds at the subsequent wave loading stage were discussed in chapter 5 on the basis of centrifugal wave tank testing, and through the analytical model for progressive liquefaction/solidification developed in chapter 3. The principal results obtained may be summarized as follows.

(a) It is important to distinguish preshearing effects into that due to low-level preshearing and that due to high-level preshearing. The low-level preshearing with $\chi_0<\chi_{cr}$, which was accompanied by a marginally discernible densification, significantly increased the resistance to liquefaction. The high-level preshearing with $\chi_0>\chi_{cr}$, which brought about an appreciable densification, did not improve the liquefaction resistance.

(b) The solidification front extends upwards to a shallower soil level as the number of wave loading cycles is increased. Such a prolonged high-level preshearing makes the resistance to re-liquefaction in the solidified zone significantly larger than the liquefaction resistance of the fresh deposits of the sand.

(c) The proposed analytical model for progressive liquefaction/solidification is capable of predicting the behaviour of sand beds under complex wave loading histories. It is demonstrated that in each of the imposed groups of waves, the re-liquefaction extended down to a horizon slightly above the previously solidified zone, forming the alternating bands of markedly densified and less densified soil.

In chapter 6, the energy dissipation in a system that consists of fully destructured liquefied soil, structured liquefied soil and sub-liquefied soil was discussed. It was shown that the structured liquefied soil could play a most important role in dissipating

the wave energy in the system. The possible energy loss in the layer of the structured liquefied soil was estimated, concluding that the structured liquefied sand has the ability to dissipate much energy in such a way as to account for the energy dissipation that was observed to occur in the total system.

Lastly, chapter 7 was devoted to discussing the behaviour of granular slopes on liquefiable sand beds and the liquefaction-related flow deformation in foundation sand, on the basis of centrifugal wave tank testing. It was found that the significant settlement of the granular slope was ascribed to the liquefaction-related flow deformation that occurred in the foundation sand. In fact, it was observed that the toe of the granular slopes started settling upon occurrence of liquefaction in the free field, and then the granular slopes penetrated markedly in the foundation sand with significant flow deformation of the sand bed.

Suggestions for future studies

For wider practical applications of the outcome of the researches described in this thesis, the following will be worth exploring in the future:

(1) The seabed responses to storm waves were examined in this thesis through experimental and analytical studies. In order for studies of fluid-soil interaction to advance on a sound basis, it will always be instructive to think of the synergies among field observation, physical modelling and numerical analysis. In particular, field observations will be of utmost significance in the future, focusing on developments of residual pore pressures in the sediments during storms, aging effects of soil, depositional environments and effects of complex wave loading history.
(2) The approaches adopted in this thesis were exclusively from a standpoint of continuum mechanics. In order to investigate not only transport phenomena of soil particles related to scouring or beach erosion but also convection or diffusion of chemical substances affecting the hydrospheric environment, integration of continuum- and particulate-mechanics approaches will certainly be a target worth exploring.
(3) Loosely packed soil deposits that have high liquefaction potential may frequently be formed in river delta fronts or in reclaimed zones as natural or artificial deposits.

The knowledge pertaining to the performance of liquefaction in loose deposits may have direct practical implications in the design of coastal structures on artificial deposits, in the prediction of liquefaction-related submarine landslide involving natural loose deposits, and in the use of imitational liquefied zone as an effective means for dampening out storm waves.

(4) The framework of progressive liquefaction/solidification presented in this thesis is considered to have a potential that may contribute to expounding the dynamics of gravity flow including sedimentation. For laboratory experimentation on gravity currents, use of drum centrifuge testing with PIV and/or X-ray TV techniques will be worth attempting.